University of Szeged

Faculty of Medicine

Doctoral School of Multidisciplinary Medicine

Lab-on-a-chip tool for the investigation of biological barriers

PhD Thesis

András Kincses

Supervisor:

András Dér PhD; DSc, scientific adviser

Biological Research Centre, Institute of Biophysics

Biomolecular Electronics Research Group

Szeged

2021

List of Publications

1. List of full papers directly related to the subject of the thesis

I. Walter FR, Valkai S., **Kincses A**, Petneházi A, Czeller T, Veszelka S, Ormos P, Deli MA, Dér A. A versatile lab-on-a-chip tool for modeling biological barriers. Sensors and Actuators B: Chemical. 2016;222:1209-1219. IF: 5.401

II. Kincses A, Santa-Maria AR, Walter FR, Dér L, Horányi N, Lipka DV, Valkai S, Deli MA, Dér A. A chip device to determine surface charge properties of confluent cell monolayers by measuring streaming potential. Lab. Chip. 2020;20(20):3792-3805. IF: 6.774

Cumulative impact factor of papers directly related to the subject of thesis: 12.175

2. List of other full papers

I. Kincses A, Toth-Boconadi R, Dér A. 2D measurement of ion currents associated to the signal transduction of the phototactic alga Chlamydomonas reinhardtii. J Photochem Photobiol B 2012;114:147-52. IF: 3.110

II. Sántha P, Veszelka S, Hoyk Z, Mészáros M, Walter FR, Tóth AE, Kiss L, **Kincses A**, Oláh Z, Seprényi G, Rákhely G, Dér A, Pákáski M, Kálmán J, Kittel Á, Deli MA. Restraint Stress-Induced Morphological Changes at the Blood-Brain Barrier in Adult Rats. Frontiers in molecular neuroscience. 2016; 8(88). IF: 5.076

III. Lázár V, Martins A, Spohn R, Daruka L, Grézal G, Fekete G, Számel M, Jangir PK, Kintses B, Csörgő B, Nyerges Á, Györkei Á, **Kincses A**, Dér A, Walter FR, Deli MA, Urbán E, Hegedűs Z, Olajos G, Méhi O, Bálint B, Nagy I, Martinek TA, Papp B, Pál C. Antibiotic-resistant bacteria show widespread collateral sensitivity to antimicrobial peptides. Nat Microbiol. 2018;3(6):718-731. IF=14.633

IV. Hoyk Z, Tóth ME, Lénárt N, Nagy D, Dukay B, Csefová A, Zvara Á, Seprényi G, **Kincses A**, Walter FR, Veszelka S, Vígh J, Barabási B, Harazin A, Kittel Á, Puskás LG, Penke B, Vígh L, Deli MA, Sántha M. Cerebrovascular Pathology in Hypertriglyceridemic APOB-100 Transgenic Mice. Front Cell Neurosci. 2018;12:380. IF=3.9

V. Harazin A, Bocsik A, Barna L, **Kincses A**, Váradi J, Fenyvesi F, Tubak V, Deli MA, Vecsernyés M. Protection of cultured brain endothelial cells from cytokine-induced damage by α-melanocyte stimulating hormone. PeerJ. 2018;15;6:e4774. IF=2.353

VI. Santa-Maria AR, Walter FR, Valkai S, Brás AR, Mészáros M, **Kincses A**, Klepe A, Gaspar D, Castanho MARB, Zimányi L, Dér A, Deli MA. Lidocaine turns the surface charge of biological membranes more positive and changes the permeability of blood-brain barrier culture models. Biochim Biophys Acta Biomembr. 2019;1861(9):1579-1591. IF=3.411

VII. Barna L, Walter FR, Harazin A, Bocsik A, **Kincses A**, Tubak V, Jósvay K, Zvara Á, Campos-Bedolla P, Deli MA. Simvastatin, edaravone and dexamethasone protect against kainate-induced brain endothelial cell damage. Fluids Barriers CNS. 2020;17(1):5. IF=4.47

VIII. Taneva SG, Krumova S, Bogár F, **Kincses A**, Stoichev S, Todinova S, Danailova A, Horváth J, Násztor Z, Kelemen L, Dér A. Insights into graphene oxide interaction with human serum albumin in isolated state and in blood plasma. Int J Biol Macromol. 2021;175:19-29. IF=5.162

IX. Santa-Maria AR, Walter FR, Figueiredo R, **Kincses A**, Vigh JP, Heymans M, Culot M, Winter P, Gosselet F, Dér A, Deli MA. Flow induces barrier and glycocalyx-related genes and negative surface charge in a lab-on-a-chip human blood-brain barrier model. J Cereb Blood Flow Metab. 2021;271678X21992638. IF=5.681

X. Dukay B, Walter FR, Vigh JP, Barabási B, Hajdu P, Balassa T, Migh E, **Kincses A**, Hoyk Z, Szögi T, Borbély E, Csoboz B, Horváth P, Fülöp L, Penke B, Vígh L, Deli MA, Sántha M, Tóth ME. Neuroinflammatory processes are augmented in mice overexpressing human heat-shock protein B1 following ethanol-induced brain injury. J Neuroinflammation. 2021 Jan 10;18(1):22. IF=5.793

Cumulative impact factor of other full papers: 53.589

Total cumulative impact factor: 65.764

Table of contents

List of abbreviations

Ag/AgCl: silver/silver chloride

BBB: blood-brain barrier

BCv1: barrier chip

BCv2: barrier chip version 2

BDF: Backward Differentiation Formula

bFGF: basic fibroblast growth factor

BSA: bovine serum albumin

Caco-2: intestinal colon carcinoma derived epithelial cell line

DMEM: Dulbecco's modified Eagle medium

EBA: Evans blue-labeled albumin

EDTA: Ethylenediaminetetraacetic acid

FD: FITC-dextran 4.4 kDa

FBS: fetal bovine serum

GCL: Gouy-Chapman layer

GFAP: glial fibrillary acidic protein

hCMEC/D3: human brain microvascular endothelial cell line

ITO: Indium tin oxide

LDv: laser-Doppler velocimetry

LOC: lab-on-a-chip

OC: organ-on-chip

Papp: apparent permeability coefficient

PBS: phosphate buffered saline

PDMS: Polydimethylsiloxane

PEI: polyethylenimine

PET: Polyethylene terephthalate

SF: sodium fluorescein

α-SM: α-smooth muscle actin

Summary

The importance of integrated biochips for studying biological barriers has been increased in the last decade. These lab-on-a-chip (LOC) devices offer effective ways to understand physiological functions, transport mechanisms, drug delivery and pathologies. However, there are only a few integrated biochips which are able to monitor several of the crucial parameters of cell-culture-based barrier models. The first aim of the study was to develop a simple but versatile LOC device that enables the complex investigation of barrier function. It's main features are the possibility of co-culturing of 2 or 3 types of cells, automatic feeding of the cells, constant flow of culture medium, visual monitoring of the entire cell layer by microscopy, measurement of trans-endothelial/epithelial electric resistance, permeability assays. A poly(dimethylsiloxane)-based biochip with integrated transparent gold electrodes and with the possibility to connect tubing was built.

Cell surface charge is a key element of biological barriers. The zeta potential of barrier forming cells is generally measured on cell suspensions but no chip device has been described to measure cell surface charge properties of confluent barrier cell monolayers, so far. The second aim of the study was to upgrade the LOC device to make it suitable for monitoring the streaming potential parallel to the surface of cell layers.

Unlike previous systems, the structure of the new LOC device allowed a constant visual observation of cell growth over the whole membrane surface. Morphological characterization of the layers was also accomplished by immunohistochemical staining. The chip was applied to monitor and characterize models of the intestinal and the blood–brain barrier. The models were established using human Caco-2 intestinal epithelial cell line, hCMEC/D3 human brain endothelial cell line and primary rat brain endothelial cells co-cultured with primary astrocytes and brain pericytes. This triple primary co-culture blood–brain barrier model was assembled on a lab-on-a-chip device, and investigated under fluid flow for the first time.

The streaming potential was successfully measured with the LOC device equipped with a pair of Ag/AgCl electrodes. The inclusion of these "zeta electrodes", a voltage pre-amplifier and an oscilloscope in the set-up made it possible to record transient streaming potential signals describing the surface charge properties of blood-brain barrier model endothelial cell monolyaers. The data were verified by comparing the streaming potential results with those of commonly used laser-Doppler velocimetry and model simulations. Changes in the negative surface charge of the barrier model by treatments with neuraminidase enzyme modifying the

cell membrane glycocalyx or lidocaine altering the lipid membrane charge could be measured by both the upgraded LOC device and LDv.

This versatile LOC device is expected to facilitate the kinetic investigation of various biological barriers. The new streaming potential function can help to gain meaningful new information on how surface charge is linked to barrier function in both physiological and pathological conditions.

Introduction

Epithelial outer, and endothelial inner barriers of the body are important defense systems to maintain homeostasis and play a crucial role in drug absorption and transport (1). Culture models of biological barriers are important tools to study physiological functions, transport mechanisms, drug delivery and pathological processes (2). Tight intercellular junctions are fundamental features of epithelial and endothelial barriers *in vivo,* which are reflected in high electrical resistance and low passive permeability for hydrophilic compounds (1, 2). These physical and physico-chemical parameters describe the barrier integrity and function accurately. In more detail, the trans-endothelial/epithelial electric resistance (TEER) represents the paracellular ion mobility which gives information about the tightness of the intercellular junctions. The passive permeability of small, charged or electroneutral molecules describe the para- and transcellular pathways. Another important contributor to the barrier function could be the high negative surface charge of the cell monolayers, yet this is the least explored field of the physical properties of the biological barriers.

The first *in vitro* models to measure these parameters, the cell culture inserts, were introduced in the 1980s. In the past 10 years, besides static models cultured on inserts (3, 4), dynamic lab-on-a-chip (LOC)/organ-on-chip (OC) devices were developed to study cell-cell interactions, molecular pathways, pathological conditions and drug delivery in biological barriers (5-8). These models incorporate the use of fluid flow enabling the investigation of physiological-like functions such as receptor and mechanosensor expression, transport mechanisms, pathologies and drug delivery (9-16). LOC/OC devices became important tools since they provide controlled conditions for cellular signaling and external stimulus, and are able to track the development and changes in the barrier function. Integrated electrodes and sensors enable the monitoring of barrier functions real-time. Besides TEER, the impedance spectrum can be measured which gives further information about cell proliferation, differentiation, degeneration processes and cell recognition. Multi-electrode arrays are used to record field potential of electrically active cells. Programmable pumps and valves provide constant fluid flow to mimic blood flow and the possibility of switching medium composition for treatments. The hydrodynamic effects of the flow, such as the shear stress and hydrodynamic pressure are measured indirectly, based on the physical parameters of the barrier integrity and also the morphological changes of the monolayer-forming cell.

Confluent monolayers of adherent epithelial or endothelial cells grown on culture inserts are widely used static models for intestinal, lung and blood-brain barriers (BBB). The Caco-2 human epithelial cell line is a well characterized model of the intestinal barrier applied for screening of drug candidates (13, 17-19). Culture-based BBB models greatly differ in complexity. Immortalized cell lines and mono-cultures of brain endothelial cells can be used as simplified BBB models (20-22), but the barrier properties of primary cell-based co-culture models are better (2, 23, 24). The field of biochips modeling gut and blood-brain barriers is rapidly evolving, and several models were developed in the last fifteen years which are listed in Table 1. These complex biochips integrate different types of imaging, microfluidics, measurement of resistance in mono- and co-culture systems. As all model systems, the focus of the devices shifts based on the main interest of the corresponding study. Our aim was to develop a versatile LOC device that can be used for different kinds of biological barriers and thus different kinds of approaches. Also, the measurement of all cucial physical parameters, such as TEER and pemeability assays are included.

The negative surface charge of the cell layers is an important element of the defense system of barriers. The role of the negatively charged glycocalyx of the vascular endothelial barrier, for example, is well known in the protection of the cardiovascular system which can be damaged in diseases like atherosclerosis, ischemia due to blood vessel occlusion, diabetes, nephropathy, inflammation and sepsis (25, 26). The glycocalyx of biological barriers is also important in microbiological infections: the neuraminidase enzyme of different bacteria and viruses contribute to their virulence: for example, the neuraminidase of influenza viruses, causing pandemics, facilitates virus release by cleaving sialic acid residues (27).

The blood-brain barrier (BBB), is a complex interface separating the central nervous system and the blood circulation. Cerebral endothelial cells lining the blood vessels in the brain have very specific properties within the vascular system (28). Brain capillary endothelial cells have an inherent role in forming the gatekeeping functions of the BBB, which consist of interendothelial tight junctions, low amount of intracellular vesicles, specialized and polarized influx and efflux transport systems (23, 29). The overall negative surface charge of endothelial cells of brain microvessels is higher than that of other vascular endothelial cells, as measured by laser-Doppler velocimetry (LDv) (30). On one hand, this negative charge of cerebral endothelial cells correlated with their higher phosphatidylserine and phosphatidylinositol content in the plasma membrane (30). On the other hand, the glycocalyx of cerebral endothelial

Microdevice						Culture model				Refs.
Imaging		Flow	Perm.	TEER		Biological barrier	Cell type	Human	Co-culture with	
PhC	Fluo			Instrument	Elec-trode					
-	+	+	+	-	-	Gut	Caco-2 cell line	+	-	(31)
-	-	+	+	-	-	Gut	Caco-2 cell line	+	vascular endothelial cell	(32)
+	+	+	+	87V Industrial Multimeter	Ag/AgCl wire	Gut	Caco-2 cell line	+	bacteria	(33)
+	+	+	+	-	-	Gut	Caco-2 cell line	+	-	(34)
-	+	+	-	-	-	Gut	HT29 cell line	+	primary neurons	(35)
+	+	+	-	-	-	Gut	Caco-2 cell line	+	-	(36)
-	+	+	+	-	-	BBB	primary brain endothelial	+	astrocytes	(37)
-	-	+	+	Flocel volt-ohm meter	built- in	BBB	hCMEC/D3 cell line	-	-	(38)
-	+	+	-	HP4194A impedance analyzer	Pt wire	BBB	hCMEC/D3 cell line	+	-	(39)
+	+	-	+	-	-	BBB	RBE4 cell line	-	mixed glia & neuron culture	(40)
+	+	+	+	-	-	BBB	RBE4 cell line	-	-	(11)
-	-	+	+	Flocel volt-ohm meter	built- in	BBB	primary brain endothelial	+	astroglia, muscle	(12)
+	+	+	+	-	-	BBB	hBMVEC cell line	+	human astro-glia cell line	(41)
-	+	+	+	EVOM2 volt-ohm meter	Au/Ag/ AgCl film	BBB	bEnd.3 cell line	-	glia/glioma cell line	(10, 42, 43)
+ + + +	+ + + +	- - + +	+ + + +	EVOM2 volt-ohm meter	Transpa-rent Au film	Gut BBB BBB	Caco-2 cell line hCMEC/D3 cell line primary brain endothelial	+ + -	- - pericyte, astroglia	Present model, 2016/ 2020 paper
-	+	+	+	EVOM2 volt-ohm meter	Ti/Au film	BBB	primary brain endothelial	-	glial cell	(44)
-	+	+	+	PGstat128N	NA.	BBB	iPS-BMVEC stem cells	+	pericyte, glial cell	(16)

Table 1. Comparison of microdevices developed for modeling biological barriers. PhC: phase contrast microscopy; Fluo: fluorescent microscopy; TEER: transendothelial electrical resistance, Perm.: permeability; BBB: blood-brain barrier; Caco-2 cell line; HT29 cell line: human colon epithelial cell line; bEnd.3: mouse brain endothelial cell line; RBE4: rat brain endothelial cell line; hCMEC/D3: human brain microvascular endothelial cell line; hBMVEC: human brain microvascular endothelial cell line.

cells is denser, and covers larger areas of the microvessel lumen, than in the heart or lung (45). In addition, after vascular injury induced by lipopolysaccharide, the endothelial glycocalyx coverage decreased in the brain, but almost completely disappeared in the peripheral organs, heart and lung, indicating that the brain-specific ultrastructure of the glycocalyx is an important element of the defense system of the BBB (45). This surface glycocalyx on brain endothelial cells is built from a mesh of glycolipids, sialo-glycoconjugates and heparan sulfate proteoglycans (46, 47). The negative surface charge at the BBB is not only providing an extra barrier function for the brain endothelial layer, but is also important in the regulation of the passage of charged molecules including drugs, delivery vectors and nanoparticles across the monolayer (46, 48-51).

Therefore, a quantitative description of the surface electric properties of cell layers forming biological barriers is essential for the broader understanding of their function in physiological processes and diseases. A well-measurable physical quantity to characterize the charge density of surfaces in contact with fluids is the so-called zeta potential (52). Counter-ions of the liquid solution are distributed close to the charged surface of the particle, where, subjected to Coulomb force and Brownian motion, form a diffuse, electric double layer. Part of the ions inside the double layer is occluded in an adsorbed layer of water molecules (the “shear layer”), which, under flow conditions, does not move with the stream. The surface potential, therefore, cannot be measured directly, only the potential difference between the surface of the shear layer and the bulk of the liquid solution, which is called zeta potential. The most widely used method to measure zeta potential of suspended particles in a solvent (colloid particles or cells in an aqueous electrolyte) is LDv, which is able to detect the electrophoretic mobility of the microscopic particles with high precision (53), from which the zeta potential can be calculated. The group of Castanho measured the zeta potential of different mammalian cells in single-cell suspension by the LDv method, and revealed that brain endothelial cells have more negative zeta potential than other types of cells or endothelial cells from other vascular bed (30). Using this technique, Santa-Maria et al. have directly measured zeta potential changes in brain endothelial cells treated with lidocaine, a cationic lipophilic drug molecule, and discovered that lidocaine can alter the passage of positively charged molecules across a BBB culture model, indicating possible drug interactions due to charge at the level of BBB (51).

While the surface charge of individual cells can be determined by LDv, for the *in situ* measurement of zeta potential of biological barrier layers forming large surfaces, this method cannot be applied. Nevertheless, in the vicinity of macroscopic surfaces (e.g., when fluids are

moving due to pressure difference through a channel of charged walls), a special electrokinetic technique, the streaming potential measurement can be used, instead, to determine the zeta potential at the channel wall (54, 55). Streaming potential refers to the transient potential difference developing under fluid flow conditions inside the channel along the flow direction, due to the migration of mobile counter-ions from the vicinity of the charged surface of the channel. Streaming potential, measured via a pair of electrodes, is considered to be proportional to the zeta potential of the surface, under laminar flow conditions (54).

Experiments to measure streaming potential in animals or in *ex vivo* tissues have been made since the late 60's (Table 2). Streaming potentials due to the bloodstream in rabbit aorta and vena cava were measured by microelectrodes inserted into the vessels (measurement direction parallel to the vessel surface), and the endothelial surface lining these large vessels were highly negatively charged at physiological pH (56). In addition to these studies, parts of the

Method to measure surface charge / zeta pontential				**Tissue/Cell**			**Refs.**
Streaming potential / measurement direction	**Chip device**	**Verifi-cation by LDv**	**Built in TEER electrodes**	**Tissue / Cell type**	**Human**	**Biological Barrier**	
Yes / parallel	No	No	No	Aorta and vena cava	No	Yes	(56)
Yes / perpendicular	No	No	No	Small intestine	No	Yes	(57)
Yes / perpendicular	No	No	No	Buccal mucosa	No	Yes	(58)
No (electro-osmosis) / parallel	No	No	No	BGM (kidney) Hep-2 (laryngeal carcinoma) RPMI-1846 (melanoma)	No Yes No	Yes No No	(59)
Yes / parallel	No	No	No	3T12 (fibroblast)	No	No	(60)
Yes / perpendicular	No	Yes	No	HEK293 (kidney epithelial) EA926 (endothelial) Caco-2	Yes Yes Yes	Yes Weak Yes	(61, 62)
Yes / parallel	Yes	Yes	Yes	hCMEC/D3 cell line	Yes	Yes	Present model

Table 2. Studies measuring streaming potential on tissues and cells. TEER: transendothelial electrical resistance; LDv: laser-Doppler velocimetry, hCMEC/D3: human brain microvascular endothelial cell line.

gastrointestinal tract, namely the small intestine (57) and the buccal mucosa (58) were also investigated by streaming potential measurements. In the latter case, however, the fluid flow was typically directed across the epithelial barrier layers (measurement direction perpendicular to the surface). Although, these pioneering papers have given important insight into the major role of surface charge of biological barriers in basic physiological mechanisms, with the increasing use of cell cultures in biomedical research new methods and devices are needed.

Despite the recent boom in LOC devices, no biochip to determine the surface charge of intact cell layers forming biological barriers has been published, yet. Table 2 summarizes the studies in which the measurement of streaming potential of biological cell surfaces, including culture models, was investigated. In Table 2 we refer to four studies performed on cultured cells in which cell surface charge properties were determined (59-62). One of them used electroosmosis (59), three of them streaming potential (60-62), but none of them were using an LOC device. Other differences, as compared to the present study, include the use of non-barrier forming cells (60) and measurement of streaming potential across the cell layer (measurement direction perpendicular to the surface) (61, 62).

Goals of the thesis

The first aim of the study was to design and fabricate a versatile lab-on-a-chip device that can monitor all the crucial properties of biological barrier models. The structure is based on the commercially available culture inserts, so a top and bottom channel is separated by a PET porous culture membrane that supports the barrier forming cells. The design should enable the mono- and co-culturing of different types of biological barriers. The trans-endohtelial/epithelial electric resistance can be measured with integrated, transparent gold electrodes, and the top and bottom channel enable permeability assays. The whole surface of the culture membrane can be monitored by phase contrast microscopy. Immunohistochemistry can be performed, and the cells on the removable culture membrane can be investigated by fluorescence microscopy. In addition, tubes and pumps can easily be connected to the device, thus the introduction of periodic or constant fluid flow can mimic certain biological processes, for instance blood flow in veins.

The second goal was to improve the LOC device with the possibility of zeta potential measurement on cell monolayers. The strategy was to develop a streaming potential-based measurement technique, that can be used for determining the zeta potential. The transient signal of the streaming potential was planned to be recorded with a pair of Ag/AgCl electrodes, a voltage pre-amplifier and an oscilloscope. The results were supposed to be compared to model simulations and laser-Doppler velocimetry method.

Materials and Methods

LOC design and fabrication process

The device was formed by top and bottom channels, separated by a porous polyester (PET) membrane with 0.45 µm pore size, 2×10^6 /cm^2 pore density and 23 µm thickness (It4ip, Belgium) (Figure 1A). The geometry of the channels enabled the measurement of trans-endothelial electric resistance (TEER) and performance of permeability assays. The channels were fabricated from poly(dimethylsiloxane) (PDMS, Sylgard 184, Dow Corning GmbH, Germany) by injection moulding. In the first version of the Barrier Chip (BCv1), the dimensions for the top channel were 37 mm×2 mm×2 mm, while the bottom channel was 42 mm long with the same diameter and height. In the upgraded version (BCv2) for the second paper, the dimensions were slightly changed. In that case the length, width and height of the top and bottom channels were 36 mm×2 mm×1 mm and 57 mm×2 mm×2 mm, respectively. The initiator and base polymer were mixed in 1:10 ratio, and subsequently degassed by vacuum. The mixture was injected in brass molds that were the negatives of the channels. The PDMS was cured on 80 °C for 15 min to reach a rigid structure. To bind the channels to each other, the surfaces of the PDMS channels were treated with oxygen plasma. The vacuum chamber of the plasma cleaner (PDC-002, Harrick Plasma, USA) was evacuated to 200 mtorr then a steady 400 mtorr pressure was set by oxygen stream. When the 400 mtorr oxygen pressure became stable, radio frequency (RF) excitation was used for oxygen plasma treatment for 45 seconds. Thus, the PDMS channels became adhesive and could be assembled with the porous membrane between. During the biochip fabrication process, several membrane types were tested for cell cultivation. Only one type of membrane from it4ip proved to be suitable for cell culture. This membrane, receiving the same treatment as the PDMS components, was mechanically sandwiched between the oxygen plasma treated PMDS parts at its circumference as shown in Figure 1A. There was no surface reaction between these two materials, the oxygen plasma treated PDMS had a poor adhesion to the PET membrane. There is a small area (2 mm × 2 mm) where the adhesion between the PET membrane and the PDMS for perfect sealing was provided by a droplet of a silicone sealant adhesive (Aquarium RTV Silicone Sealant, Adarsha Specialty Chemicals Pvt. Ltd., India). This sealant adhesive has a relatively high viscosity, so it can be applied precisely while it is soft for about 15 minutes. It reaches the fully cross-linked, solid state in 24 hours.

For the top and bottom side of the LOC device, plastic microscope slides (polystyrene, Ted Pella USA) were used. The top slide and the flat part of the male luer lock (Rotilabo, Carl Roth, Germany) inlets/outlets were drilled with a diameter of 2 mm using a commercial drilling machine (Figure 1A). The inlets were glued on the top slide using a photoresin (Norland optical adhesive 81, Norland Products, USA). The bottom sides of the luer locks were painted with the photoresin then placed above the holes on the top slide. After 30 seconds of exposure with a UV lamp (Newport New Illumination System, Newport Corp, USA), the resin reached the required structural rigidity. The gold electrodes for TEER measurement were formed on plastic microscope slides using sputter-coating (K975X, Emitec, France). The thickness of the gold layer was 25 nm, providing low enough resistance (ca. 10 Ohms), and approximately 70% transmission in the visible spectrum, to allow TEER measurements and simultaneous microscopic observation. Therefore, the cell growth could be monitored with a phase contrast microscope throughout the whole length of the channel. Conductive epoxy glue (CW2400,

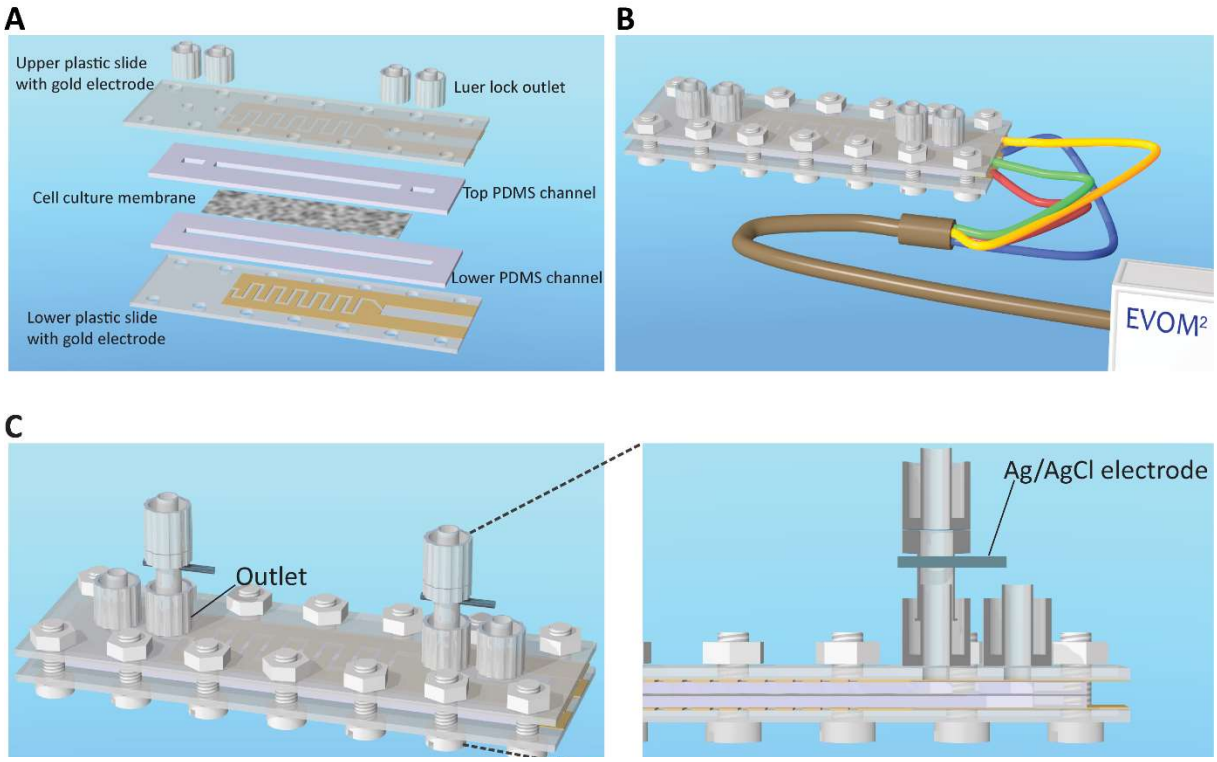

Figure 1 *The structure of the biochip. (A) The two PDMS channels are separated by a porous PET culture membrane. The top and bottom plastic slides coated with the gold electrodes are closing down the two channels. The PDMS and the plastic slides are assembled with plastic screws to avoid shortcut between the electrodes. Luer-lock inlets/outlets on the top slide provide easy access to the channels. The culture medium is circulated in the top channels, while the bottom channel is closed down using male luer cups (not shown). (B) Copper wires are glued to gold electrodes using conductive epoxy, so the instrument (EVOM²) to measure transendothelial electric resistance can be connected easily. (C) The biochip and the zeta electrodes. The PDMS channels and the plastic slides containing the electrodes for transendothelial electric resistance measurement were joined together with screws. The female luer inlets were located on the top, and provided easy access for both top and bottom channels. The Ag/AgCl electrodes were fit in a drilled channel of male-female luer lock caps, and fixed using Norland optical adhesive, thus the electrodes were easy to mount to the biochip for the experiments.*

Chemtronics) was applied in order to link copper wires to the electrodes, and a 4-channel voltohmmeter (EVOM^2, World Precision Intruments, USA) could be connected to the LOC device. The oxygen treated PDMS does not bond very well to metal surfaces either, so the microscope slides with gold electrodes were fixed to the PDMS with either silicone sealant adhesive (BCv1) or plastic screws (BCv2). In case of BCv1, the sealant was applied as a thin, continuous line on the surface of the PDMS. The fabrication procedure was monitored under a stereo microscope. In the end, we had a 0.1 mm thick sealant layer that provided a good adhesion for the glass slides, and sealed well both channels. For the easier assembly of BCv2, the top and bottom slides and the PDMS channels were screwed together. To avoid shortcut of the TEER electrodes, plastic screws were used in the process (Figure 1B). The ready-to-use devices were sterilized with oxygen plasma for 10 min and 70% ethanol for 30 min before cells were seeded to the system.

Electrode fabrication for TEER and streaming potential detection

For the resistance measurements, a pair of 25-nm thick, transparent, gold electrodes was formed on each glass slide using sputter-coating (sputtering machine: K975X, EMITEC, France). Thin copper wires were glued to the gold electrodes with conductive epoxy drops (CW2400, ITW Chemtronics, USA) in order to connect them with the 4-channel input of the voltohmmeter (EVOM, World Precision Instruments, USA). For comparison to the common indium tin oxide (ITO) electrodes, we performed a recording of impedance spectra in the chip with transparent gold (Au) and ITO electrodes (Figure 2A). A voltage source (sinus function generator, TE 8020, 20 MHz), the sample using one electrode on the top and one on the bottom plate of the chip and a reference resistance (100 Ω) were switched in series, and the voltage drop on the resistance was registered by a storage oscilloscope (LeCroy Wave Runner 6010A), from which the sample resistance values were calculated at different frequencies. The frequency range span from 1 Hz to 20 MHz, with 3 records in each decade. Prior to the measurements, both of the channels were filled up with the same buffer as used in the cell culture experiments. Transmission spectra of gold and ITO electrodes were also evaluated (Figure 2B).

For the detection of streaming potentials, Ag/AgCl electrodes were prepared and placed in luer lock connectors (Figure 1C), so they could be easily connected to the inlet and outlet side of the biochip. The silver wires (10 mm long, 0.5 mm width) were polished with a sandpaper and washed with ethanol, then were soldered to copper wires. The connectors were drilled at their diameter, and the silver wires were fitted in. Small drops of the Norland photoresin were applied

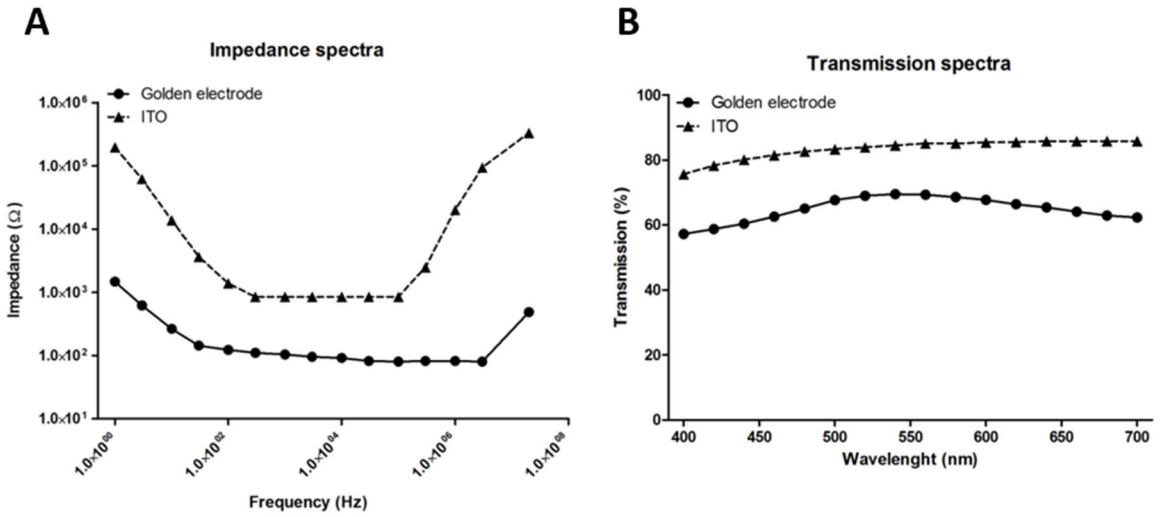

Figure 2 *Impedance and transmission spectra of the transparent gold and ITO electrodes on the chip. (A) Impedance is given in Ohm (Ω), frequency is in hertz (Hz). Measurements were performed between 1 Hz – 100MHz. (B) Transmission spectra were recorded at wavelengths between 400 and 700 nm.*

at openings between the connector and the silver cord to fix them, and were exposed to UV light using a mercury arch lamp for 30 seconds. The end of the copper wire connecting the silver was sealed with silicon glue to avoid shortcut during the subsequent electrolytic chloridisation. For this, the wires were immersed in 3 M KCl solution, one at the time, and a 3 mA DC current was applied for 1 minute. The ready Ag/AgCl electrodes were rinsed with distilled water and dried under N_2 stream.

Zeta potential measurements: Detection of streaming potential

Development of streaming potential is a well-known electrokinetic phenomenon occurring in microfluidic channels (20, 62). If the inner surface of the channel is covered with charges (intrinsic or adsorbed), it attracts counterions from the solution, and keeps them near the surface. Due to a balance of Coulomb attraction and Browninan motion, a diffuse double layer is formed by the mobile ions and the fixed surface charges, the Gouy-Chapman layer (GCL). As a consequence, an electric potential gradient develops perpendicular to the membrane plane, screening the surface potential of the membrane across the GCL. If a fluid flow is applied in the channel, a major part of the counterion cloud of GCL, divided by a “slipping plane” to a moving part and a layer sticking the channel wall, will be grabbed by the solution under Poisseuille flow. The resulting flow of net charge along the channel represents an electric current called streaming current, and the accompanying streaming potential can be detected by an electrode pair separated alongside the channel. The streaming potential under stationary conditions is proportional to the surface potential of the shear plane called zeta potential,

according to the Helmholtz-Smoluchowski equation (52). Since the zeta potential can be relatively easily measured by electrokinetic methods, this is the very quantity that is used to characterize surface charge densities of artificial membranes or colloid particles. In this work, we measure a nonstationary (transient) streaming potential, in order to maximize the signal amplitude by applying high inlet flow rates. We provide both theoretical and experimental evidences that the amplitude of the transient signal is proportional to the zeta-potential at the surface, in this case, too. (For more details, see below, and under the Simulation section).

The transient signal was gained and filtered with a low-noise voltage pre-amplifier (SR560, Stanford Research Systems, USA) (Figure 3A), recorded by a digital oscilloscope (Wave Ace, Teledyne LeCroy, USA), and further analysed via the Wavestudio software (Teledyne LeCroy, USA). The amplitude of the transient streaming potential signals was calculated with Matlab (MathWorks, USA). The difference between the baseline and the maximum of the curve defined the amplitude. The noise of the signals was eliminated with the function estimation of smoothing splines. (Figure 4A)

Experimental validation of the system was performed by using a Nafion membrane inserted between the two PDMS channels. For the measurements performed on the confluent monolayer of hCMEC/D3 after 24 h flow, first the background streaming potential was registered under a 1 ml/min flow rate, then cells were treated with 1 mM lidocaine for 30 min at 37 ºC or with 1 U/ml neuraminidase in a serum-free medium for 1 h at 37ºC. After treatments, the streaming potential was measured again with the same electrodes and under the same conditions, and

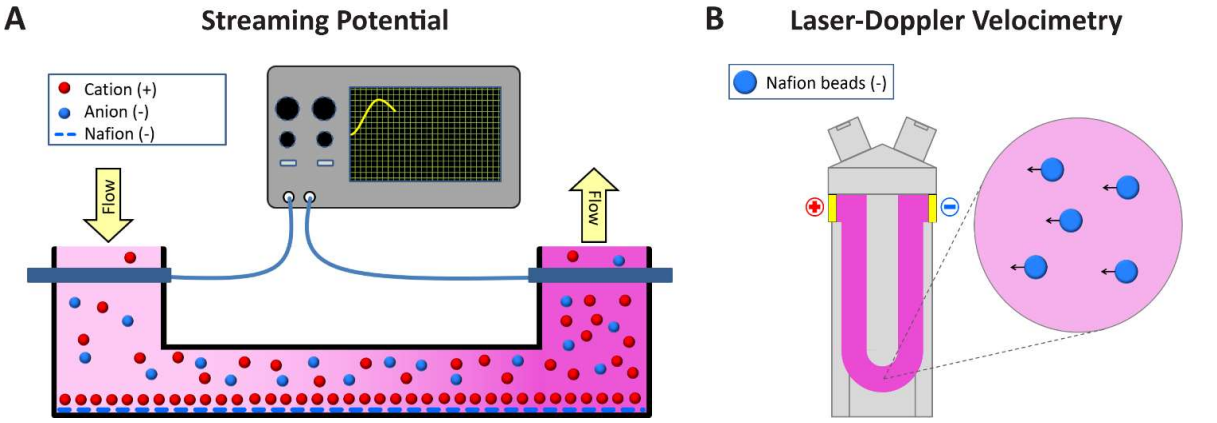

Figure 3 *Methods of zeta potential measurement. (A) Sreaming potential. The counterions of the solution have a higher local concentration close to the negatively charged surface due to the electric double layer. The ion concentration of the diffuse layer was constant (fix cations close to the surface) while the cations of the slipping plane move towards the outlet under flow conditions and temporarily accumulate in the larger vicinity of the electrode resulting in a potential difference compared to the reference (inlet) electrode. (B) Laser-Doppler velocimetry. Electric field was applied on a suspension of charged particles (e.g. the Nafion beads) in the capillary channel and the beads moved toward the direction of the field. The electrophoretic mobility was measured with the intensity shift between two collimated, monochromatic, and coherent Laser beams, thus the zeta potential of the particles could be calculated.*

changes were calculated. In case of cell monolayers in the control group, instead of any treatment, the medium was changed and incubated for 30 min or 1h at 37 ºC, before the streaming potential was measured.

Zeta potential measurements: Laser-Doppler velocimetry

LDv measures the electrophoretic mobility of charged particles with two collimated, monochromatic, and coherent laser light beams, forming a set of straight fringes by interference (53). The moving particles go through the fringes and reflect light to a photodetector. The frequency of the reflected light's intensity fluctuation is proportional to the Doppler shift between the scattered and incident light, and the velocity of the particles is proportional to the Doppler shift. Using the Smoluchowski equation, the zeta potential ζ can be calculated as follows:

$$\zeta = \frac{4\pi\mu\eta}{\varepsilon}$$

where μ is the electrophoretic mobility, η is the viscosity of the solvent and ε is the dielectric constant.

In the experiments, a Zetasizer Nano ZS instrument (Malvern, UK) was used. First, LDv was performed using Nafion beads as a simple model for ionic surface changes. Nafion belongs to a class of polymers with ionic properties whose unique characteristics result from the incorporation of perfluorovinyl ether groups terminated with sulfonate groups onto a tetrafluoroethylene strength (63). To alter the negative surface charge of the Nafion particles, cationic polyethylenimine (PEI) polymer with good attachment properties was used. Nafion beads were stored in a mixture of water and ethanol. To measure the LDv of the Nafion beads, they were

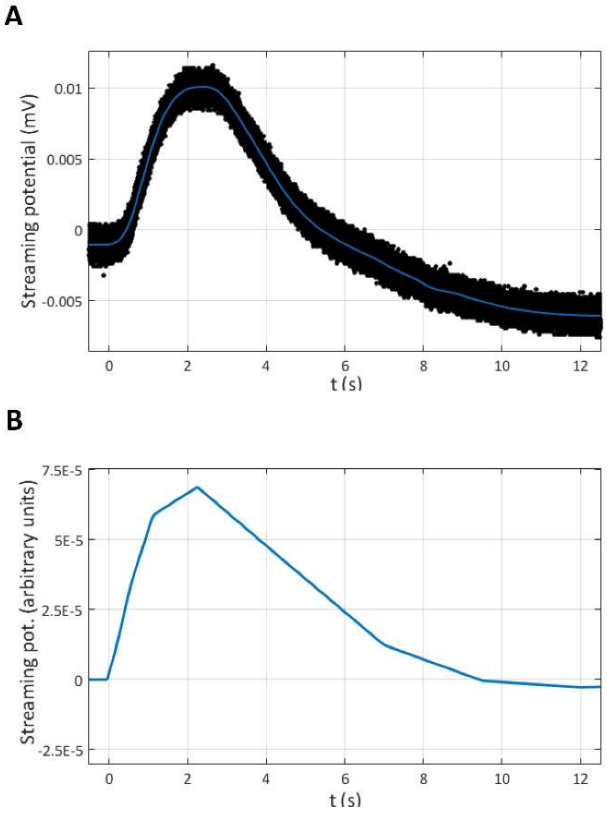

Figure 4 *Comparison of the registered streaming potential and the model simulations. In both cases the reference was on the low-pressure end, so the positive potential difference corresponds to negative zeta potential since it measured the concentration of the counterions. (A) The registered signal on Nafion membrane measured in the biochip. (B) The result of the simulation. The streaming potential is shown in arbitrary units because the geometry of the model was proportionally decreased as compared to the chip device. The dynamics of the transient streaming potential signal is identical.*

transferred into the same ionic solution used for measuring the surface charge of endothelial cells. First, 2 × 1 ml Nafion stock solution was spinned down with ultracentrifugation (T-1270 fixed angle titanium rotor, Sorvall WX+100 Ultracentrifuge, ThermoFisher Scientific, USA) at 45000 rpm for 30 min on 4 °C. The pellet in one of the vials was resuspended in 2 ml phosphate buffered saline (PBS) solution containing Ca^{2+} and Mg^{2+}, while the other vial was resuspended in 3 ml PEI. Both samples were sonicated for 60 min. The PEI-treated sample was ultacentrifuged once more with the same settings and was resuspended in 2 ml of PBS containing Ca^{2+} and Mg^{2+} and sonicated for 1 hour. This step was repeated once more to remove any PEI which was not attached to the Nafion beads. Samples were measured by Zetasizer Nano ZS using a disposable zeta potential cuvette with gold plated beryllium/copper electrodes (DST1070, Malvern, UK). Before measurements cuvettes were rinsed with 100 % ethanol for activation and washed twice with distilled water. Then zeta cuvettes were calibrated with zeta standard solution (Malvern, UK), as described by the manufacturer's protocol. Samples were measured at 25 ºC, with a minimum of 6 rounds (12 runs each), with an applied 40 V voltage (Figure 3B).

Zeta potential of hCMEC/D3 brain endothelial cells was measured similarly (51). Before the cells in Petri dishes reached full confluence, were trypsinized and 10^5 cells were re-suspended for treatment in the appropriate buffer. As described in our previous work, 1 mM lidocaine was added to the cell suspension and incubated at 37ºC for 30 minutes (51). For neuraminidase treatment, cells in suspension were incubated with 1 U/ml of neuraminidase in a serum-free medium for 1 h at 37 ºC, before measurement. The zetasizer software v.7.12. calculated the zeta potential using the Smoluchowski equation.

Simulations

Model calculations were carried out on a flow channel by the COMSOL Multiphysics work package (Comsol Inc., USA) run on a personal computer, to describe time- and zeta potential dependence of the transient streaming potential signal. To optimize simulation time and disencumber processor capacity, a rectangular channel of proportionally reduced size and simplified geometry was used in the simulations. The average flow velocity at the inlet (3.8×10^{-4} m/s) was adjusted to the reduced size, in order to be able to mimic the time course of the measured transient electric signal. The dimensions of the channel were 100 µm x 200 µm x 1200 µm. In the middle of this channel a 200 µm by 300 µm inner wall segment, representing the slipping plane, was carrying a surface charge density of 0.172 C/m^2. The electrolyte

comprised of a NaCl - water solution of 137 mM concentration, with ambient pressure and temperature values, to mimic typical measuring conditions. The simulations were carried out by solving coupled differential equations of the Electrostatics, Transport of diluted species and Creeping flow work packages, using the Poisson approximation (1-3) and the Nernst-Planck (4), and Navier-Stokes equations for the creeping flow of an incompressible fluid (5-6), respectively:

$$\nabla \cdot \boldsymbol{D} = \rho_V \quad (1)$$

$$-\boldsymbol{n} \cdot \boldsymbol{D} = \sigma_s \quad (2)$$

$$\boldsymbol{E} = -\nabla \mathrm{V} \quad (3)$$

$$\frac{\partial c_j}{\partial t} + \nabla \cdot \left(-D_j \nabla c_j - z_j u_{m,j} F c_j \nabla V\right) + \boldsymbol{u} \cdot \nabla \boldsymbol{c_j} = 0 \quad (4)$$

$$0 = \nabla \cdot [-p\boldsymbol{I} + \mu(\nabla \boldsymbol{u} + (\nabla \boldsymbol{u})^T)] + \boldsymbol{F} \quad (5)$$

$$\rho \nabla \cdot (\boldsymbol{u}) = 0 \quad (6)$$

Here $\boldsymbol{D}$ and $\boldsymbol{E}$ are the electric displacement and field strength, respectively, ρ_V and σ_S are the volume and surface charge densities, $\boldsymbol{n}$ is the normal vector of the surface, V is the electric potential, c_j is the concentration of the jth ion of z_j valency and $u_{m,j}$ mobility, F is the Faraday constant, $\boldsymbol{u}$ is the flow velocity, p is the pressure, $\boldsymbol{I}$ is the volumetric current flux, μ is the dynamic viscosity, $\boldsymbol{F}$ is the volumetric force, and $(\nabla \boldsymbol{u})^T$ is the shear stress term. The simulations were carried out in two steps: first, under no-flow conditions a stationary state was developed, while in the second step, a creeping flow was also introduced. The coupled differential equations were solved by the implicit method of Backward Differentiation Formula (BDF).

Statistics

Data of the standardization of BCv1 are presented as means ± SD. Statistical significance between treatment groups was determined using two-way ANOVA following Bonferroni multiple comparison posttest (GraphPad Prism 5.0; GraphPad Software, USA). Changes were considered statistically significant at $p < 0.05$ (a, compared to Transwell inserts and b, compared to static chip conditions). All experiments were repeated at least three times, the number of parallel samples was 3-5.

Data of the streaming potential measurements are presented as means ± SD. Statistical significance between groups was determined by one-way ANOVA with Bonferroni multiple

comparison test, by unpaired t-test or by paired t-test (GraphPad Prism 5.0, GraphPad software, USA). The number of parallel samples were minimum 3, and significance was considered at $p<0.05$. Experiments were repeated at least two times with multiple parallels.

Cell cultures

To test the versatility of the barrier chip, both epithelial and endothelial monolayers were cultured and monitored under static and flow conditions, as was appropriate. The transparent gold electrodes enabled a continuous visualization by phase contrast microscopy on the entire membrane surface, every day during the experiments. Visually confirmed leakage, holes on monolayers accompanied by low TEER resulted in the exclusion of the barrier chip from the experiments. Data were compared to measurements performed on Transwell cell culture inserts (Corning, USA). Cell cultures were grown in a humidified, 37 °C incubator with 5 % CO_2 in both experimental setups.

Epithelial cells

A human immortalized cell line, Caco-2 intestinal epithelial cells (ATCC, USA) were cultured under static conditions to model epithelial barrier on the chip. Vinblastine-selected Caco-2 cells (≤passage number 75; (17)) were cultured on rat tail collagen- (prepared in the laboratory with acetic acid extraction) coated Petri dishes in Dulbecco's modified Eagle medium (DMEM, Biochrom, Germany) supplemented with 10 % fetal bovine serum (FBS, Pan Biotech, Germany) and 50 µg/ml gentamicin. The porous membrane of the chip was coated with rat tail collagen overnight at 4°C. After cell cultures reached 80 % confluency in the dishes, Caco-2 cells (7×10^4 cells / chip) were subcultured to the chip using 0.05 % trypsin-EDTA solution (Pan Biotech, Germany). Confluent layers at maximal resistance were used for permeability measurements and immunolabeling (Figure 5A). Cells were also cultured on Transwell inserts for resistance and permeability data comparison (Figure 5B). Caco-2 cells were passaged to inserts at a cell number of 10^5 cells / insert (insert: 1.12 cm^2, 0.4 µm pore size, 10^8 pores / cm^2).

Endothelial cells

Brain microvascular endothelial cell line hCMEC/D3 (20) and primary rat brain endothelial cells (64-66) were used as models of the blood-brain barrier on the chip. Cultures of hCMEC/D3 cells (≤ passage number 35) were grown in MCDB 131 medium (Pan Biotech) supplemented with 5 % FBS, GlutaMAX (100 x, Life Technologies, USA), lipid supplement (100 x, Life Technologies, USA), 10 µg/ml ascorbic acid, 550 nM hydrocortisone, 100 µg/ml heparin, 1

ng/ml basic fibroblast growth factor (bFGF, Roche, USA), insulin (2.5 µg/ml), transferrin (2.5 µg/ml), sodium selenite (2.5 ng/ml) and 50 µg/ml gentamicin. hCMEC/D3 brain endothelial cells (6 x 10^4 cells / chip) were seeded to microdevices similarly to epithelial cells (Figure 5A). Static cultures were kept for 5 days before the permeability experiment. For flow studies cells were grown under static conditions until day 3, and left 48 h under dynamic conditions before permeability studies. After the first day in culture both models received 10 mM lithium chloride (Merck, USA) to induce barrier properties (20, 67, 68). D3 cells were also subcultured to Transwell inserts (1.12 cm^2, 0.4 µm pore size, 4 × 10^6 pores / cm^2) at a cell number of 4 x 10^4 cells / insert (Figure 5B).

Primary rat brain endothelial cells, pericytes and astroglia cells were isolated and cultured according to the method described in our previous studies (17, 64). To establish the triple culture model the upper compartment of the barrier chip was coated with rat tail collagen for endothelial cells and with collagen type IV. for pericytes and glial cells overnight at 4°C. Pericytes at passage number 3 (1.5 x 10^4 cells / chip) were seeded to the bottom side of the porous membrane according to the method of Nakagawa et al. (69, 70). Primary glial cells (10^5 cells / chip) were seeded to the bottom of the lower chamber directly to the coated glass surface. Primary rat brain endothelial cells (7 x 10^4 cells / chip) were passaged to the upper side of the coated membrane with endothelial culture medium: DMEM/F12 supplemented with plasma-derived bovine serum (15 %; First Link, UK), heparin (100 µg/ml), bFGF (1 ng/ml; Roche, Switzerland), insulin (5 µg/ml), transferrin (5 µg/ml), sodium selenite (5 ng/ml) and gentamycin (50 µg/ml). Static co-cultures were kept for 6 days before the permeability experiment. For flow measurements, cultures were grown under static conditions until day 4, and were kept for 48 h under dynamic conditions before permeability studies. After the second day in culture both models received 550 nM hydrocortisone. One day before the static permeability test or the beginning of flow experiments cells were treated with chlorophenylthio-adenosine-3',5'-cyclic monophosphate (250 µM, CPT-cAMP) and RO 201724 (17.5 µM, Roche) to tighten junctions and elevate resistance (2, 71). For comparison cells were also kept on Transwell inserts (1.12 cm^2, 0.4 µm pore size, 4 × 10^6 pores / cm^2). Triple primary co-culture BBB model was assessed as shown in Figure 5A and B and described previously (65, 69, 72).

Automation of cell feeding and the dynamic flow conditions

A syringe (20 ml plastic disposable syringe with luer cone, Braun) containing the culture medium was placed in a syringe pump (Legato 110, KDS products, USA) and connected to the device. The tubes (1 mm inner, 3 mm outer diameter, Carl Roth, Germany) were connected to the inlets/outlets via female luer-locks (Rotilabo, Carl Roth, Germany) to allow feeding during cell growth and constant medium-supply. During the cell growth phase, the syringe pump was

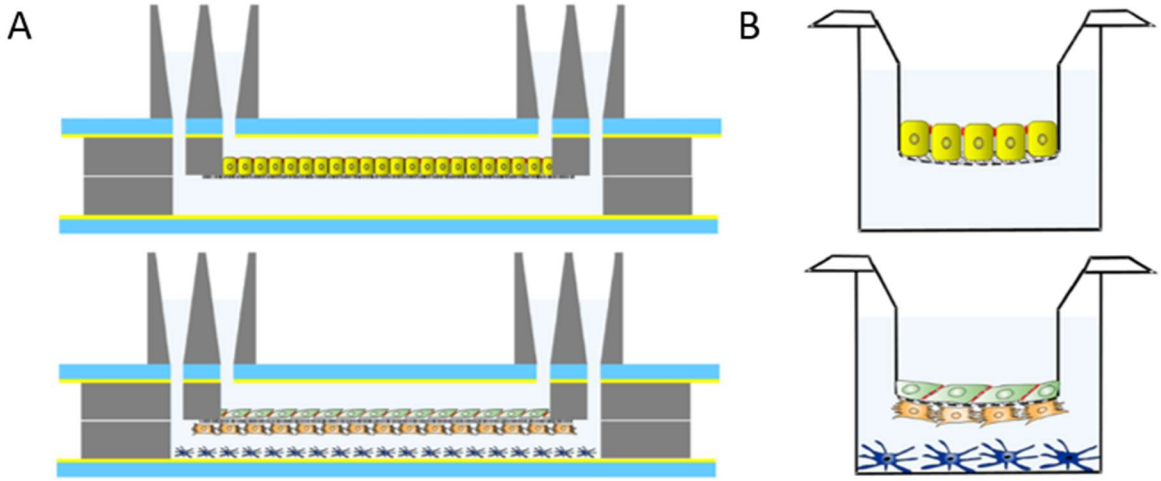

Figure 5 *Cell growth in the LOC device and culture inserts. (A) LOC setups with two types of cells. Epithelial cells (top, yellow cells) grow as monolayers on the porous membrane of the chip. Triple culture blood-brain barrier model using rat primary endothelial cells (green), pericytes (orange) and glial cells (blue) assembled in the biochip. (B) Transwell cell culture inserts with the same arrangements for epithelial or endothelial cell models as shown in the microchip.*

programed to change the medium above the cell monolayer (static condition) with 500 µl/min flow rate every 8 hours. The transparency of the gold electrodes let us monitor the growth of the cell monolayer by phase contrast microscopy on the entire surface, and TEER was measured every day. If the cell layer was not continuous as reflected in low TEER values and visually detected holes, the device was excluded from the experiments. After the cell layer reached 90% confluency, a constant stream of culture medium was introduced by a peristaltic pump (Masterflex, Cole-Parmer, USA) for 24 hours (1 ml/min, flow condition) before zeta measurement and/or permeability studies.

Cell culture treatments

Lidocaine (Sigma L7757) was dissolved in water at 30°C to prepare a 20 mM stock solution. Working solutions of 1 mM concentration were prepared freshly before each experiment in culture medium and added to the cells. Neuraminidase from *Clostridium perfringens* (Sigma N2876) was dissolved in Dulbecco's Modified Eagle's Medium (DMEM) and aliquots of a 10 U/ml stock were stored at -20ºC. A new neuraminidase stock vial was thawed before each

experiment. For the treatment, neuraminidase was applied at 0.1, 0.3 and 1 U/ml concentrations to the cells, based on a preliminary study and literature data.

Evaluation of barrier integrity

Cells in the LOC device received fresh medium every 8 hours automatically, and TEER measurement was performed each day to follow barrier formation. Under dynamic flow conditions, no medium change was required, because the cell culture medium was moved continuously by the peristaltic pump positioned after the chip in the circuit. Permeability measurements as layer integrity tests and immunohistochemical labeling for morphological characterization were performed at the end of all experiments. Cells on Transwell inserts received fresh culture medium every second day. TEER was also measured according to culture protocols. After reaching appropriate TEER values, permeability experiments were performed. These methods are accepted and widely used in the barrier field as integrity measurements and testing model applicability.

The flux of the hydrophilic tracers, sodium fluorescein (SF, MW: 376 Da) and fluorescein isothiocyanate-labeled dextran (FD, MW: 4.4 kDa) indicating paracellular permeability, was measured. Permeability of Evans blue-labeled albumin (EBA, MW: 67 kDa) was also tested across cell monolayers as previously described (65, 66). For the assay, cell culture medium was changed in the lower compartment of the chip to 500 µl Ringer-Hepes solution (118 mM NaCl, 4.8 mM KCl, 2.5 mM $CaCl_2$, 1.2 mM $MgSO_4$, 5.5 mM D-glucose, 10 mM Hepes, pH 7.4). In the upper compartment, the culture medium was replaced by 250 µl Ringer-Hepes solution containing either 10 µg/ml SF or 100 µg/ml FD and 165 µg/ml Evans blue bound to 1 % bovine serum albumin (BSA) simultaneously. At 20, 40 and 60 min of the permeability assay Ringer-Hepes solution in the lower compartment was changed to a fresh 500 µl buffer. Samples from the luminal and abluminal compartments were collected. Permeability measurements were also performed on Transwell inserts using 500 µl volumes with marker molecules for the upper and 1500 µl for the lower compartments (65, 66). During the experiments inserts were kept in 12-well plates (Corning, USA) and inserts were moved after 20, 40 and 60 min to the next well of the plate. Barrier chips and plates with inserts were incubated on a horizontal shaker in the CO_2 incubator (100 rpm; Biosan, Latvia) at 37 °C for 1 h. SF and FD concentrations were determined by the same instrument using 485 nm excitation and 520 nm emission wavelengths. EBA content of samples was measured at 584 nm excitation and 680 nm emission wavelengths

(Fluostar Optima, BMG Labtechnologies, Germany). Apparent permeability coefficient (P_{app}) was calculated as described previously (17).

Fluorescent immunostaining

Morphological characterization of epithelial and endothelial cell lines grown in the barrier chip was performed by immunohistochemical staining for ZO-1 and β-catenin tight and adherens junction associated cytoplasmic linker proteins. In the triple co-culture model, endothelial cells were stained for ZO-1 and β-catenin, pericytes for α-smooth muscle actin (α-SM) and astroglial cells for glial fibrillary acidic protein (GFAP). Before ZO-1 labeling, double cell nucleus staining with ethidium homodimer-1 and bis-benzimide was performed to reveal cell death. After the permeability tests, cells were fixed with cold acetone-methanol solution (1:1) for 10 min, washed with phosphate buffered saline (PBS), and non-specific binding sites were blocked with 3 % BSA-PBS for 1 h at room temperature. Incubation with rabbit-anti-ZO-1, rabbit anti-β-catenin, mouse anti-α-SM (Dako, USA) and mouse-anti-GFAP primary antibodies lasted overnight at 4 °C. Cells were incubated with anti-rabbit secondary antibody labeled with CY3 or anti-mouse secondary antibody labeled with Alexa Fluor 488 (Life Technologies, USA) and H33343 dye to stain nuclei for 1 h at room temperature. Between incubations, cells were washed three times with PBS. Chips were disassembled, cell culture membranes were removed from the chip, and were mounted in Fluoromount-G (Southern Biotech, USA), except for astroglia which were photographed *in situ* in PBS. Stainings were visualized by a Leica TCS SP5 confocal laser scanning microscope (Leica Microsystems, Germany).

Surface glycocalyx staining

Endothelial cells were cultured on rat tail collagen coated glass cover slips. After reaching confluence, cells were treated either with culture medium (control group) or with neuraminidase, as described in the Cell Culture Treatment section. After treatment, cells were fixed with 1% paraformaldehyde in PBS for 15 min at room temperature. To visualize the surface glycocalyx, fixed but unpermeabilized cells were incubated with wheat germ agglutinin (WGA) lectin conjugated with Alexa Fluor 488 (Invitrogen, W11261). WGA is specific for sialic acid and N-acetyl-D-glucosamine residues within the glycocalyx. The final concentration of WGA was 5 µg/ml in PBS and the incubation lasted for 10 min at room temperature (73). After thorough washing steps, preparations were mounted and pictures were taken with an Olympus FV1000 confocal microscope at different random positions. Minimum of 5 pictures were taken from each group at each experiment. The images were analyzed for staining intensity using the FIJI (ImageJ) software.

Results and discussion

Design and operation of the device

The basic structure of the barrier device mimics that of the culture inserts: top and bottom channels separated by a porous PET membrane (Figure 1A). The two parallel channels were made of PDMS. There are several setups have been built for similar purposes. Most of them consist of two channels, either parallel (31) or perpendicular to each other (39, 43), with a relatively small overlapping area. The arrangement of our channels enables a much larger overlapping area (ca. 1 cm^2), allowing a larger surface and a bigger sampling size for *in vitro* permeability studies. The main difference between the BCv1 and BCv2 is the smaller hight of the top channel (2 mm and 1 mm, respectively). The reason of the decreased channel hight is that we wanted higher shear stress in the latter.

The thin, transparent electrodes grant a special advantage to the chip, permitting a continuous visual monitoring of the cells by a microscope, above the entire membrane surface, during the full time span of the experiment. Such a feature is missing in other model systems using nontransparent electrodes that allow visual observation limited to the narrow slits between the electrodes (10, 43), therefore a full microscopic screening of the sample can only be done on the disassembled chip. This is a critical point for such assays that include monitoring of TEER or paracellular permeability of the barrier membrane, since local faults in the confluence of the cell layer, occurring usually at its perimeter and invisible for other methods, might seriously tamper the results.

We tested transparent ITO electrodes as possible candidates, and measured their resistance. Figure 2A shows the impedance spectra of chips equipped either with a pair of transparent gold electrodes or ITO electrodes placed at the outer walls of the top and bottom channel, and separated by the porous membrane. In the low-frequency regime (between 1Hz and 1kHz) the electric double layer formed upon electrode polarization hinders the correct measurement of the ohmic resistance of the chip, while in the high-frequency regime (above 3 MHz), the reduced values of ionic mobilities limit conductivity. In between the two extremes, the sample resistance is nearly constant, but its value is an order of magnitude smaller with gold electrodes than with the ITO ones. This was the primary reason for which we used gold electrodes instead of ITO. Proper electrode patterning with ITO glass was not feasible with our laboratory

technique, therefore the standard four-electrode method, eliminating the effect of electrode polarization on TEER, could not be applied.

On the other hand, low-resistance “non-polarizable” electrodes (platinized platinum or Ag/AgCl) proved not to be transparent enough (extinction coefficient > 1), hampering visual observation. The choice of a 25-nm inert, gold layer for TEER electrodes was found to be the best compromise between the opposing requirements of conductance and transparency (10 Ohms, extinction coefficient 0.4, Figure 2A and B). Possible artifacts of the resistance measurements due to polarization of the gold electrodes were avoided by the four-electrode method. Rectangular pulses (12.5 Hz) were applied on the sample and kept controlled by a pair of electrodes, while another electrode pair was supplying load current via a feedback loop, to keep the transmembrane voltage constant during each half-period. The electric resistance of the system was found to be characteristic to the cell culture layer.

The plastic tubes and the zeta electrodes were connected to the device via luer lock inlets. The Ag/AgCl zeta electrodes were inserted in luer connectors, so they could be mounted easily (Figure 1C). A programmable syringe pump fed the cells during the growth period (3 days) every 8 hours, while the TEER values were recorded and the monolayer was monitored with a phase contrast microscope, each day. Automatic feeding decreased the chances of contamination, too. The devices were connected in line (3 to 6 at one experiment), thus the flow rate and shear stress were the exact same in all cultures. After cell monolayers reached about 90% confluency, a peristaltic pump was introduced for constant flow, to mimic the shear stress of the blood stream for 1 day. The flow rate was 500 µl/min during feeding, 1 ml/min during the constant flow and the shear stress values were 0.1 and 0.4 for BCv1 and BCv2, respectively. Under dynamic flow conditions, the input tube was immersed in the cell culture medium in the reservoir, and was connected to the inlet of the chip, while the output tube was connected to the reservoir via the peristaltic pump. This arrangement has three advantages: (i) the liquid pressure is always less than the air pressure outside, therefore there was no simmering or jamming failure (no „explosion”), (ii) the reservoir also acts as a bubble trap, since all bubbles (eg. from leakages) burst as the liquid is dripping out from the output tube, and none of them can reach the input of the chip at the bottom of the reservoir, (iii) since the reservoir of the circulated medium is located after the pump, it is not pressurized, and the medium inside can be promptly and continuously sampled or treated very easily. That could be very useful for both long- and short-term tests of various drugs influencing the permeability of the barrier layer.

The streaming potential was measured with the Ag/AgCl electrodes (Figure 1C) between the inlet and outlet sides of the top channel (Figure 3A). For the recording, the flow was periodically stopped and restarted after equilibration of the ions close to the surface of the cell monolayer. Please note that contrary to the usual streaming potential measurements working with moderate flow rates, we do not operate our device under stationary conditions where the forward streaming current and the backward conductive current keep an equilibrium, but rather measure transient signals (Figure 4A) by applying a strong input flow, in order to increase the signal-to-noise ratio. Although, this case is beyond the scope of the Helmholtz-Smoluchowsky equation establishing a linear relationship between the zeta and steady-state streaming potentials, here we present experimental and theoretical evidence for the proportionality of the zeta potential and the amplitude of the transient streaming potential in our approach, as well.

On the whole, the device enables several ways to study the barrier layer simultaneously: electric conductivity and streaming potetential measurement, molecule permeability and microscopic visualization of the (co-)cultured cells. In addition, morphological characterization of the layers is also possible by immunohistochemical staining.

The streaming potential feature

Experimental validation of the method

In this work, the streaming potential was measured in BCv2 either on a test membrane or on cell monolayers, in the form of a transient potential difference evolving between the inlet and outlet electrodes, due to migration of ions from the vicinity of the negatively charged surface of the channel under flow conditions (Figure 3A). The negative charge derives from the overwhelming anionic groups on the surface of the confluent cell monolayer due to the lipid headgroups (30) and the surface glycocalyx in the BBB experiments (49), or from the sulfate groups of the Nafion membrane in the control measurements. The electric double layer close to a charged surface has a different ion concentration compared to the solution. If flow is applied to the system, the mobile part of the GCL containing an excess number of positive counterions move towards the outlet electrode, and temporarily increase the positive charge density in the larger volume of the socket of the electrode, giving rise to an increase in electric potential, as compared to the reference electrode (Figure 4A). As we show by both model calculations (Figure 4B) and control experiments using the LDv method, the amplitude of this transient streaming potential signal is proportional to the zeta potential of the membrane surface.

A highly negatively charged Teflon derivative, the sulfonated tetrafluoroethylene-based fluoropolymer-copolymer called Nafion was selected to perform the proof-of-concept experiments by the streaming potential electrodes incorporated in the chip. Since Nafion is available both in 183-µm thick membrane sheets and in liquid suspension, it is suitable for both the transient streaming potential measurements and for LDv (Figure 6A and B), where the latter can serve as a control for calibration.

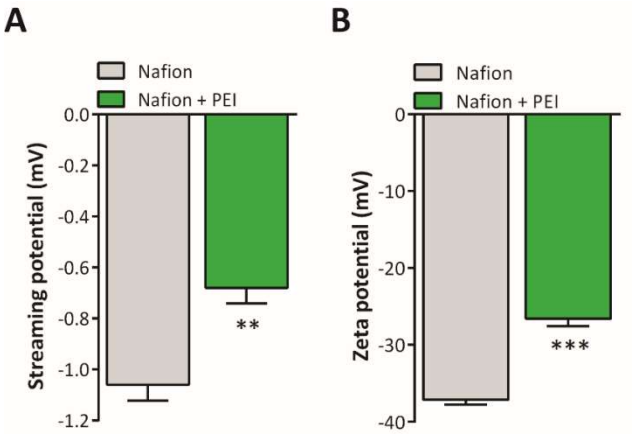

Figure 6 *Measurement of the surface charge of Nafion by streaming potential and by laser-Doppler velocimetry (LDv) methods. (A) Nafion film replaced the culture membrane in the biochip. It was treated with polyethyleneimine and the streaming potential was measured before and after the treatment. Values are presented as means ± SD, n=4. Data was analysed by unpaired t- test. **, p<0.01, compared to control. (B) Nafion beads were treated with PEI, and the samples were measured with LDv before and after the treatment. Values are presented as means ± SD, n=5. Data was analysed by unpaired t-test. ***, p<0.001, compared to control groups.*

For the streaming potential study, the PET membrane of the chip was replaced by a Nafion membrane, and the adjacent microfluidic channels were filled up by PBS, in order to mimic the ionic conditions of the incubating solution of endothelial cells, most frequently used in our earlier BBB chip experiments. Following the application of an inflow on the upper microfluidic channel of the device (Figure 3A), a well-measurable transient electric potential change could be recorded under 1 ml/min flow rate, using a voltage preamplifier and an oscilloscope (Figure 4A). The sign of the transient signal corresponded to a displacement of positive charges in the direction of the flow, indicating an overall negative zeta potential of the surface of the channel. After a 1-minute post-measurement incubation time without flow, the signal could be quantitatively reproduced. As a single-parameter descriptor of the transient signal, we chose its amplitude for comparison with the results of subsequent measurements. Note that here the convention of the sign was the opposite compared to the traditional streaming potential measurements (74), as the reference electrode was on the low-pressure end of the channel. Hence, the sign of the measured signal was the opposite of that of the zeta potential since the amplitude was proportional to the concentration of the counterions. According to the convention, the amplitude of the streaming potential of the untreated Nafion membrane was found to be -1.06 ± 0.0625 mV (Figure 6A).

To change the surface charge density, the Nafion membrane, was treated for 30 min with PEI, known to be able to attach via highly positively charged ethyleneimine residues to the surface.

Its access quantity was subsequently washed away with PBS, and the streaming potential was measured again. The result showed a pronounced decrease of the absolute value of the amplitude to -0.68 ± 0.061 mV (Figure 6A). Control measurements without Nafion membrane showed negligible streaming potential signal, indicating that the zeta potential of the PDMS channel walls was insignificant, as compared to the highly negatively charged Nafion membranes (17).

In order to calibrate the results gained by the transient streaming potential method with well-established techniques, LDv was applied to measure the zeta potential of Nafion beads prepared of identical material characteristics to those of the membrane. The Nafion stock solution (pH=1.5) had a -76.2 ± 2.08 mV zeta potential measured with Malvern Zetasizer nano ZS. Then the stock was centrifuged and resuspended in PBS (pH=7.2), therefore the Nafion beads had the same ionic conditions as in the streaming potential experiments, and had a zeta potential of -37.13 ± 0.63 mV. Another batch of beads was then treated with PEI, and subsequently re-centrifuged and resuspended in PBS. The PEI-treated beads showed a similar ratio of increase in zeta potential up to -26.58 ± 0.94 mV (Figure 6B), as it was observed for the streaming potentials of analogously treated Nafion membranes (Figure 6B).

Based on the fact that the ratios of the zeta and streaming potentials of the native and PEI-treated Nafion surfaces were the same within the experimental error, a proportionality between the data measured by the two different methods was suggested. Below, we present both theoretical and further experimental evidences supporting this finding.

Simulations

In order to give a theoretical background for the measured transient streaming potential signals, we carried out model calculations on a flow channel by the COMSOL Multiphysics work package. The dynamics of the system was modelled in two steps: 1) to establish stationary conditions without flow, first the system was let to equilibrate according to the Poisson-Botzmann-Nernst-Planck approximation, assuming electro-neutrality of the channel-fluid system; 2) in the second step, a creeping flow with an average velocity of $3.8 \cdot 10^{-4}$ m/s was applied to the inlet of the channel, and the electric potential was measured on two probe planes placed in front of and behind the charged surface, along the long axis of the channel. A typical voltage signal received by subtracting the two potentials is shown in Figure 4B, faithfully reflecting the time-evolution of the measured signal (Figure 4A). In order to establish the connection between the simulated signal amplitudes and the zeta potential, the latter was swept two orders of magnitude, and the simulated time-evolution of the streaming potential functions was recorded (Figure 7). Figure 8B shows the dependence of the amplitudes of these curves as

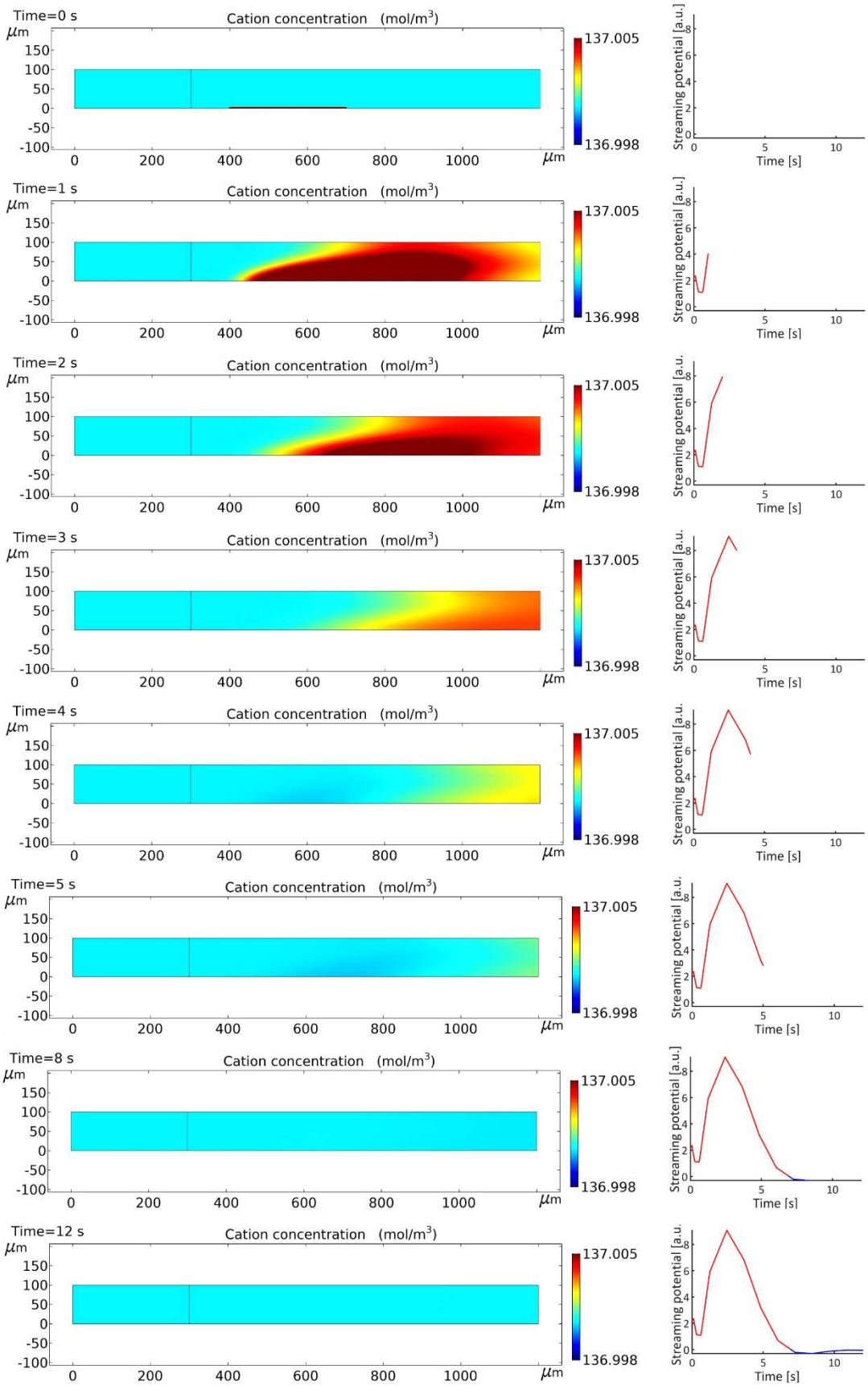

Figure 7 *Simulated movement of the counterion cloud under creeping flow, and the time evolution of potential difference between the measuring and reference electrodes. Note that the vertical line at 300 μm represents the reference electrode.*

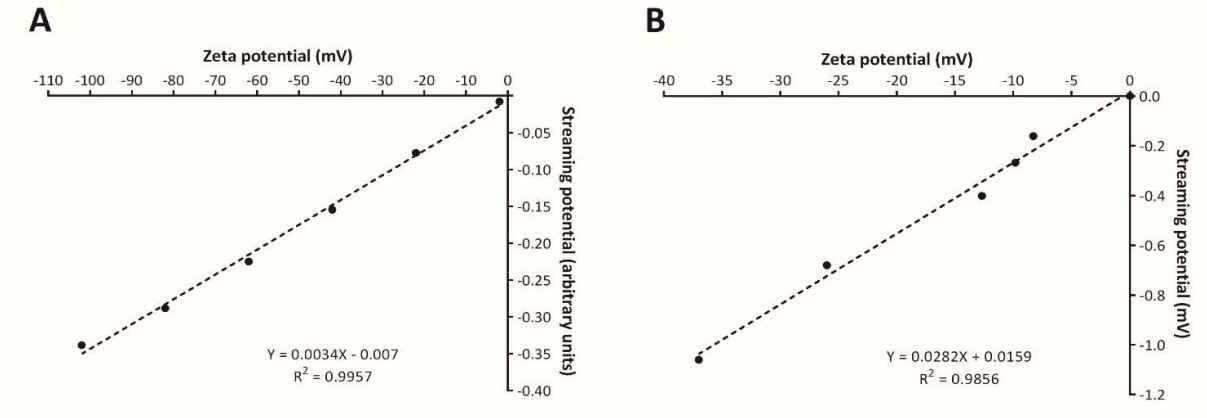

Figure 8 *Correlation between streaming potential and laser-Doppler velocimetry data. (A) Correlation in the simulation. The zeta potential was set in the channel as a charged section of the wall and the corresponding streaming potential was calculated by the simulation. (B)The streaming potential and laser-Doppler velocimetry data measured on Nafion or the confluent brain endothelial cell layers were plotted and fitted with linear regression. The two goodness-of-fits are R^2=0.996 and R^2=0.986 respectively, which shows a clear linear relationship between the zeta and streaming potential.*

a function of the zeta potential, showing a clear linear relationship, in full concert with the experiments (see the previous section, and Figure 8A).

The above experimental and model calculation results proved that the concept of upgrading our chip device by a streaming potential unit, to detect the zeta potential of the membrane insert and monitor its changes, is feasible. Nevertheless, it remained an important question whether the method is appropriate (i.e. sensitive enough) to characterize changes in the surface charge properties of cellular monolayers, such as those in biological barriers. We address this problem via the experimental investigation of the hCMEC/D3 BBB model system in later sections.

Cell cultures

In order to illustrate the main features of our LOC device, it was used to model three different biological barriers with cell cultures: human intestinal epithelial and brain endothelial cell lines as well as a triple primary co-culture BBB model were tested for barrier function in the chip.

Barrier integrity of cell monolayers in the LOC device

The two major passive permeability routes of biological barriers, including the BBB, are the transcellular and the paracellular or junctional pathways. The tightness of the paracellular pathway, restricted by tight intercellular junctions, can be tested with hydrophilic molecules (2, 23, 75, 76). Electrical impedance measurement at low frequency (called as TEER) is the most sensitive method to characterize the paracellular barrier integrity for ions (2, 76).

Intestinal model

The Caco-2 intestinal epithelial cell line formed the tightest monolayer among the 3 models in the microdevice, with a TEER value of 578.3 ± 29.6 Ω cm^2 (Figure 9). The tightness of the barrier was also indicated by the low P_{app} for all markers (SF: 0.55 × 10^{-6} cm/s; FD: 0.36 × 10^{-6} cm/s; EBA: 0.10 × 10^{-6} cm/s). Cells had a cuboidal shape, grew in monolayers and stained well for ZO-1 and β-catenin. Cell morphology, good resistance and permeability properties of Caco-2 cells in the new device were similar to data obtained on Transwell culture inserts after 10 days of culturing. On culture inserts, TEER of Caco-2 monolayers reached 546.5 ± 33.9 Ω cm^2. There was a significant difference in the measured permeability for SF (0.30 × 10^{-6} cm/s) compared to the biochip, but permeability for EBA (0.03 × 10^{-6} cm/s) shows no difference between the insert and the chip setup. There was a higher standard deviation for TEER in biochips during the growing phase. Since it was not possible to use the same membrane type as for Transwell inserts, there could be a difference in the kinetics of cell growth due to the different culture membranes, but after cells reach confluency and begin to form the barrier, TEER values become more uniform between the parallels, and reflect good barrier properties. Higher Lucifer yellow permeability has been described for the same cell type cultured in a microfluidic chamber, but that system did not allow measurement of TEER (31). Note that Caco-2 cells in a gut-on-a-chip model have reached tighter barrier properties when co-cultured with bacteria and/or immune cells, and exposed to low shear stress and cyclic strain to mimic peristaltic motion (13, 33).

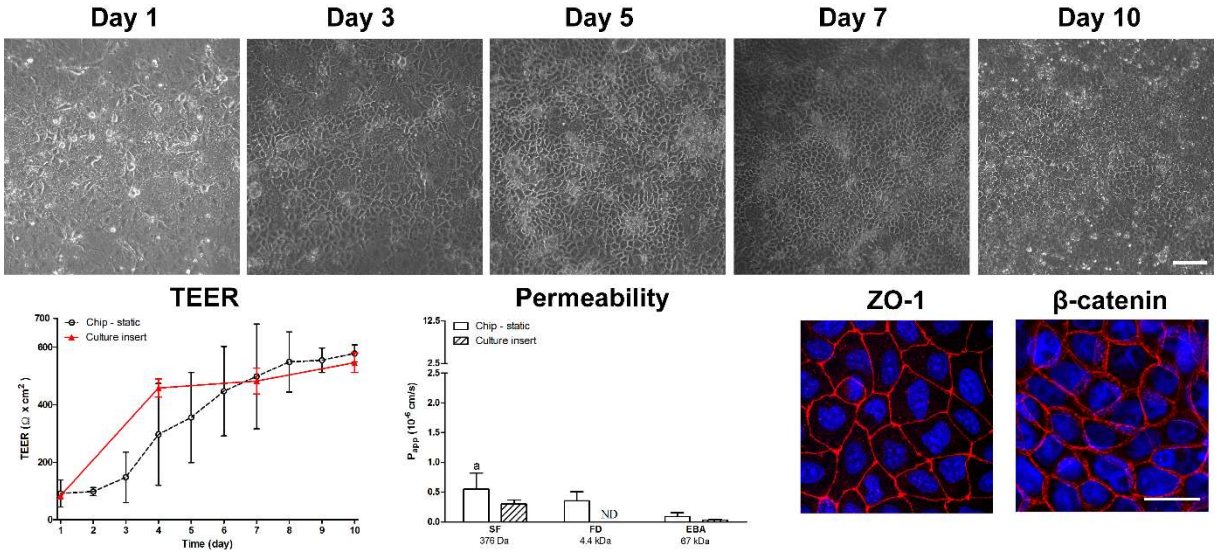

Figure 9 *Characterization of the intestinal barrier model on the chip. Phase contrast microscopy images of Caco-2 cells grown in the biochip on culture days 1-10, electrical resistance and permeability measurement data (day 10) are presented. Resistance and permeability values for cell culture inserts are also indicated. Cell morphology was characterized by ZO-1 and β-catenin immunostaining in the device and visualized by confocal microscopy. Bar = 100 µm (phase contrast images), bar = 25 µm (confocal images), ND: no data available.*

Blood-brain barrier models

Brain endothelial cell line model

The human hCMEC/D3 brain endothelial cell line is a well-characterized, simplified *in vitro* model of the BBB (21). Still, a comprehensive study on a human brain endothelial cell line in a microdevice, with a complex characterization of barrier properties including microscopy, has so far been missing. Previously, the rat cell line RBE4 was studied for a similar purpose (11, 40). Biochips modeling the vascular system also widely use peripheral endothelial cells (77-80).

In our miniaturized model, D3 cells grew to confluency (Figure 10). After 3 days of static followed by 2 days of dynamic culture conditions, TEER values increased to 28.5 ± 7.2 Ω cm^2. TEER values of the 5-day-old static culture were in the range of 19.0 ± 2.8 Ω cm^2. The resistance values measured by the device were in concert with the ones obtained on culture inserts by our group (23.7 ± 3.5 Ω cm^2), and with those described in the literature (21, 39). Permeability data were also compared between the static and dynamic cultures. On the static hCMEC/D3 barrier chip model, the permeability was 1.61 × 10^{-6} cm/s for SF, 1.55 × 10^{-6} cm/s for FD and 0.51 × 10^{-6} cm/s for EBA. Under dynamic culture conditions P_{app} of 1.57×10^{-6} cm/s for SF, 1.32 × 10^{-6} cm/s for FD and 0.15 × 10^{-6} cm/s for EBA was measured. In dynamic

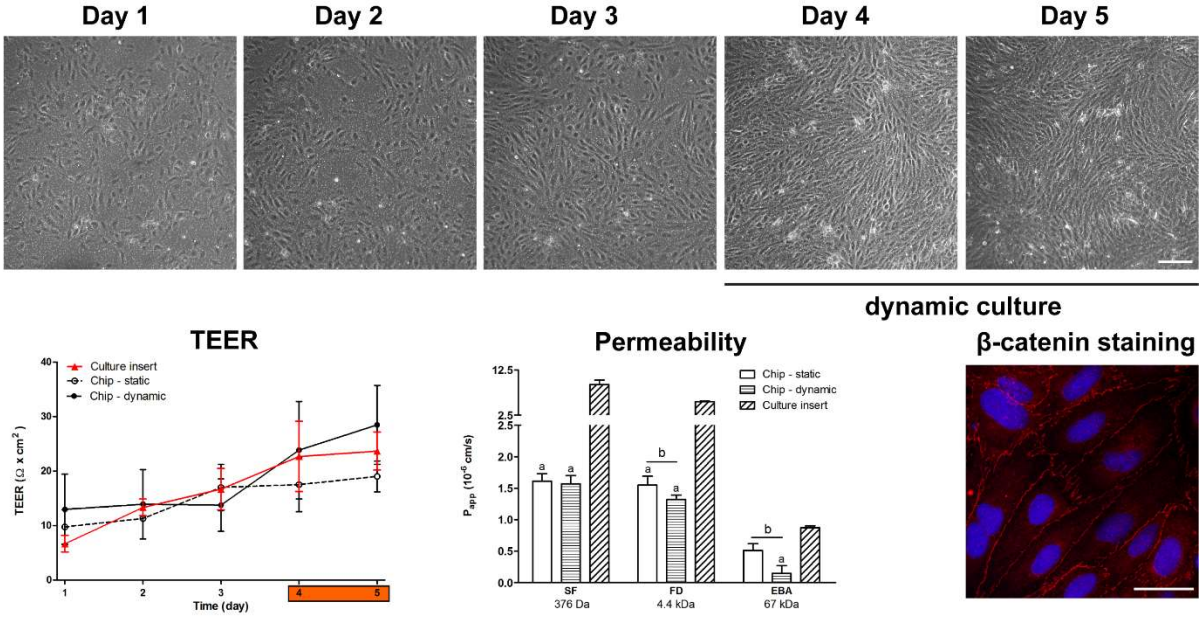

Figure 10 *Characterization of a simplified blood-brain barrier model on the chip. Phase contrast microscopy images of hCMEC/D3 human brain endothelial cells grown in the biochip on culture days 1-5, electrical resistance and permeability measurement data (day 5) are presented. Brain endothelial cells were kept under static conditions for 3 days followed by 2 days of flow (0.15 dyn) in the dynamic setup. Resistance and permeability values for cell culture inserts are also indicated. Cell morphology was characterized by ZO-1 and β-catenin immunostaining in the device and visualized by confocal microscopy. Statistically significant differences p<0.05 (a, compared to culture inserts; b, compared to static chip cultures) are indicated. Bar = 100 µm (phase contrast images), bar = 25 µm (confocal images).*

cultures, brain endothelial permeability for FD and EBA markers was significantly lower compared to the static model in the same device. Permeability data obtained on Transwell inserts (9.31×10^{-6} cm/s for SF, 5.47×10^{-6} cm/s for FD and 0.87×10^{-6} cm/s for EBA) are in good correlation with the literature (20), but those measured in the biochip were found to be significantly lower for all marker molecules. Since we could not use the exactly same membrane type in both the Transwell and chip models (Figure 10), the effect of membrane thickness on permeability coefficients cannot be excluded. In the present study we could not reproduce the intensive increase of resistance after exposing hCMEC/D3 to shear stress (38, 39), but we could observe a significantly reduced tracer permeability for larger marker molecules, indicating a barrier-tightening effect. Cells in both dynamic and static cultures were elongated, formed close contacts typical for endothelial monolayers, and stained well for ZO-1 and β-catenin.

Primary cell based co-culture model of the BBB

Our primary-cell-based triple co-culture BBB model (69) was characterized for the first time in a miniaturized flow chip device. Co-culturing with glial cells and pericytes on Transwell inserts in the anatomical position (Figure 5) have proved to be the most efficient in the induction of barrier properties in brain endothelial cells; better than double cultures using only brain endothelial cell and glial cell or brain endothelial cell and pericyte combination as described previously by our group (69). In this model, brain endothelial cells are not directly contacting pericytes or glial cells (Figure 2). In the Transwell inserts a membrane with 0.4 μm pore size, 12 μm thickness is used. A membrane with a same pore size was used in the chip, which does not allow cell migration. Growth factors and other barrier property inducing molecules are secreted into the common cell culture medium enabling communication between the three cell types through the porous culture membrane.

Cell growth in the triple BBB model was followed by phase contrast microscopy. Immunolabeling showed a typical cell shape for all three kinds of cells (Figure 11). Endothelial cells had an elongated shape, and formed tight intercellular connections. Pericytes and glial cells were also stained by their cellular marker proteins, α-SM actin and GFAP. The rat primary triple co-culture BBB model on the chip formed a barrier with a TEER value of 114.2 ± 35.7 Ω cm^2. TEER values measured under static and dynamic conditions were not significantly different. These values are lower than data obtained on culture inserts (173.3 ± 21.6 Ω cm^2). Compared to the results of our previous papers the TEER of the present triple model on

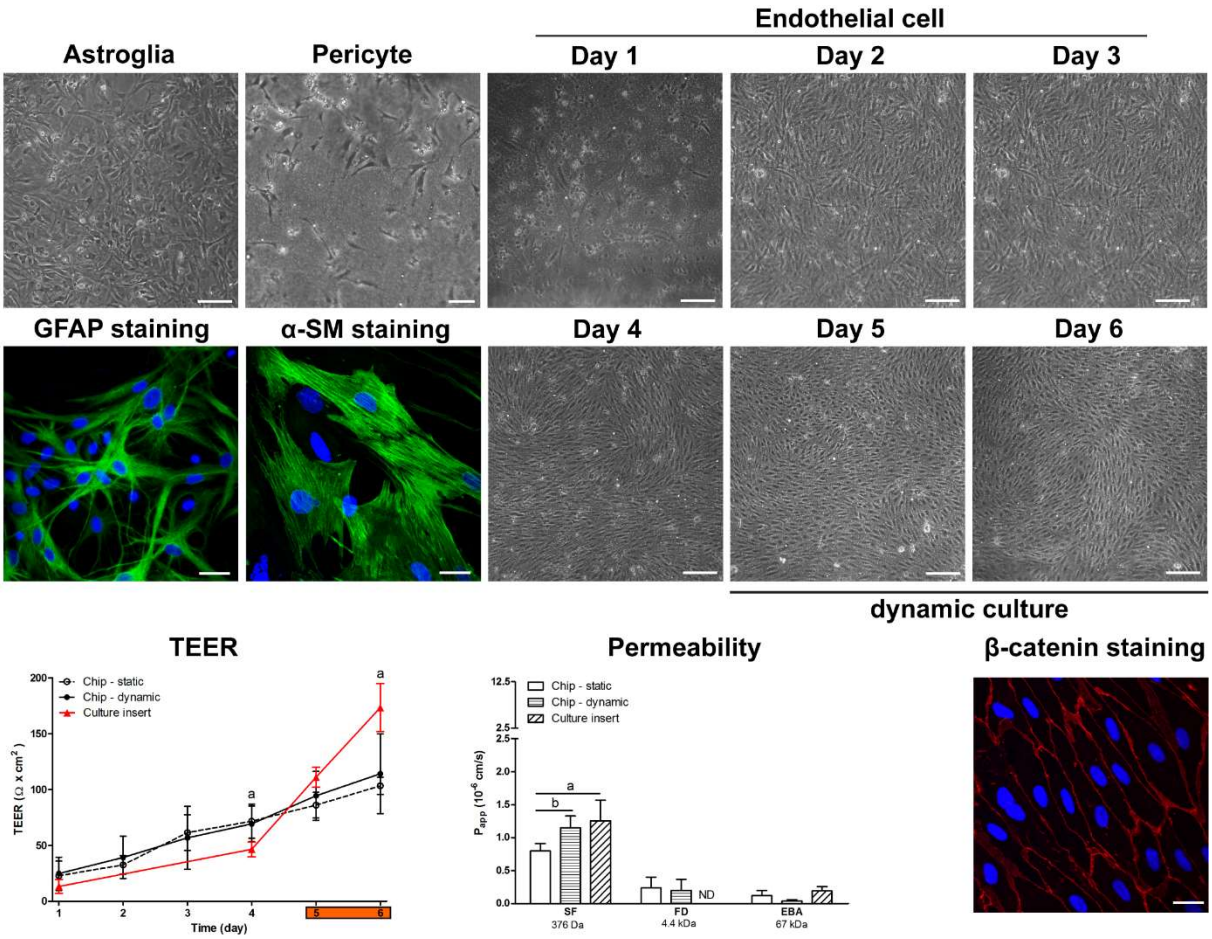

Figure 11 *Characterization of a triple co-culture blood-brain barrier model on the chip. Phase contrast microscopy images of primary rat brain endothelial cells (culture days 1-6), primary rat pericytes and glial cells (day 1), electrical resistance and permeability measurement data (day 6) are presented. Primary endothelial cells in co-culture were kept under static conditions for 3 days followed by 2 days of flow (0.15 dyn) in the dynamic setup. Cell morphology was characterized by ZO-1 and β-catenin (endothelial cells), α-smooth muscle actin (pericyte) and glial fibrillary acidic protein (astroglia) immunostaining in the device and visualized by confocal microscopy. Statistically significant difference $p<0.05$ (a, compared to culture inserts; b, compared to static chip cultures) is indicated. Bar = 100 µm (phase contrast images), bar = 25 µm (confocal images), ND: no data available.*

Transwell inserts was lower (173 vs. 350 Ω × cm^2; (69)), but the permeability coefficient for fluorescein was better, 0.8×10^{-6} cm/s vs. 4×10^{-6} cm/s indicating a good barrier. In static conditions permeability values were 0.80×10^{-6} cm/s for SF, 0.24×10^{-6} cm/s for FD and 0.12×10^{-6} cm/s for EBA on the BBB model. These permeability coefficient values are similar to data of previously described BBB models on Transwell inserts (17) and indicate a tight barrier. Dynamic cultures were kept under flow conditions for 48 h, then permeability measurements were performed. P_{app} values for the dynamic model were 1.15×10^{-6} cm/s for SF, 0.20×10^{-6} cm/s for FD and 0.04×10^{-6} cm/s for EBA. An elevated flux of SF across the monolayer was found after introducing low shear stress on the triple model. The permeability

for SF on the triple BBB model grown on cell culture inserts was higher compared to the static biochip model (1.25×10^{-6} cm/s for SF and 0.19×10^{-6} cm/s for EBA). There was no difference in the flux of the other two permeability markers after flow conditions, neither in the static chip compared to the dynamic model, nor in the chip models compared to the Transwell inserts. In our setup, the low-shear-stress exposure did not elevate the resistance of primary endothelial cells. All these data indicate that under low flow conditions, barrier properties typical for venules may develop in a BBB model (12). The different biological response in a brain endothelial cell line as compared to primary cells emphasizes the difference between such models (38).

Effects of surface charge modifications and measurement of streaming potential on the brain endothelial cell line model hCMEC/D3

There is an increasing number of direct and indirect evidence that simple physical parameters such as surface charge density or the related zeta potential might control physiological functions of barrier properties (30, 51). The main sources of the, usually negative, surface charge densities of cells are the lipid head groups of the plasma membrane, and the so-called glycocalyx, composed of highly negatively charged polysaccharide chains at the surface of the cells (Figure 12A). Glycocalyx forms a continuous coat on the luminal surface and plays important roles as both a mechanosensor (73) and as a physical barrier for nanoparticle permeability (50). The negative surface charge derived from the lipid head groups of the BBB regulates both drug delivery to the brain (48) and drug interaction at the level of brain endothelial cells (51). Therefore, the surface charge density of brain endothelial cells can be modified by both enzymatic digestion of the glycocalyx or cationic lipophilic molecules which are inserted to the plasma membrane (Figure 12A). To determine changes in the surface charge of individual cells, LDv measurements are used (30, 51).

In this study we measured the streaming potential on confluent monolayers of hCMEC/D3 barrier cells cultured in the LOC device for the first time. We used two clinically relevant surface charge modulators (Figure 12A). The antiarrhythmic intravenous drug, lidocaine incorporates into the plasma membrane of vascular endothelial cells and as it was demonstrated in a recent study it changes the zeta potential of brain endothelial cells (51). Neuraminidase, a glycoside-hydrolase enzyme, cleaves sialic acids and reduces the amount of negative charge on the glycocalyx, thus mimics glycocalyx shedding observed in sepsis. The efficiency of cleavage of sialic acid residues from the glycocalyx by neuraminidase was determined by the sialic acid-

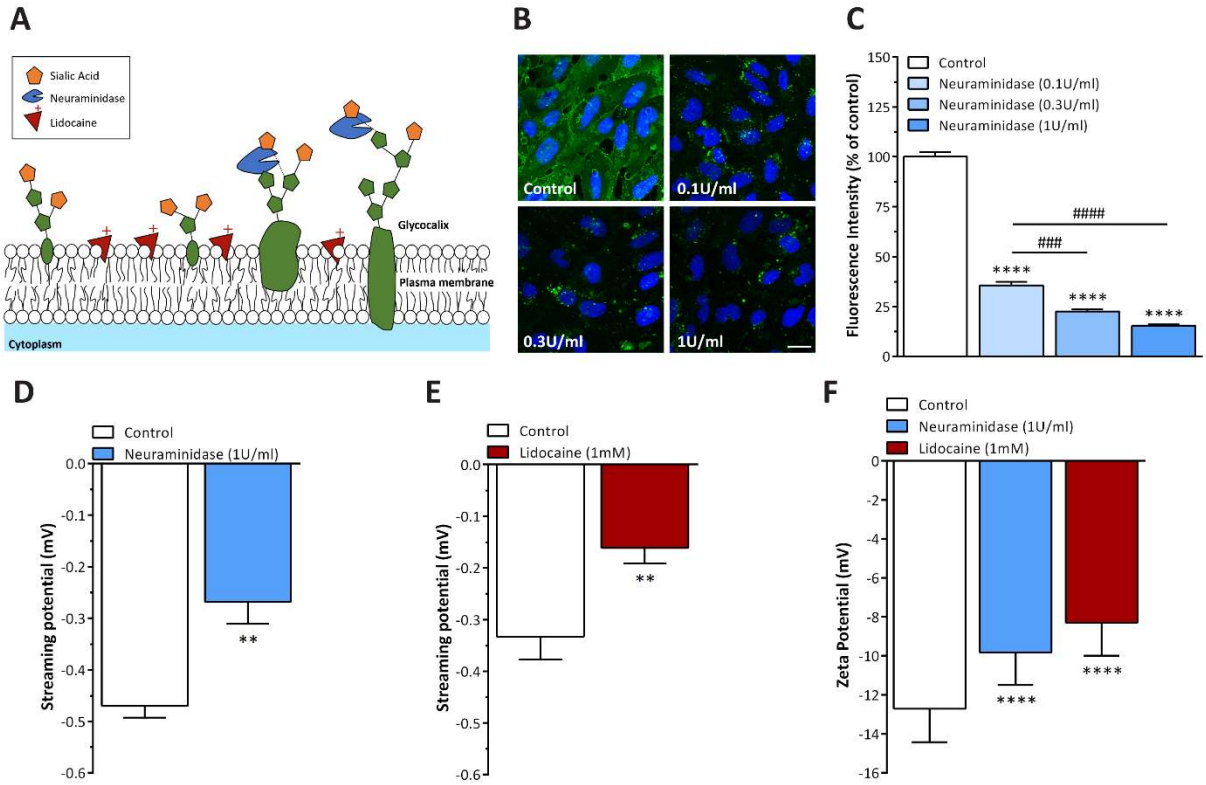

Figure 12 *Measurement of surface charge and its modification on brain endothelial cells by streaming potential in the chip device and by laser-Doppler velocimetry (LDv). (A) The two strategies to modify the zeta potential were the cleavage of the glycocalyx or the insertion of positively charged molecules in the membrane. Neuraminidase enzyme cleaves the sialic acids of the polysaccharide sidechains, thus decreases the amount of negative charges on the cell surface. Lidocaine incorporates into the cell membrane and makes it more positive. (B) Representative pictures of the staining with wheat germ agglutinin (WGA) lectin labeled with Alexa 488, with or without treatments with different concentrations of neuraminidase, bar: 20µm. (C) Image analysis of the fluorescent intensity of the lectin labeling on pictures taken by confocal microscopy. Values are presented as means ± SD, n=30-66. Data was analysed by one-way ANOVA with Bonferroni post-test. ****, #### p<0.0001, ### p<0.001. (D, E) Streaming potential values measured in the chip device. Values are presented as means ± SD, n=4. Data was analysed by unpaired t-test. **, p<0.01, compared to control. (F) Zeta potential results obtained with LDv method. Values are presented as means ± SD, n=12-60. Data was analysed by one-way ANOVA with Bonferroni post-test. ****, p<0.0001, compared to control.*

specific lectin WGA-Alexa 488 staining, followed by confocal microscopy and image analysis for staining intensity Cleavage of glycocalyx elements turns cellular surface charge more positive, although this change has not been measured directly on brain endothelial cells yet. The efficiency of cleavage of sialic acid residues from the glycocalyx by neuraminidase was determined by the sialic acid-specific lectin WGA-Alexa 488 staining, followed by confocal microscopy and image analysis for staining intensity (Figure 12B-C). A concentration-dependent effect of the enzyme on lectin staining was obtained: neuraminidase treatment at 1U/ml concentration reduced the labeling by 80% on the surface of BEC after 1h treatment, while lower concentrations were less effective (Figure 12B-C).

The effects of the two different treatments were tested by measuring transient streaming potential signals on the chip (Figure 12D-E). To this end, a fluid flow of 1 ml/min was applied

on the upper channel of the device, containing the brain endothelial cell monolayer and the flow of charges were registered. As shown in Figure 12D-E, both treatments increased the streaming potential of the cell monolayers. Neuraminidase treatment was performed at a concentration of 1 U/ml, since it was the most effective concentration in reducing sialic acids from the glycocalyx (Figure 12B-C). Addition of neuraminidase increased the streaming potential of cell layers to -0.268 ±-0.086 mV from -0.470 ± 0.047 mV (Figure 12D). Lidocaine, the other surface charge modulator in our experiments, is widely used as an anaesthetic or antiarrhythmic drug. It was demonstrated in a previous study by LDv that it modifies the zeta potential of brain endothelial cells (51). Since there found to be no toxic effect of lidocaine at 1 mM concentration (51), this concentration was used on the D3 monolayers cultured in the LOC device. In Figure 12E, the streaming potential is shown to increase from -0.333 ± 0.089 mV to -0.161 ± 0.061 mV upon lidocaine treatment.

For comparison with the results obtained by the streaming potential measurements, single-cell experiments were performed using the same treatments but the LDv method. As shown in Figure 12F, neuraminidase treatment significantly increased the surface charge of D3 to -9.83 ± 1.67 mV, while lidocaine elevated it to -8.29 ± 1.71 mV from the -12.7 ± 1.71 mV measured in basal conditions when no treatment was applied. The efficiency of cleavage of sialic acid residues from the glycocalyx by neuraminidase was determined by the sialic acid specific lectin WGA-Alexa 488 staining, followed by confocal microscopy and image analysis for staining intensity (Figure 12B-C). The neuraminidase treatment (1U/ml) reduced the labeling by 80% on the surface of D3 after 1h treatment.

After completing the experiments on both Nafion and cells, the streaming potential amplitudes recorded on the LOC device and the zeta potential values measured by the LDv technique were compared to seek possible correlation. Figure 8B shows the streaming potential results plotted as a function of zeta potential, including the Nafion results. The graph was fitted with linear regression, and the result showed a clear linear relationship between the data gathered by the two methods, with a goodness-of-fit of R^2=0.988.

The results clearly prove the feasibility of the new “zeta-feature” of the device, at the same time provide a calibration factor for the determination of the zeta potential of the cell layer. It was also shown that the sensitivity of the technique is sufficient to measure changes of the surface charge properties of the BBB layer that was demonstrated to be linked to altered penetration of charged molecules and nanoparticles (30, 50, 51). The question arises, however, whether the changes in surface charge measured by streaming or zeta potential were accompanied by

alterations in barrier parameters, such as permeability for ions (TEER) or neutral hydrophilic molecules. To investigate whether zeta potential changes are linked to changes in passive paracellular permeability or are independent indicators of barrier function, further experiments were performed.

Barrier integrity of cell monolayers in the LOC device

The resistance of the D3 cultures in the LOC device did not change after treatments (Figure 13A), and the same result was shown on culture inserts for neuraminidase. Since the paracellular permeability for both ions and neutral hydrophilic molecules is regulated by the tight intercellular junctions, changes in the cell surface zeta potential are not expected to affect this pathway. The removal of the sialic acid residues from the glycocalyx or the insertion of a positively charged molecule in the plasma membrane of the cells did not result in any statistical difference in the paracellular permeability for dextran as compared to the control group, as it was expected for a neutral large tracer molecule (Figure 13B). The same was observed on culture inserts. These data are in agreement with a previous study describing that treatment of BBB culture models with lidocaine did not change the permeability of neutral hydrophilic markers such as dextran (51). In concordance with TEER and permeability data, the cell morphology of D3 was unchanged as the same immunostaining pattern was observed for the junctional linker protein β-catenin after treatments as compared to the control cells (Figure C). Similar D3 morphology was also observed after neuraminidase treatment by phase contrast microscopy. These control experiments prove that modulation of endothelial cellular surface charge with neuraminidase or lidocaine did not affect barrier integrity of the cell layers and that both TEER and zeta potential, two independent essential parameters can be measured with the device.

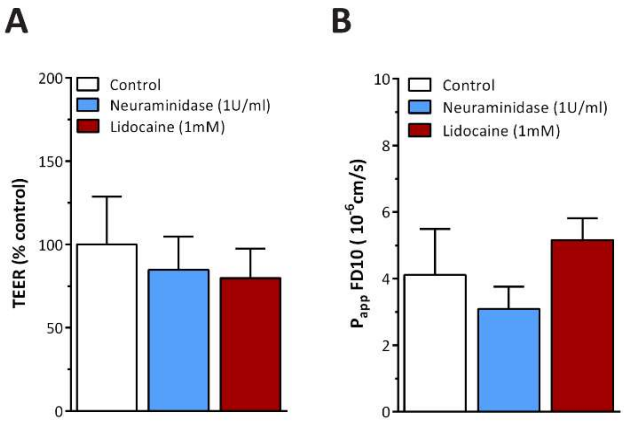

Figure 13 *The effects of the treatments modifying the surface charge of confluent brain endothelial cells on the paracellular barrier properties measured in the chip device. (A) Transendothelial electric resistance (TEER) results were normalised to the values of the control group which received culture medium instead of treatments for the same period. (B) Apparent permeability coefficient (P_{app}) of the brain endothelial monolayers for the neutrally charged fluorescently labeled 10 kDa dextran (FD10), a marker of paracellular permeability.*

Conclusion

The first goal of the study was to develop a general-purpose device that can be used to investigate multiple types of biological barriers as mono-, double- or triple cultures monitoring the electric conductivity and molecular permeability of the (co-)cultured cells under no-flow or low-flow conditions, at the same time allowing microscopic visualization of the whole membrane surface. The miniaturized chip was successfully used to model two different biological barriers with three types of cell cultures. Human intestinal epithelial and brain endothelial cells grew all well in the new microdevice, and showed cell morphology and barrier functions similar to cultures on inserts. The biochip was suitable for modeling the BBB: formation of barriers was observed for both the brain endothelial cell line and the co-culture model. The triple primary co-culture blood-brain barrier model was established on a lab-on-a-chip device and investigated under fluid flow for the first time. The barrier-inducing effect of flow could be observed for the brain endothelial cell line. This was the first LOC device where resistance is measured by transparent gold electrodes, so that cellular growth can be monitored through the whole length of the device, not only through a small window and used for several different types of barrier models.

The second goal was to develop a method to quantify the surface charge properties of cell monolayers. We successfully measured the streaming potential of a biological barrier culture model with the help of our versatile lab-on-a-chip device upgraded with two Ag/AgCl electrodes. The inclusion of the “zeta electrodes”, a voltage preamplifier and an oscilloscope in our set-up made it possible to successfully record signals describing the surface charge properties of brain endothelial cell monolayers used as a barrier model in our experiments. The new technique was verified by comparing streaming potential data obtained in the LOC device and zeta potential results by the commonly used LDv method. Changes in the negative surface charge of the barrier model by treatments with neuraminidase enzyme modifying the plasma membrane glycocalyx, or lidocaine altering the lipid membrane charge could be measured by both the novel LOC device and LDv.

The device can be used for different types of biological barriers, such as respiratory and intestinal epithelial cell cultures and co-culture models of the BBB. Potential application of the new LOC zeta device can be two-fold. Surface charge and its changes can be measured by registering the streaming potential on other epithelial and endothelial barrier systems including lung, intestine, kidney and cornea. On the other hand, changes in either the glycocalyx of the

vascular-, or other barriers caused by pathologies such as diabetes, sepsis, hypertension or virus infection, or changes in the plasma membrane caused by charged molecules or drugs can be modeled and directly measured on intact cell layers. The new device can help to gain meaningful novel information on how surface charge is linked to barrier function in both physiological and pathological conditions.

Acknowledgements

I would like to express my gratitude to Prof. Dr. András Dér, the head of the Biomolecular Electronics Research Group, for providing me the opportunity to work under his supervision at Institute of Biophysics in the Biological Research Centre.

I wish to thank Dr. Sándor Valkai and the late Dr. Rudolf Boconádi-Tóth for all their teaching and guidance throughout my undergraduate and PhD student years.

I would like to express my appreciation to Prof. Dr. Mária Deli, head of Biological Barriers Research Group, for her great support during our collaboration.

I would like to offer my special thanks to Dr. Fruzsina Walter and Dr. Ana Raquel Santa Maria for all the work together, their significant contribution and friendship throughout the years.

I wish to thank the members of the Biomolecular Electronics and Biological Barriers Research Groups and all the colleagues of the Institute of Biophyisics. I received generous support and assistance from Dániel Petrovszki, Dr. Alexandra Bocsik, Dr. Mária Mészáros, Judit Vigh, Dr. Gaszton Vizsnyiczai, Tamás Fekete, Dr. Lóránd Kelemen, László Dér, Dr. Krisztina Nagy, Dr. Péter Galajda, Dr. László Zimányi and Prof. Pál Ormos.

Above all, I am deeply thankful for the support of my family. Without their support this thesis would have never been accomplished. I wish to dedicate this work to my wife, Zsófia Melczer.

References

1. Deli MA. Potential use of tight junction modulators to reversibly open membranous barriers and improve drug delivery. Biochim Biophys Acta. 2009;1788(4):892-910.
2. Deli MA, Abraham CS, Kataoka Y, Niwa M. Permeability studies on in vitro blood-brain barrier models: physiology, pathology, and pharmacology. Cell Mol Neurobiol. 2005;25(1):59-127.
3. Helms HC, Abbott NJ, Burek M, Cecchelli R, Couraud PO, Deli MA, et al. In vitro models of the blood-brain barrier: An overview of commonly used brain endothelial cell culture models and guidelines for their use. J Cereb Blood Flow Metab. 2016;36(5):862-90.
4. Veszelka S, Toth A, Walter FR, Toth AE, Grof I, Meszaros M, et al. Comparison of a Rat Primary Cell-Based Blood-Brain Barrier Model With Epithelial and Brain Endothelial Cell Lines: Gene Expression and Drug Transport. Front Mol Neurosci. 2018;11:166.
5. Sakolish CM, Esch MB, Hickman JJ, Shuler ML, Mahler GJ. Modeling Barrier Tissues In Vitro: Methods, Achievements, and Challenges. EBioMedicine. 2016;5:30-9.
6. van der Helm MW, van der Meer AD, Eijkel JC, van den Berg A, Segerink LI. Microfluidic organ-on-chip technology for blood-brain barrier research. Tissue Barriers. 2016;4(1):e1142493.
7. Kratz SRA, Holl G, Schuller P, Ertl P, Rothbauer M. Latest Trends in Biosensing for Microphysiological Organs-on-a-Chip and Body-on-a-Chip Systems. Biosensors (Basel). 2019;9(3).
8. Raimondi I, Izzo L, Tunesi M, Comar M, Albani D, Giordano C. Organ-On-A-Chip in vitro Models of the Brain and the Blood-Brain Barrier and Their Value to Study the Microbiota-Gut-Brain Axis in Neurodegeneration. Front Bioeng Biotechnol. 2019;7:435.
9. Neuhaus W, Lauer R, Oelzant S, Fringeli UP, Ecker GF, Noe CR. A novel flow based hollow-fiber blood-brain barrier in vitro model with immortalised cell line PBMEC/C1-2. J Biotechnol. 2006;125(1):127-41.
10. Booth R, Kim H. Characterization of a microfluidic in vitro model of the blood-brain barrier (muBBB). Lab Chip. 2012;12(10):1784-92.
11. Prabhakarpandian B, Shen MC, Nichols JB, Mills IR, Sidoryk-Wegrzynowicz M, Aschner M, et al. SyM-BBB: a microfluidic Blood Brain Barrier model. Lab Chip. 2013;13(6):1093-101.
12. Cucullo L, Hossain M, Tierney W, Janigro D. A new dynamic in vitro modular capillaries-venules modular system: cerebrovascular physiology in a box. BMC Neurosci. 2013;14:18.

13. Ramadan Q, Jafarpoorchekab H, Huang C, Silacci P, Carrara S, Koklu G, et al. NutriChip: nutrition analysis meets microfluidics. Lab Chip. 2013;13(2):196-203.
14. Wang YI, Carmona C, Hickman JJ, Shuler ML. Multiorgan Microphysiological Systems for Drug Development: Strategies, Advances, and Challenges. Adv Healthc Mater. 2018;7(2).
15. Maoz BM, Herland A, FitzGerald EA, Grevesse T, Vidoudez C, Pacheco AR, et al. A linked organ-on-chip model of the human neurovascular unit reveals the metabolic coupling of endothelial and neuronal cells. Nat Biotechnol. 2018;36(9):865-74.
16. Park TE, Mustafaoglu N, Herland A, Hasselkus R, Mannix R, FitzGerald EA, et al. Hypoxia-enhanced Blood-Brain Barrier Chip recapitulates human barrier function and shuttling of drugs and antibodies. Nat Commun. 2019;10(1):2621.
17. Hellinger E, Veszelka S, Toth AE, Walter F, Kittel A, Bakk ML, et al. Comparison of brain capillary endothelial cell-based and epithelial (MDCK-MDR1, Caco-2, and VB-Caco-2) cell-based surrogate blood-brain barrier penetration models. Eur J Pharm Biopharm. 2012;82(2):340-51.
18. Kiss L, Walter FR, Bocsik A, Veszelka S, Ozsvari B, Puskas LG, et al. Kinetic analysis of the toxicity of pharmaceutical excipients Cremophor EL and RH40 on endothelial and epithelial cells. J Pharm Sci. 2013;102(4):1173-81.
19. Kiss L, Hellinger E, Pilbat AM, Kittel A, Torok Z, Furedi A, et al. Sucrose esters increase drug penetration, but do not inhibit p-glycoprotein in caco-2 intestinal epithelial cells. J Pharm Sci. 2014;103(10):3107-19.
20. Weksler BB, Subileau EA, Perriere N, Charneau P, Holloway K, Leveque M, et al. Blood-brain barrier-specific properties of a human adult brain endothelial cell line. FASEB J. 2005;19(13):1872-4.
21. Weksler B, Romero IA, Couraud PO. The hCMEC/D3 cell line as a model of the human blood brain barrier. Fluids Barriers CNS. 2013;10(1):16.
22. Toth AE, Walter FR, Bocsik A, Santha P, Veszelka S, Nagy L, et al. Edaravone protects against methylglyoxal-induced barrier damage in human brain endothelial cells. PLoS One. 2014;9(7):e100152.
23. Deli MA. Drug Transport and the Blood-Brain Barrier. In: Tihanyi K, Vastag M, editors. Solubility, Delivery and ADME Problems of Drugs and Drug-Candidates. Washingon DC: Bentham Science Ltd; 2011. p. 144-65.
24. Toth A, Veszelka S, Nakagawa S, Niwa M, Deli MA. Patented in vitro blood-brain barrier models in CNS drug discovery. Recent Pat CNS Drug Discov. 2011;6(2):107-18.

25. van den Berg BM, Nieuwdorp M, Stroes ES, Vink H. Glycocalyx and endothelial (dys) function: from mice to men. Pharmacol Rep. 2006;58 Suppl:75-80.
26. Dogne S, Flamion B. Endothelial Glycocalyx Impairment in Disease: Focus on Hyaluronan Shedding. Am J Pathol. 2020;190(4):768-80.
27. Krammer F, Smith GJD, Fouchier RAM, Peiris M, Kedzierska K, Doherty PC, et al. Influenza. Nat Rev Dis Primers. 2018;4(1):3.
28. Abbott NJ, Patabendige AA, Dolman DE, Yusof SR, Begley DJ. Structure and function of the blood-brain barrier. Neurobiol Dis. 2010;37(1):13-25.
29. Campos-Bedolla P, Walter FR, Veszelka S, Deli MA. Role of the blood-brain barrier in the nutrition of the central nervous system. Arch Med Res. 2014;45(8):610-38.
30. Ribeiro MM, Domingues MM, Freire JM, Santos NC, Castanho MA. Translocating the blood-brain barrier using electrostatics. Front Cell Neurosci. 2012;6:44.
31. Imura Y, Asano Y, Sato K, Yoshimura E. A microfluidic system to evaluate intestinal absorption. Anal Sci. 2009;25(12):1403-7.
32. Pusch J, Votteler M, Gohler S, Engl J, Hampel M, Walles H, et al. The physiological performance of a three-dimensional model that mimics the microenvironment of the small intestine. Biomaterials. 2011;32(30):7469-78.
33. Kim HJ, Huh D, Hamilton G, Ingber DE. Human gut-on-a-chip inhabited by microbial flora that experiences intestinal peristalsis-like motions and flow. Lab Chip. 2012;12(12):2165-74.
34. Gao D, Liu H, Lin JM, Wang Y, Jiang Y. Characterization of drug permeability in Caco-2 monolayers by mass spectrometry on a membrane-based microfluidic device. Lab Chip. 2013;13(5):978-85.
35. Gress C, Jeziorski M, Saumer M, Schafer KH. Simulation of in-vivo-equivalent epithelial barriers using a micro fluidic device. Biomed Microdevices. 2014;16(2):191-8.
36. Guo Y, Li Z, Su W, Wang L, Zhu Y, Qin J. A Biomimetic Human Gut-on-a-Chip for Modeling Drug Metabolism in Intestine. Artif Organs. 2018;42(12):1196-205.
37. Siddharthan V, Kim YV, Liu S, Kim KS. Human astrocytes/astrocyte-conditioned medium and shear stress enhance the barrier properties of human brain microvascular endothelial cells. Brain Res. 2007;1147:39-50.
38. Cucullo L, Couraud PO, Weksler B, Romero IA, Hossain M, Rapp E, et al. Immortalized human brain endothelial cells and flow-based vascular modeling: a marriage of convenience for rational neurovascular studies. J Cereb Blood Flow Metab. 2008;28(2):312-28.

39. Griep LM, Wolbers F, de Wagenaar B, ter Braak PM, Weksler BB, Romero IA, et al. BBB on chip: microfluidic platform to mechanically and biochemically modulate blood-brain barrier function. Biomed Microdevices. 2013;15(1):145-50.

40. Achyuta AK, Conway AJ, Crouse RB, Bannister EC, Lee RN, Katnik CP, et al. A modular approach to create a neurovascular unit-on-a-chip. Lab Chip. 2013;13(4):542-53.

41. Takeshita Y, Obermeier B, Cotleur A, Sano Y, Kanda T, Ransohoff RM. An in vitro blood-brain barrier model combining shear stress and endothelial cell/astrocyte co-culture. J Neurosci Methods. 2014;232:165-72.

42. Booth R, Kim H. Permeability analysis of neuroactive drugs through a dynamic microfluidic in vitro blood-brain barrier model. Annals of Biomedical Engineering. 2014;42:12.

43. Booth R, Noh S, Kim H. A multiple-channel, multiple-assay platform for characterization of full-range shear stress effects on vascular endothelial cells. Lab Chip. 2014;14(11):1880-90.

44. Jeong S, Kim S, Buonocore J, Park J, Welsh CJ, Li J, et al. A Three-Dimensional Arrayed Microfluidic Blood-Brain Barrier Model With Integrated Electrical Sensor Array. IEEE Trans Biomed Eng. 2018;65(2):431-9.

45. Ando Y, Okada H, Takemura G, Suzuki K, Takada C, Tomita H, et al. Brain-Specific Ultrastructure of Capillary Endothelial Glycocalyx and Its Possible Contribution for Blood Brain Barrier. Sci Rep. 2018;8(1):17523.

46. Herve F, Ghinea N, Scherrmann JM. CNS delivery via adsorptive transcytosis. AAPS J. 2008;10(3):455-72.

47. Fu BM, Tarbell JM. Mechano-sensing and transduction by endothelial surface glycocalyx: composition, structure, and function. Wiley Interdiscip Rev Syst Biol Med. 2013;5(3):381-90.

48. Ribeiro MM, Pinto AR, Domingues MM, Serrano I, Heras M, Bardaji ER, et al. Chemical conjugation of the neuropeptide kyotorphin and ibuprofen enhances brain targeting and analgesia. Mol Pharm. 2011;8(5):1929-40.

49. Li G, Fu BM. An electrodiffusion model for the blood-brain barrier permeability to charged molecules. J Biomech Eng. 2011;133(2):021002.

50. Meszaros M, Porkolab G, Kiss L, Pilbat AM, Kota Z, Kupihar Z, et al. Niosomes decorated with dual ligands targeting brain endothelial transporters increase cargo penetration across the blood-brain barrier. Eur J Pharm Sci. 2018;123:228-40.

51. Santa-Maria AR, Walter FR, Valkai S, Bras AR, Meszaros M, Kincses A, et al. Lidocaine turns the surface charge of biological membranes more positive and changes the permeability of blood-brain barrier culture models. Biochim Biophys Acta Biomembr. 2019;1861(9):1579-91.

52. Hunter RJ. Zeta Potential in Colloid Science. San Diego: Academic Press; 1981.

53. Malher E, Martin D, Duvivier C, Volochine B, Stoltz JF. New device for determination of cell electrophoretic mobility using doppler velocimetry. Biorheology. 1982;19(5):647-54.

54. Oldham IB, Young FJ, Osterle JF. Streaming potential in small capillaries. Journal of Colloid Science. 1963;18(4):8.

55. Van Wagenen RA, Andrade JD. Flat plate streaming potential investigations: Hydrodynamics and electrokinetic equivalency. Journal of Colloid and Interface Science. 1980;76(2):8.

56. Sawyer PN, Himmelfarb E, Lustrin I, Ziskind H. Measurement of streaming potentials of mammalian blood vessels, aorta and vena cava, in vivo. Biophys J. 1966;6(5):641-51.

57. Smyth DH, Wright EM. Streaming potentials in the rat small intestine. J Physiol. 1966;182(3):591-602.

58. Gandhi RB, Robinson JR. Permselective characteristics of rabbit buccal mucosa. Pharm Res. 1991;8(9):1199-202.

59. Fike RM, van Oss CJ. Zeta-protentials of intact cell monolayers determined by electro-osmosis. In Vitro. 1976;12(6):428-36.

60. van Wagenen RA, Andrade JD, Hibbs JB. Streaming Potential Measurements of Biosurfaces. J Electrochem Soc. 1976;123.

61. Vandrangi P, Jreij P, Rajapaksa TE, Bansal N, Lo DD, Rodgers VG. Novel in situ normal streaming potential device for characterizing electrostatic properties of confluent cells. Rev Sci Instrum. 2012;83(7):074302.

62. Vandrangi P, Lo DD, Kozaka R, Ozaki N, Carvajal N, Rodgers VG. Electrostatic properties of confluent Caco-2 cell layer correlates to their microvilli growth and determines underlying transcellular flow. Biotechnol Bioeng. 2013;110(10):2742-8.

63. Singh A, Satchell SC, Neal CR, McKenzie EA, Tooke JE, Mathieson PW. Glomerular endothelial glycocalyx constitutes a barrier to protein permeability. J Am Soc Nephrol. 2007;18(11):2885-93.

64. Veszelka S, Pasztoi M, Farkas AE, Krizbai I, Ngo TK, Niwa M, et al. Pentosan polysulfate protects brain endothelial cells against bacterial lipopolysaccharide-induced damages. Neurochem Int. 2007;50(1):219-28.

65. Veszelka S, Toth AE, Walter FR, Datki Z, Mozes E, Fulop L, et al. Docosahexaenoic acid reduces amyloid-beta induced toxicity in cells of the neurovascular unit. J Alzheimers Dis. 2013;36(3):487-501.

66. Hulper P, Veszelka S, Walter FR, Wolburg H, Fallier-Becker P, Piontek J, et al. Acute effects of short-chain alkylglycerols on blood-brain barrier properties of cultured brain endothelial cells. Br J Pharmacol. 2013;169(7):1561-73.

67. Liebner S, Corada M, Bangsow T, Babbage J, Taddei A, Czupalla CJ, et al. Wnt/beta-catenin signaling controls development of the blood-brain barrier. J Cell Biol. 2008;183(3):409-17.

68. Ramirez SH, Fan S, Zhang M, Papugani A, Reichenbach N, Dykstra H, et al. Inhibition of glycogen synthase kinase 3beta (GSK3beta) decreases inflammatory responses in brain endothelial cells. Am J Pathol. 2010;176(2):881-92.

69. Nakagawa S, Deli MA, Kawaguchi H, Shimizudani T, Shimono T, Kittel A, et al. A new blood-brain barrier model using primary rat brain endothelial cells, pericytes and astrocytes. Neurochem Int. 2009;54(3-4):253-63.

70. Nakagawa S, Deli MA, Nakao S, Honda M, Hayashi K, Nakaoke R, et al. Pericytes from brain microvessels strengthen the barrier integrity in primary cultures of rat brain endothelial cells. Cell Mol Neurobiol. 2007;27(6):687-94.

71. Perriere N, Demeuse P, Garcia E, Regina A, Debray M, Andreux JP, et al. Puromycin-based purification of rat brain capillary endothelial cell cultures. Effect on the expression of blood-brain barrier-specific properties. J Neurochem. 2005;93(2):279-89.

72. Jahne EA, Eigenmann DE, Culot M, Cecchelli R, Walter FR, Deli MA, et al. Development and validation of a LC-MS/MS method for assessment of an anti-inflammatory indolinone derivative by in vitro blood-brain barrier models. J Pharm Biomed Anal. 2014;98:235-46.

73. Kostiuchenko ZA, Cui JZ, Lemay SG. Electrochemistry in Micro- and Nanochannels Controlled by Streaming Potentials. J Phys Chem C Nanomater Interfaces. 2020;124(4):2656-63.

74. Mauritz KA, Moore RB. State of understanding of nafion. Chem Rev. 2004;104(10):4535-85.

75. Betteridge KB, Arkill KP, Neal CR, Harper SJ, Foster RR, Satchell SC, et al. Sialic acids regulate microvessel permeability, revealed by novel in vivo studies of endothelial glycocalyx structure and function. J Physiol. 2017;595(15):5015-35.

76. Morgan FD, Williams ER, Madden TR. Streaming potential properties of westerly granite with applications. JGR Solid Earth. 1989;94(B9):12.

77. Khan OF, Sefton MV. Endothelial cell behaviour within a microfluidic mimic of the flow channels of a modular tissue engineered construct. Biomed Microdevices. 2011;13(1):69-87.

78. Chau LT, Rolfe BE, Cooper-White JJ. A microdevice for the creation of patent, three-dimensional endothelial cell-based microcirculatory networks. Biomicrofluidics. 2011;5(3):34115-3411514.

79. Kim S, Lee H, Chung M, Jeon NL. Engineering of functional, perfusable 3D microvascular networks on a chip. Lab Chip. 2013;13(8):1489-500.

80. Fede C, Fortunati I, Petrelli L, Guidolin D, De Caro R, Ferrante C, et al. An easy-to-handle microfluidic device suitable for immunohistochemical procedures in mammalian cells grown under flow conditions. Eur J Histochem. 2014;58(2):2360.

Annex

I.

Walter FR, Valkai S., **Kincses A**, Petneházi A, Czeller T, Veszelka S, Ormos P, Deli MA, Dér A. A versatile lab-on-a-chip tool for modeling biological barriers. Sensors and Actuators B: Chemical. 2016;222:1209-1219. IF: 5.401

Sensors and Actuators B 222 (2016) 1209–1219

Contents lists available at ScienceDirect

Sensors and Actuators B: Chemical

journal homepage: www.elsevier.com/locate/snb

A versatile lab-on-a-chip tool for modeling biological barriers

Fruzsina R. Walter[1], Sándor Valkai[1], András Kincses, András Petneházi, Tamás Czeller, Szilvia Veszelka, Pál Ormos, Mária A. Deli*, András Dér*

Institute of Biophysics, Biological Research Centre, Hungarian Academy of Sciences, Temesvári krt. 62, H-6726 Szeged, Hungary

ARTICLE INFO

Article history:
Received 13 April 2015
Received in revised form 24 July 2015
Accepted 28 July 2015
Available online 30 July 2015

Keywords:
Microfluidics
Lung and intestinal epithelial cells
Endothelial cells
Blood–brain barrier
Permeability
Trans-epithelial/endothelial electric resistance

ABSTRACT

Models of biological barriers are important to study physiological functions, transport mechanisms, drug delivery and pathologies. However, there are only a few integrated biochips which are able to monitor several of the crucial parameters of cell-culture-based barrier models. The aim of this study was to design and manufacture a simple but versatile device, which allows a complex investigation of barrier functions. The following functions and measurements are enabled simultaneously: co-culture of 2 or 3 types of cells; flow of culture medium; visualization of the entire cell layer by microscopy; real-time transcellular electrical resistance monitoring; permeability measurements. To this end, a poly(dimethylsiloxane)-based biochip with integrated transparent gold electrodes and with a possibility to connect to a peristaltic pump was built. Unlike previous systems, the structure of the device allowed a constant visual observation of cell growth over the whole membrane surface. Morphological characterization of the layers was also accomplished by immunohistochemical staining. The chip was applied to monitor and characterize models of the intestinal and lung epithelial barriers, and the blood–brain barrier. The models were established using human Caco-2 intestinal and A549 lung epithelial cell lines, hCMEC/D3 human brain endothelial cell line and primary rat brain endothelial cells co-cultured with primary astrocytes and brain pericytes. This triple primary co-culture blood–brain barrier model was assembled on a lab-on-a-chip device and investigated under fluid flow for the first time. Such a versatile tool is expected to facilitate the kinetic investigation of various biological barriers.

1. Introduction

Epithelial outer, and endothelial inner barriers of the body are important defense systems to maintain homeostasis and play a crucial role in drug absorption and transport [1]. Culture models of biological barriers are important tools to study physiological functions, transport mechanisms, drug delivery and pathological processes [2]. Tight intercellular junctions are fundamental features of epithelial and endothelial barriers *in vivo* which are reflected in high electrical resistance and low passive permeability for hydrophilic compounds [1,2]. Cell culture inserts with porous membrane were introduced to measure these parameters on *in vitro* models in the 1980s. Confluent monolayers of adherent epithelial or endothelial cells grown on culture inserts are widely used static models for intestinal, lung and blood–brain barriers (BBB). The Caco-2 human epithelial cell line is a well characterized model of the intestinal barrier applied for screening of drug candidates [3–6]. Several studies describe the lung epithelial cell line A549 as a model of the lung barrier [7,8]. Culture-based BBB models greatly differ in complexity. Immortalized cell lines and mono-cultures of brain endothelial cells can be used as simplified BBB models [9–11], but the barrier properties of primary cell-based co-culture models are better [2,12,13]. We established a syngeneic rat BBB model based on the co-culture of primary brain endothelial cells with pericytes and glial cells mimicking the *in vivo* anatomical position of the cells. This triple co-culture BBB model displays barrier properties and in drug permeability assays shows good correlation with *in vivo* BBB permeability data [14,15].

Microtechnology and new lab-on-chip devices with integrated functions offer the possibility to study the barriers real-time, and

Abbreviations: A549, human alveolar type II like lung epithelial cell line; BBB, blood–brain barrier; BSA, bovine serum albumin; Caco-2, intestinal colon carcinoma derived epithelial cell line; DMEM, Dulbecco's modified Eagle medium; EBA, Evans blue-labeled albumin; FBS, fetal bovine serum; FD, FITC-dextran 4.4 kDa; bFGF, basic fibroblast growth factor; GFAP, glial fibrillary acidic protein; hCMEC/D3, human brain microvascular endothelial cell line; ITO, indium tin oxide electrode; P_{app}, apparent permeability coefficient; PBS, phosphate buffered saline; PDMS, poly(dimethylsiloxane); SF, sodium fluorescein; α-SM, α-smooth muscle actin; TEER, transendothelial/epithelial electrical resistance (TEER).

* Corresponding authors.
E-mail addresses: deli.maria@brc.mta.hu (M.A. Deli), der.andras@brc.mta.hu (A. Dér).

[1] These authors contributed equally to this manuscript.

http://dx.doi.org/10.1016/j.snb.2015.07.110
0925-4005/

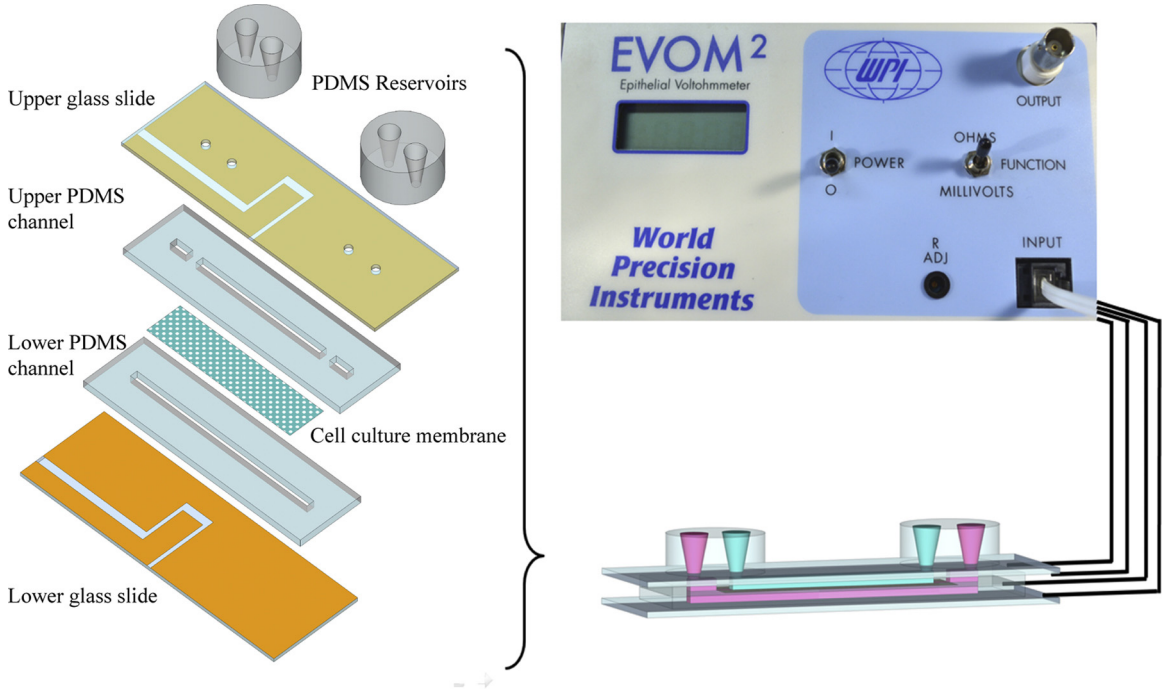

Fig. 1. Structural assembly of the chip showing all layers of the device (on the left). PDMS reservoirs (gray) holding the inlet and outlet tubes are fixed to the top of the chip. The porous cell culture membrane (dotted sheet) is situated between the upper and the lower channels made of PDMS (light blue). This core is sandwiched by two glass slides with gold electrodes (yellow). 3D structural view of the chip connected to the EVOM2 voltohmmeter (on the right). Electrodes and the connecting wires are shown as black lines.

under more physiological conditions [16,17]. In contrast to the static culture inserts, the cells can be exposed to fluid flow and shear stress, which are especially important for the vascular endothelium [18–20]. Although a dynamic BBB model on a 3-dimensional tube structure with a continuous flow of culture medium has been published, the real-time visualization of the cells is not possible with the hollow fiber system [18,21].

The aim of this study was to design and manufacture a versatile microdevice, which enables the co-culture of 2 or 3 cell types, the flow of the culture medium, visualization of the cells by microscopy, monitoring of the transcellular electrical resistance, and the measurement of monolayer permeability. An integrated lab-on-a-chip measuring chamber was built and applied to monitor and characterize four different barrier models. The chip proved to be suitable for the complex characterization of Caco-2 human intestinal and A549 human lung epithelial cell lines, hCMEC/D3 human brain endothelial cell line and primary rat brain endothelial cells co-cultured with primary astrocytes and brain pericytes.

2. Materials and methods

2.1. Ethics statement

All animal studies were done according to the 1998. XXVIII. Hungarian law and the EU Directive 2010/63/EU about animal protection and welfare. Approval for animal studies was obtained from the local animal health authority, the Governmental Office for Csongrád County, Directorate of Food Chain Safety and Animal Health (Permit number: XVI./834/2012).

2.2. Materials

All reagents were purchased from Sigma–Aldrich Ltd., Hungary, unless otherwise indicated.

2.3. Microfabrication process

The barrier chip device, which is a two-layered, porous membrane based model, was fabricated using poly(dimethylsiloxane) (PDMS, Sylgard 184, Dow Corning GmbH, Germany). Dimensions for the top channel were 3.7 cm × 0.2 cm × 0.2 cm, while the bottom channel was 4.2 cm long with the same diameter and height. For the chip parts, a 1:10 mixture of initiator and base material (silicone elastomer) was used, mixed and degassed by vacuum. After this step the material was poured on brass molds defining the shape of the channels. On the filled molds PDMS was cured at 75 °C on a hot plate for 30 min to achieve structural rigidity. To enable the composition of the model, the PDMS surfaces had to be treated with oxygen plasma. The plasma cleaner (PDC-002, Harrick Plasma, USA) and its chamber were evacuated to 150 mtorr, then a constant 400 mtorr pressure was set by excess oxygen. Having the oxygen pressure been stabilized, oxygen plasma was induced in the chamber by RF excitation (13.56 MHz, 29.6 W) for 30 s. The treated upper and lower PDMS parts became highly adhesive and ready to assemble the microfluidic channels. A porous membrane (It4ip, Belgium; PET, thickness: 23 μm, pore size 0.45 μm, pore density $2 \times 10^6/cm^2$) was used for separating the upper and lower channels. During the biochip fabrication process several membrane types were tested for cell cultivation (Fig. S1). Only one type of membrane from it4ip proved to be suitable for cell culture (Fig. S1). This membrane, receiving the same treatment as the PDMS components, was mechanically sandwiched between the oxygen plasma treated PMDS parts at its circumference as shown in Fig. 1. There was no surface reaction between these two materials, the oxygen plasma treated PDMS had a poor adhesion to the PET membrane. There is a small area (2 mm × 2 mm, Fig. 1) where the adhesion between the PET membrane and the PDMS for perfect sealing was provided by a droplet of a silicone sealant adhesive (Aquarium RTV Silicone Sealant, Adarsha Specialty Chemicals Pvt. Ltd., India). This sealant adhesive has a relatively high viscosity so it can be applied precisely

while it is soft for about 15 min. It reaches the fully cross linked, solid state in 24 h. The oxygen treated PDMS does not bond very well to metal surfaces either, so the microscope slides with gold electrodes were fixed to the PDMS with the same sealant adhesive. The sealant was applied as a thin, continuous line on the surface of the PDMS. The fabrication procedure was monitored under a stereo microscope. In the end, we had a 0.1 mm thick sealant layer that provided a good adhesion for the glass slides and sealed well both channels. PDMS blocks holding the inlet and outlet tubes (PCR tubes, Eppendorf, Germany) were fixed to the upper glass surface after plasma treatment. These parts served as medium reservoirs for the cell cultivation period (when flow was not applied). Four holes were drilled across the top glass slide for medium transport. Drilling was performed using a 1.5 mm diamond core drilling bit (Eternal Tools, UK) and a commercial drilling machine with some droplet of water added on the glass surface as coolant liquid at the spot of the hole.

Cell culture medium flow was driven by a peristaltic pump (Masterflex, Cole-Parmer) through silicone tubing (1 mm inner, 3 mm outer diameter, Carl Roth, Germany). The input tube was connected to the inlet of the chip, while the output tube was connected to the reservoir *via* the peristaltic pump. For all flow experiments low-shear-stress conditions (0.15 dyn) were used.

For the resistance measurements, a pair of 25-nm thick, transparent, gold electrodes was formed on each glass slide using sputter-coating (sputtering machine: K975X, EMITEC, France). The exact dimensions of the glass slides were $26 \times 76^{\circ}$mm (Menzel-Glaser, Germany). Thin copper wires were glued to the gold electrodes with conductive epoxy drops (CW2400, ITW Chemtronics, USA) in order to connect them with the 4-channel input of the voltohmmeter (EVOM, World Precision Instruments, USA). For comparison to the common indium tin oxide (ITO) electrodes, we performed a recording of impedance spectra in the chip with transparent gold (Au) and ITO electrodes. A voltage source (sinus function generator, TE 8020, 20 MHz), the sample using one electrode on the top and one on the bottom plate of the chip and a reference resistance (100 Ω) were switched in series, and the voltage drop on the resistance was registered by a storage oscilloscope (LeCroy Wave Runner 6010A), from which the sample resistance values were calculated at different frequencies. The frequency range span from 1 Hz to 20 MHz, with 3 records in each decade. Prior to the measurements both of the channels were filled up with the same buffer as used in the cell culture experiments. Transmission spectra of gold and ITO electrodes was also evaluated (see Supplemetary material, Fig. S4).

The ready-to-use device was sterilized using 70% ethanol for 2 h then was washed with sterile distilled water 6 times, and the chip was treated with oxygen plasma again to turn the naturally hydrophobic PDMS surface hydrophilic.

2.4. Cell cultures

To test the versatility of the barrier chip, both epithelial and endothelial monolayers were cultured and monitored under static and flow conditions, as was appropriate. The transparent gold electrodes enabled a continuous visualization by phase contrast microscopy on the entire membrane surface. Cells were checked every day during the experiments. Visually confirmed leakage, holes on monolayers were accompanied by low TEER and resulted in the exclusion of the barrier chip from the experiments. Data were compared to measurements performed on Transwell cell culture inserts (Corning, USA). Cell cultures were grown in a humidified, 37°C incubator with 5% CO_2 in both experimental setups. A detailed description of the laboratory setup is available in the Supplementary material (Fig. S3).

2.4.1. Epithelial cells

Two human immortalized cell lines, Caco-2 intestinal epithelial cells and human alveolar type II like lung epithelial cells A549 (both from ATCC, USA) were cultured under static conditions to model epithelial barriers on the chip. A549 (≤passage number 35) and vinblastine selected Caco-2 cells (≤passage number 75; [22]) were cultured on rat tail collagen (prepared in the laboratory with acetic acid extraction) coated Petri dishes in Dulbecco's modified Eagle medium (DMEM, Biochrom, Germany) supplemented with 10% fetal bovine serum (FBS, Pan Biotech, Germany) and 50 μg/ml gentamicin. The porous membrane of the chip was coated with rat tail collagen overnight at 4 °C. After cell cultures reached 80% confluency in the dishes, Caco-2 cells (7×10^4 cells/chip) and A549 cells (8×10^4 cells/chip) were subcultured to the chip using 0.05% trypsin-EDTA solution (Pan Biotech, Germany). Confluent layers at maximal resistance were used for permeability measurements and immunolabeling. Cells were also cultured on Transwell inserts for resistance and permeability data comparison. Epithelial cells were passaged to inserts at a cell number of 8×10^4 cells/insert for A549 (insert: 1.12 cm^2, 0.4 μm pore size, 4×10^6 pores/cm^2) and 10^5 cells/insert for Caco-2 cells (insert: 1.12 cm^2, 0.4 μm pore size, 10^8 pores/cm^2).

2.4.2. Endothelial cells

Brain microvascular endothelial cell line hCMEC/D3 [9] and primary rat brain endothelial cells [23–25] were used as models of the blood–brain barrier on the chip. Cultures of hCMEC/D3 cells (≤passage number 35) were grown in MCDB 131 medium (Pan Biotech) supplemented with 5% FBS, GlutaMAX (100×, Life Technologies, USA), lipid supplement (100×, Life Technologies, USA), 10 μg/ml ascorbic acid, 550 nM hydrocortisone, 100 μg/ml heparin, 1 ng/ml basic fibroblast growth factor (bFGF, Roche, USA), insulin (2.5 μg/ml), transferrin (2.5 μg/ml), sodium selenite (2.5 ng/ml) and 50 μg/ml gentamicin. hCMEC/D3 brain endothelial cells (6×10^4 cells/chip) were seeded to microdevices similarly to epithelial cells. Static cultures were kept for 5 days before the permeability experiment. For flow studies cells were grown under static conditions until day 3, and left 48 h under dynamic conditions before permeability studies. After the first day in culture both models received 10 mM lithium chloride (Merck, USA) to induce barrier properties [9,26,27]. D3 cells were also subcultured to Transwell inserts (1.12 cm^2, 0.4 μm pore size, 4×10^6 pores/cm^2) at a cell number of 4×10^4 cells/insert.

Primary rat brain endothelial cells, pericytes and astroglia cells were isolated and cultured according to the method described in our previous studies [22,23]. To establish the triple culture model the upper compartment of the barrier chip was coated with rat tail collagen for endothelial cells and with collagen type IV for pericytes and glial cells overnight at 4 °C. Pericytes at passage number 3 (1.5×10^4 cells/chip) were seeded to the bottom side of the porous membrane according to the method of Nakagawa et al. [14,15]. Primary glial cells (10^5 cells/chip) were seeded to the bottom of the lower chamber directly to the coated glass surface. Primary rat brain endothelial cells (7×10^4 cells/chip) were passaged to the upper side of the coated membrane with endothelial culture medium: DMEM/F12 supplemented with plasma-derived bovine serum (15%; First Link, UK), heparin (100 μg/ml), bFGF (1 ng/ml; Roche, Switzerland), insulin (5 μg/ml), transferrin (5 μg/ml), sodium selenite (5 ng/ml) and gentamycin (50 μg/ml). Static co-cultures were kept for 6 days before the permeability experiment. For flow measurements, cultures were grown under static conditions until day 4, and were kept for 48 h under dynamic conditions before permeability studies. After the second day in culture both models received 550 nM hydrocortisone. One day before the static permeability test or the beginning

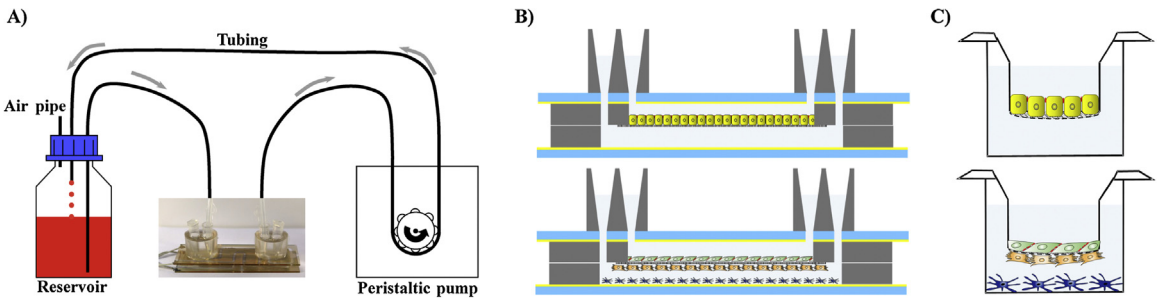

Fig. 2. (A) Schematic drawing of the flow circuit. Peristaltic pump moving the cell culture medium is positioned after the chip. Culture medium is stored in a glass reservoir bottle providing constant circulation. (B) Biochip setups with two types of cells. Epithelial cells (top, yellow cells) grow as monolayers on the porous membrane of the chip. Triple culture blood–brain barrier model using rat primary endothelial cells (green), pericytes (orange) and glial cells (blue) assembled in the biochip. (C) Transwell cell culture inserts with the same arrangements for epithelial or endothelial cell models as shown in the microchip.

of flow experiments cells were treated with chlorophenylthioadenosine-3′,5′-cyclic monophosphate (250 μM, CPT-cAMP) and RO 201724 (17.5 μM, Roche) to tighten junctions and elevate resistance [2,28]. For comparison, cells were also kept on Transwell inserts (1.12 cm^2, 0.4 μm pore size, 4×10^6 pores/cm^2). Triple primary co-culture BBB model was assessed as shown in Fig. 2 and described previously [15,24,29].

2.5. Cell culture characterization

Cells grown on the barrier chip received fresh culture medium every day. Transendothelial/epithelial electrical resistance (TEER) measurement was performed before every medium change, minimum once in every 24 h. Under dynamic flow conditions no medium change was required, because the cell culture medium was moved continuously by the peristaltic pump positioned after the chip in the circuit. Permeability measurements as layer integrity tests and immunohistochemical labeling for morphological characterization were performed at the end of all experiments. Cells on Transwell inserts received fresh culture medium every second day. TEER was also measured according to culture protocols. After reaching appropriate TEER values permeability experiments were performed. These methods are accepted and widely used in the barrier field as integrity measurements and testing model applicability.

The flux of the hydrophilic tracers sodium fluorescein (SF, MW: 376 Da) and fluorescein isothiocyanate-labeled dextran (FD, MW: 4.4 kDa) indicating paracellular permeability was measured. Permeability of Evans blue-labeled albumin (EBA, MW: 67 kDa) was also tested across cell monolayers as previously described [24,25]. For the assay cell culture medium was changed in the lower compartment of the chip to 500 μl Ringer-Hepes solution (118 mM NaCl, 4.8 mM KCl, 2.5 mM $CaCl_2$, 1.2 mM $MgSO_4$, 5.5 mM D-glucose, 10 mM Hepes, pH 7.4). In the upper compartment culture medium was replaced by 250 μl Ringer-Hepes solution containing either 10 μg/ml SF or 100 μg/ml FD and 165 μg/ml Evans blue bound to 1% bovine serum albumin (BSA) simultaneously. At 20, 40 and 60 min of the permeability assay Ringer-Hepes solution in the lower compartment was changed to a fresh 500 μl buffer. Samples from the luminal and abluminal compartments were collected. Permeability measurements were also performed on Transwell inserts using 500 μl volumes with marker molecules for the upper and 1500 μl for the lower compartments [24,25]. During the experiments inserts were kept in 12-well plates (Corning, USA) and inserts were moved after 20, 40 and 60 min to the next well of the plate. Barrier chips and plates with inserts were incubated on a horizontal shaker in the CO_2 incubator (100 rpm; Biosan, Latvia) at 37 °C for 1 h. SF and FD concentrations were determined by the same instrument using 485 nm excitation and 520 nm emission wavelengths. EBA content of samples was measured at 584 nm excitation and 680 nm emission wavelengths (Fluostar Optima, BMG Labtechnologies, Germany). Apparent permeability coefficient (P_{app}) was calculated as described previously [3].

Morphological characterization of epithelial and endothelial cell lines grown in the barrier chip was investigated by immunohistochemical staining for ZO-1 and β-catenin tight and adherens junction associated cytoplasmic linker proteins. In the triple co-culture model endothelial cells were stained for ZO-1 and β-catenin, pericytes for α-smooth muscle actin (α-SM) and astroglial cells for glial fibrillary acidic protein (GFAP). Before ZO-1 labeling double cell nucleus staining with ethidium homodimer-1 and bis-benzimide was performed to reveal cell death. After the permeability tests cells were fixed with cold acetone-methanol solution (1:1) for 10 min, washed with phosphate buffered saline (PBS) and non-specific binding sites were blocked with 3% BSA-PBS for 1 h at room temperature. Incubation with rabbit-anti-ZO-1, rabbit anti-β-catenin, mouse anti-α-SM (Dako, USA) and mouse-anti-GFAP primary antibodies lasted overnight at 4 °C. Cells were incubated with anti-rabbit secondary antibody labeled with Cy3 or anti-mouse secondary antibody labeled with Alexa Fluor 488 (Life Technologies, USA) and H33343 dye to stain nuclei for 1 h at room temperature. Between incubations cells were washed three times with PBS. Chips were disassembled, cell culture membranes were removed from the chip and were mounted in Fluoromount-G (Southern Biotech, USA), except for astroglia which were photographed *in situ* in PBS. Stainings were visualized by a Leica TCS SP5 confocal laser scanning microscope (Leica Microsystems, Germany).

2.6. Statistical analysis

Data are presented as means ± SD. Statistical significance between treatment groups was determined using two-way ANOVA following Bonferroni multiple comparison posttest (GraphPad Prism 5.0; GraphPad Software, USA). Changes were considered statistically significant at $p < 0.05$ (a, compared to Transwell inserts and b, compared to static chip conditions). All experiments were repeated at least three times, the number of parallel samples was 3–5.

3. Results and discussion

3.1. Chip structure and assembly

The structure of the barrier chip was fabricated by bonding five layers including the bottom and top glass slides with the measuring electrodes, the upper and lower channels made of PDMS, and the porous membrane (Fig. 1).

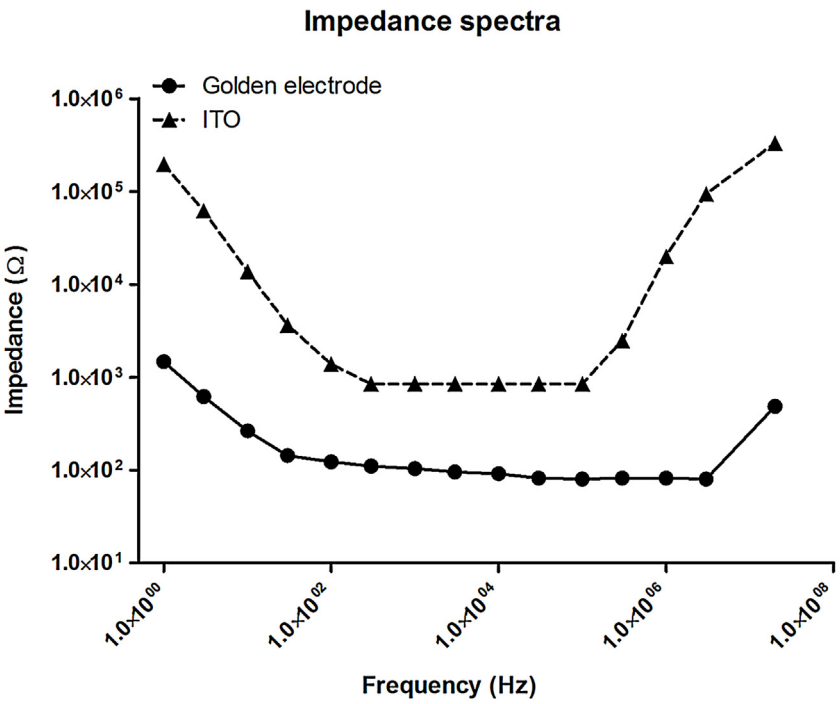

Fig. 3. Impedance spectra of the chip equipped with transparent gold and ITO electrodes, respectively. Impedance is given in Ohms (Ω), frequency is in Herz (Hz). Measurements were performed between 1 Hz and 20 MHz.

There are several setups built for similar purposes. Most of them consist of two channels, either parallel [30] or perpendicular to each other [19,31], with a relatively small overlapping area. The arrangement of our channels enables a much larger overlapping area (*ca.* 1 cm^2), allowing a larger surface and a bigger sampling size for *in vitro* permeability studies.

The thin, transparent electrodes grant a special advantage to the chip, permitting a continuous visual monitoring of the cells by a microscope, above the entire membrane surface, during the full time span of the experiment. Such a feature is missing in other model systems using nontransparent electrodes that allow visual observation limited to the narrow slits between the electrodes [16,19], therefore a full microscopic screening of the sample can only be done on the disassembled chip. This is a critical point for such assays that include monitoring of TEER or paracellular permeability of the barrier membrane, since local faults in the confluence of the cell layer, occurring usually at its perimeter and invisible for other methods, might seriously tamper the results.

We tested transparent ITO electrodes as possible candidates, and measured their resistance. Fig. 3 shows the impedance spectra of chips equipped either with a pair of transparent gold electrodes or ITO electrodes placed at the outer walls of the top and bottom channel, and separated by the porous membrane. In the low-frequency regime (between 1 Hz and 1 kHz) the electric double layer formed upon electrode polarization hinders the correct measurement of the ohmic resistance of the chip, and another dispersion process occurs in the MHz domain. In between the two extremes, the sample resistance is nearly constant, but its value is an order of magnitude smaller with gold electrodes than with the ITO ones. The high resistance of the latter (>800 Ohms) is comparable to or higher than typical TEER values of biological barriers, which might tamper the results of TEER measurements performed with ITO electrodes. This was the primary reason for which we used gold electrodes instead of ITO. Another problem was that proper electrode patterning with ITO glass was not feasible with our laboratory technique, therefore the standard four-electrode method, eliminating the effect of electrode polarization on TEER, could not be applied.

On the other hand, low-resistance "non-polarizable" electrodes (platinized platinum or Ag–AgCl) proved not to be transparent enough (extinction coefficient > 1), hampering visual observation. The choice of a 25-nm inert, gold layer for TEER electrodes was found to be the best compromise between the opposing requirements of conductance and transparency (10 Ohms, extinction coefficient 0.4, Fig. S4). Possible artifacts of the resistance measurements due to polarization of the gold electrodes were avoided by the four-electrode method. Rectangular pulses (12.5 Hz) were applied on the sample and kept controlled by a pair of electrodes, while another electrode pair was supplying load current *via* a feedback loop, to keep the transmembrane voltage constant during each half-period. The electric resistance of the system was found to be characteristic to the cell culture layer.

During the experiments, the medium was circulated by a peristaltic pump through silicone tubing (Fig. 2). PDMS blocks on the top serve both as reservoirs and in- or outlets for tubing. The input tube was immersed in the cell culture medium in the reservoir, and was connected to the inlet of the chip, while the output tube was connected to the reservoir *via* the peristaltic pump. This arrangement has three advantages: (i) the liquid pressure is always less than the air pressure outside, therefore there was no simmering or jamming failure (no "explosion"), (ii) the reservoir also acts as a bubble trap, since all bubbles (*e.g.* from leakages) burst as the liquid is dripping out from the output tube, and none of them can reach the input of the chip at the bottom of the reservoir, (iii) since the reservoir of the circulated medium is located after the pump, it is not pressurized, and the medium inside can be promptly and continuously sampled or treated very easily. That could be very useful for both long- and short-term tests of various drugs influencing the permeability of the barrier layer.

On the whole, the device enables several ways to study the barrier layer simultaneously: electric conductivity measurement, molecule permeability and microscopic visualization of the (co-)cultured cells. In addition, morphological characterization of the

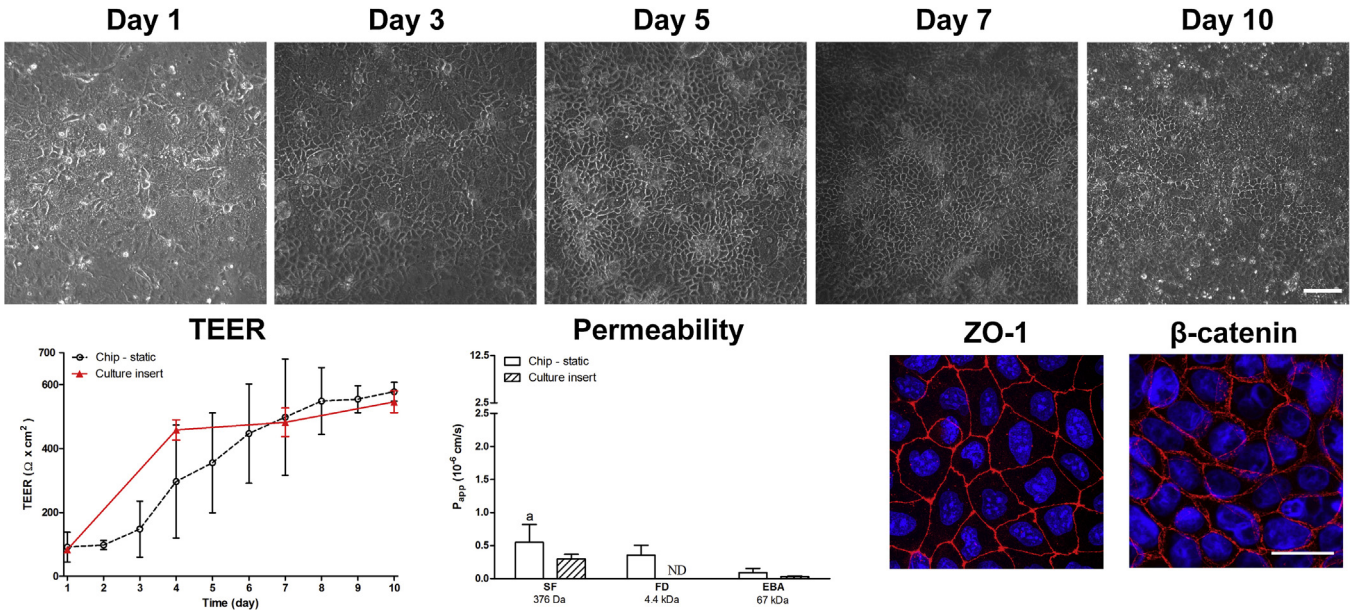

Fig. 4. Characterization of the intestinal barrier model on the chip. Phase contrast microscopy images of Caco-2 cells grown in the biochip on culture days 1–10, electrical resistance and permeability measurement data (day 10) are presented. Resistance and permeability values for cell culture inserts are also indicated. Cell morphology was characterized by ZO-1 and β-catenin immunostaining in the device and visualized by confocal microscopy. Bar = 100 μm (phase contrast images), bar = 25 μm (confocal images), ND: no data available.

layers is also possible by immunohistochemical staining. The procedure we used to create the device is not for industrial mass production. The chip is a proof-of-concept device that can be modified according to various experimental requirements. A drawback of the system is that it can be used as a disposable piece, and is not yet optimized for large scale applications like drug screening. We plan to prepare plastic, reusable versions of the chip.

3.2. Cell cultures

In order to illustrate the main features of our integrated microdevice, it was used to model four different biological barriers with cell cultures: human intestinal epithelial, lung alveolar epithelial and brain endothelial cell lines as well as a triple primary co-culture BBB model were tested for barrier function in the chip.

3.2.1. Intestinal model

The Caco-2 intestinal epithelial cell line formed the tightest monolayer among the 4 models in the microdevice, with a TEER value of $578.3 \pm 29.6\,\Omega\,cm^2$ (Fig. 4). The tightness of the barrier was also indicated by the low P_{app} for all markers (SF: 0.55×10^{-6} cm/s; FD: 0.36×10^{-6} cm/s; EBA: 0.10×10^{-6} cm/s). Cells had a cuboidal shape, grew in monolayers and stained well for ZO-1 and β-catenin. Cell morphology, good resistance and permeability properties of Caco-2 cells in the new device were similar to data obtained on Transwell culture inserts after 10 days of culturing. On culture inserts, TEER of Caco-2 monolayers reached $546.5 \pm 33.9\,\Omega\,cm^2$. There was a significant difference in the measured permeability for SF (0.30×10^{-6} cm/s) compared to the biochip, but permeability for EBA (0.03×10^{-6} cm/s) shows no difference between the insert and the chip setup. There was a higher standard deviation for TEER in biochips during the growing phase. Since it was not possible to use the same membrane type as for Transwell inserts (see Supplementary Material, Fig. S1), there could be a difference in the kinetics of cell growth due to the different culture membranes, but after cells reach confluency and begin to form the barrier, TEER values become more uniform between the parallels and reflect good barrier properties. Higher Lucifer yellow permeability has been described for the same cell type cultured in a microfluidic chamber, but that system did not allow measurement of TEER [30]. Note that Caco-2 cells in a gut-on-a-chip model have reached tighter barrier properties when co-cultured with bacteria and/or immune cells, and exposed to low shear stress and cyclic strain to mimic peristaltic motion [4,32].

3.2.2. Lung model

Lung epithelial A549 cell line grew well on the chip and easily formed monolayers (Fig. 5). Compared to the case of Caco-2 cells, these monolayers represented a weaker epithelial barrier. Lung cell layers in the chip reached a maximum TEER of a $46.4 \pm 17.0\,\Omega\,cm^2$, and these values were in concordance with our data obtained on A549 culture on Transwell inserts ($27.8 \pm 2.2\,\Omega\,cm^2$), as well as with literature data for this cell line [33]. Average P_{app} values were 1.45×10^{-6} cm/s for SF, 1.24×10^{-6} cm/s for FD and 0.17×10^{-6} cm/s for EBA markers. No significant difference was found in the permeability values as compared to data measured on culture inserts (P_{app}: 0.9×10^{-6} cm/s for FD and 0.3×10^{-6} cm/s for EBA). In accordance with the functional data, ZO-1 and β-catenin staining was not as intensive and continuous as in Caco-2 cells, indicating weaker intercellular junctions. Some lab-on-a-chip models using A549 cells [7,33,34] have already been published, but none of them offers simultaneous cell visualization, measurement of TEER and the flux of marker molecules. Concerning the lung model the chip will enable the establishment of a more complex model of the alveolar capillary unit, by the co-culture of lung epithelial cells with vascular endothelial cells at an air–liquid interface [35]. Modeling lung barriers in air–liquid interface condition is important and induces barrier properties. It is a limitation of the study that such conditions were not included.

3.2.3. Blood–brain barrier models

3.2.3.1. Brain endothelial cell line model. The human hCMEC/D3 brain endothelial cell line is a widely used, well-characterized and simplified *in vitro* model of the BBB [10]. Still, a comprehensive study on a human brain endothelial cell line in a microdevice, with a complex characterization of barrier properties including

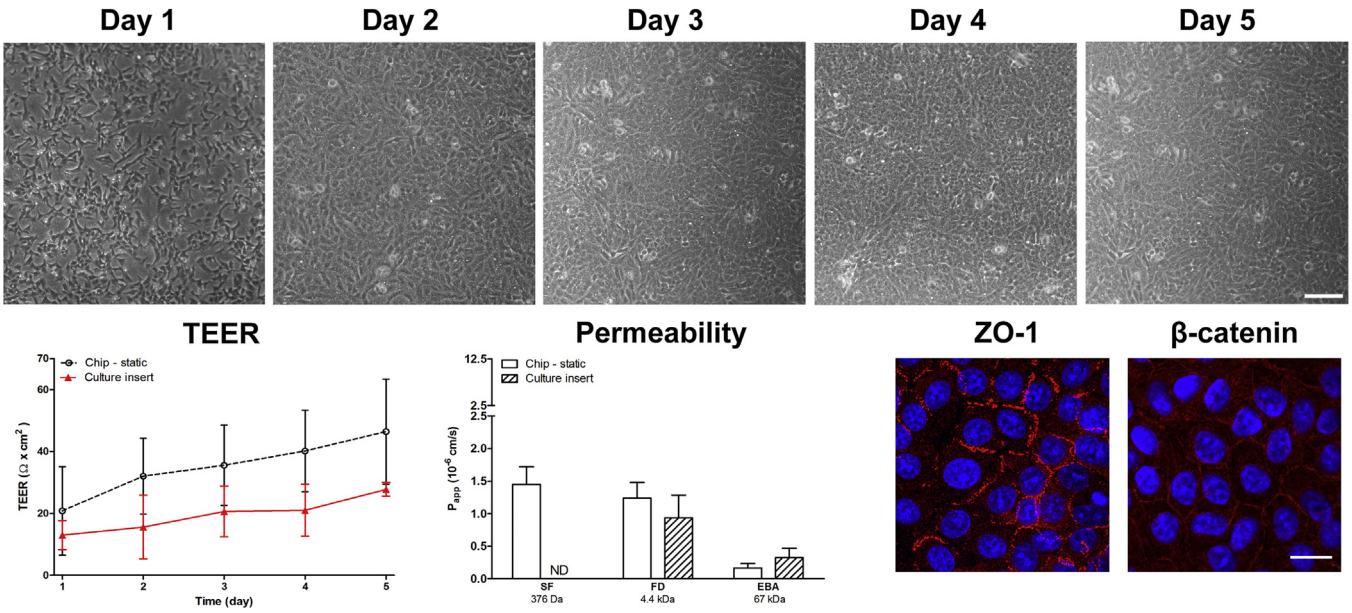

Fig. 5. Characterization of the lung epithelial barrier model on the chip. Phase contrast microscopy images of A549 cells grown in the biochip on culture days 1–5, electrical resistance and permeability measurement data (day 5) are presented. Resistance and permeability values for cell culture inserts are also indicated. Cell morphology was characterized by ZO-1 and β-catenin immunostaining in the device and visualized by confocal microscopy. Bar = 100 μm (phase contrast images), bar = 25 μm (confocal images), ND: no data available.

microscopy, has so far been missing. Previously, the rat cell line RBE4 was studied for a similar purpose [17,36]. Biochips modeling the vascular system also widely use peripheral endothelial cells [37–40].

In our miniaturized model, D3 cells grew to confluency (Fig. 6). After 3 days of static followed by 2 days of dynamic culture conditions, TEER values increased to $28.5 \pm 7.2\ \Omega\,cm^2$. TEER values of the 5-day-old static culture were in the range of $19.0 \pm 2.8\ \Omega\,cm^2$. The resistance values measured by the device were in concert with the ones obtained on culture inserts by our group ($23.7 \pm 3.5\ \Omega\,cm^2$), and with those described in the literature [10,31]. Permeability data were also compared between the static and dynamic cultures. On the static hCMEC/D3 barrier chip model, the permeability was 1.61×10^{-6} cm/s for SF, 1.55×10^{-6} cm/s for FD and 0.51×10^{-6} cm/s for EBA. Under dynamic culture conditions P_{app} of 1.57×10^{-6} cm/s for SF, 1.32×10^{-6} cm/s for FD and

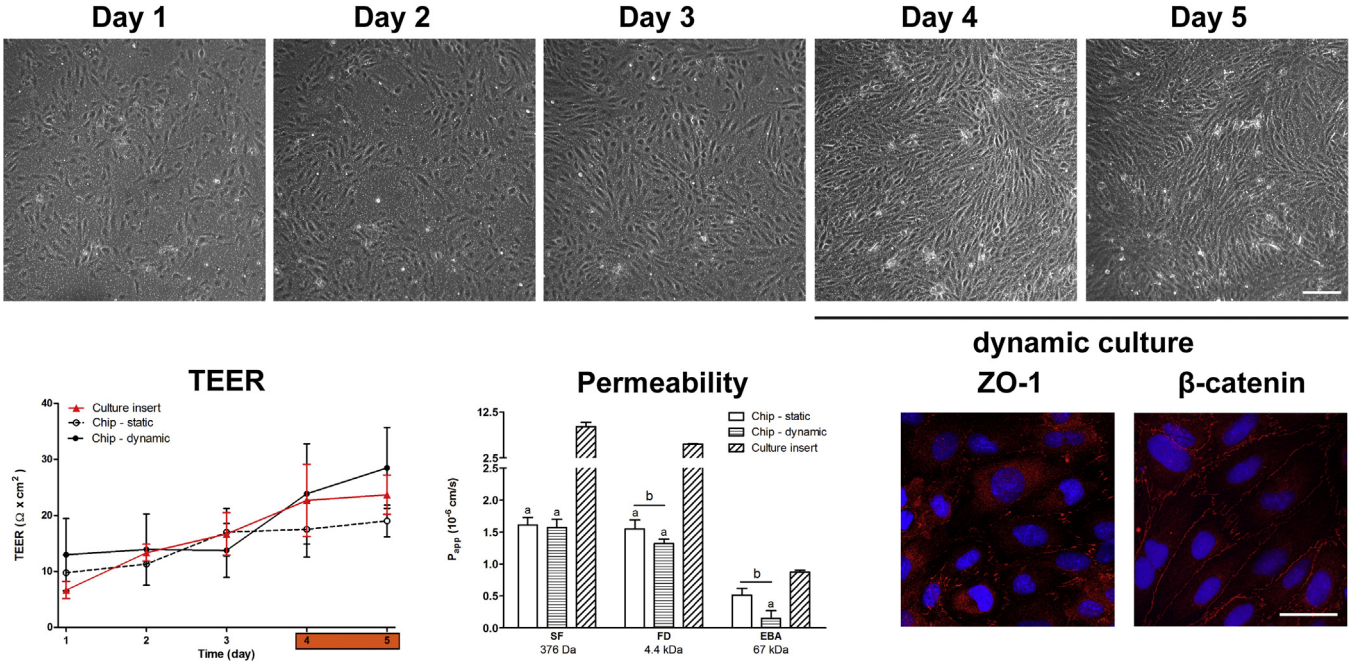

Fig. 6. Characterization of a simplified blood–brain barrier model on the chip. Phase contrast microscopy images of hCMEC/D3 human brain endothelial cells grown in the biochip on culture days 1–5, electrical resistance and permeability measurement data (day 5) are presented. Brain endothelial cells were kept under static conditions for 3 days followed by 2 days of flow (0.15 dyn) in the dynamic setup. Resistance and permeability values for cell culture inserts are also indicated. Cell morphology was characterized by ZO-1 and β-catenin immunostaining in the device and visualized by confocal microscopy. Statistically significant differences $p < 0.05$ (a, compared to culture inserts; b, compared to static chip cultures) are indicated. Bar = 100 μm (phase contrast images), bar = 25 μm (confocal images).

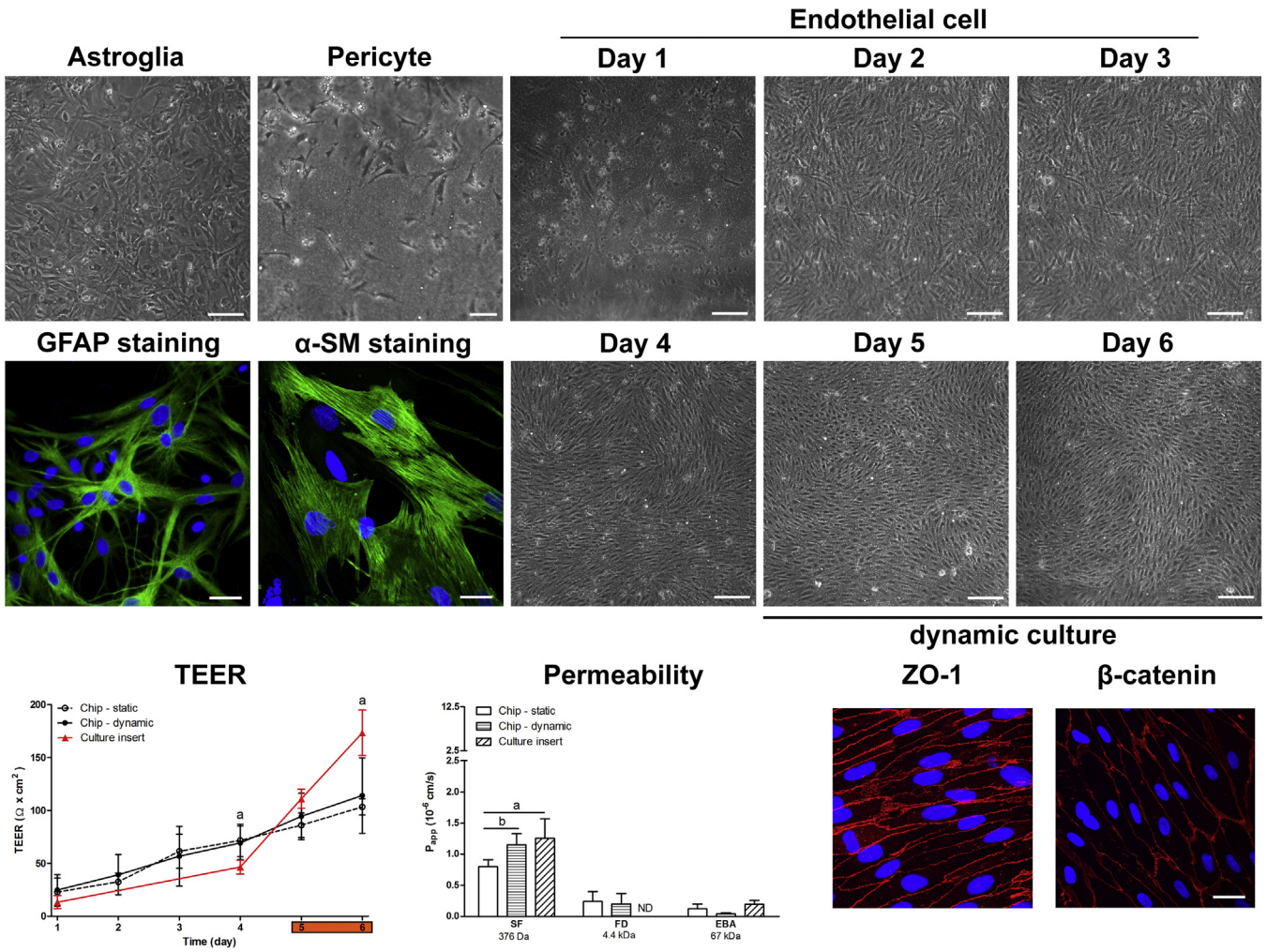

Fig. 7. Characterization of a triple co-culture blood–brain barrier model on the chip. Phase contrast microscopy images of primary rat brain endothelial cells (culture days 1–6), primary rat pericytes and glial cells (day 1), electrical resistance and permeability measurement data (day 6) are presented. Primary endothelial cells in co-culture were kept under static conditions for 3 days followed by 2 days of flow (0.15 dyn) in the dynamic setup. Cell morphology was characterized by ZO-1 and β-catenin (endothelial cells), α-smooth muscle actin (pericyte) and glial fibrillary acidic protein (astroglia) immunostaining in the device and visualized by confocal microscopy. Statistically significant difference $p < 0.05$ (a, compared to culture inserts; b, compared to static chip cultures) is indicated. Bar = 100 μm (phase contrast images), bar = 25 μm (confocal images), ND: no data available.

0.15×10^{-6} cm/s for EBA was measured. In dynamic cultures, brain endothelial permeability for FD and EBA markers was significantly lower compared to the static model in the same device. Permeability data obtained on Transwell inserts (9.31×10^{-6} cm/s for SF, 5.47×10^{-6} cm/s for FD and 0.87×10^{-6} cm/s for EBA) are in good correlation with the literature [9], but those measured in the biochip were found to be significantly lower for all marker molecules. Since we could not use the exactly same membrane type in both the Transwell and chip models as explained in the Supplementary material (Fig. S1), the effect of membrane thickness on permeability coefficients cannot be excluded. In the present study we could not reproduce the intensive increase in resistance after exposing hCMEC/D3 to shear stress [31,41], but we could observe a significantly reduced tracer permeability for larger marker molecules, indicating a barrier-tightening effect. Cells in both dynamic and static cultures were elongated, formed close contacts typical for endothelial monolayers, and stained well for ZO-1 and β-catenin (Fig. 6).

3.2.3.2. Primary cell based co-culture model of the BBB. Our primary-cell-based triple co-culture BBB model [15] was characterized for the first time in a miniaturized flow chip device. Co-culture of brain endothelial cells with glial cells and pericytes on Transwell inserts in the anatomical position (Fig. 2) was the most efficient in the induction of barrier properties as described previously by our group [15]. Brain endothelial cells in this BBB model showed higher TEER and lower permeability values, and expressed higher levels of junctional proteins than in other triple or double cultures using different combinations of brain endothelial cells, glial cells and pericytes [15] highlighting the important and functional role of pericytes. In this model, brain endothelial cells are not directly contacting pericytes or glial cells (Fig. 2). In the Transwell inserts a membrane with 0.4 μm pore size, 12 μm thickness is used (Fig. S1). A membrane with a same pore size was used in the chip, which does not allow cell migration. Growth factors and other barrier property inducing molecules are secreted into the common cell culture medium enabling communication between the three cell types through the porous culture membrane.

Cell growth in the triple BBB model was followed by phase contrast microscopy. Immunolabeling showed a typical cell shape for all three kinds of cells (Fig. 7). Endothelial cells had an elongated shape, and formed tight intercellular connections. Pericytes and glial cells were also stained by their cellular marker proteins, α-SM actin and GFAP. The rat primary triple co-culture BBB model on the chip formed a barrier with a TEER value of $114.2 \pm 35.7\ \Omega\ cm^2$. TEER values measured under static and dynamic conditions were not

significantly different. These values are lower than data obtained on culture inserts ($173.3 \pm 21.6\,\Omega\,cm^2$). Compared to the results of our previous papers the TEER of the present triple model on Transwell inserts was lower (173 *vs.* $350\,\Omega \times cm^2$; [15]), but the permeability coefficient for fluorescein was better, 0.8×10^{-6} cm/s *vs.* 4×10^{-6} cm/s indicating a good barrier. In static conditions permeability values were 0.80×10^{-6} cm/s for SF, 0.24×10^{-6} cm/s for FD and 0.12×10^{-6} cm/s for EBA on the BBB model. These permeability coefficient values are similar to data of previously described BBB models on Transwell inserts [3] and indicate a tight barrier. Dynamic cultures were kept under flow conditions for 48 h, then permeability measurements were performed. P_{app} values for the dynamic model were 1.15×10^{-6} cm/s for SF, 0.20×10^{-6} cm/s for FD and 0.04×10^{-6} cm/s for EBA. An elevated flux of SF across the monolayer was found after introducing low shear stress on the triple model. The permeability for SF on the triple BBB model grown on cell culture inserts was higher compared to the static biochip model (1.25×10^{-6} cm/s for SF and 0.19×10^{-6} cm/s for EBA). There was no difference in the flux of the other two permeability markers after flow conditions, neither in the static chip compared to the dynamic model, nor in the chip models compared to the Transwell inserts. In our setup, the low-shear-stress exposure did not elevate the resistance of primary endothelial cells. All these data indicate that under low flow conditions, barrier properties typical for venules may develop in a BBB model [21]. The different biological response in a brain endothelial cell line as compared to primary cells emphasizes the difference between such models [42].

3.3. General considerations and comparison with other biochips modeling biological barriers

In the permeability assays Caco and primary brain endothelial cell based models which have the highest resistance, have the lowest permeability and the A549 and D3 models which present low resistance show high permeability for the markers (Figs. 4–7; Fig. S2), in agreement with literature data. All barrier models were tested with double cell nucleus staining to reveal cell death. No red staining for nuclei was observed, indicating viable and functioning cells both in the static and dynamic models.

While several barrier functions were monitored, some aspects of barrier functions in the present study were not investigated. Mucus layers are present and important for intestinal and lung barriers including drug absorption [43]. In a recent three-dimensional model mimicking the microenvironment of the small intestine transport properties closer to the *in vivo* situation were measured [44]. At the blood–brain barrier the luminal surface of brain endothelium is covered by a relatively thick layer of glycocalyx which also acts as a physicochemical barrier blocking drug delivery [45]. We aim to further develop the culture models to study these more complex interactions. Culture models of barriers on planar surfaces represent simplified systems, where imaging, measurement of resistance, or drug transport studies are easier. However there are models using 3D scaffold which represent more complex systems mimicking the anatomical position of cells, for example a culture model of the small intestine [44].

The field of biochips modeling gut, lung and blood–brain barriers is rapidly evolving and several models were developed in the last ten years which are listed in Table 1. These complex biochips integrate different types of imaging, microfluidics, measurement of resistance in mono- and co-culture systems. To our best knowledge the present paper is the first in which the same device is used for three different types of barrier models, resistance is measured by transparent gold electrodes, and cellular growth can be monitored through the whole length of the device, not only through a small window. The triple cell culture model of the BBB we described on Transwell inserts was also investigated for the first time in a biochip

Table 1
Comparison of microdevices developed for modeling biological barriers.

Microdevice						Culture model				Refs.
Imaging		Flow	Permeabilty	TEER		Barrier	Cell	Human	Co-culture with	
PhC	Fluo			Instrument	Electrode					
–	+	+	+	–	–	Gut	Caco-2 cell line	+	–	[30]
–	–	+	+	–	–	Gut	Caco-2 cell line	+	Vascular endothelial cell	[44]
+	+	+	+	87V Industrial Multimeter	Ag/AgCl wire	Gut	Caco-2 cell line	+	Bacteria	[32]
–	+	+	–	–	–	Gut	HT29 cell line	+	Primary neurons	[46]
–	–	+	–	–	–	Lung	A549 cell line	+	–	[7]
–	–	+	+	EVOM volt-ohm meter	ND	Lung	A549 cell line	+	–	[33]
+	+	+	+	Modified volt-ohm meter	Ag/AgCl wire	Lung	Alveolar epithelial cell	+	Vascular endothelial cell	[47]
+	+	+	–	–	–	Lung	A549 cell line	+	–	[34]
–	+	+	+	EVOM volt-ohm meter	Ag/AgCl chopstick	Lung	Calu-3 cell line	+	–	[48]
+	+	+	–	–	–	Lung	A549 cell line	+	–	[49]
–	–	+	+	–	–	BBB	Brain endothelial	+	astrocyte	[50]
–	–	+	+	Flocel volt-ohm meter	Built in electrodes	BBB	hCMEC/D3 cell line	–	–	[41]
–	+	+	–	HP4194A impedance analyzer	Pt wire	BBB	hCMEC/D3 cell line	+	–	[31]
+	+	–	+	–	–	BBB	RBE4 cell line	–	Mixed glia and neuron culture	[36]
+	+	+	+	–	–	BBB	RBE4 cell line	–	–	[17]
–	–	+	+	Flocel volt-ohm meter	Built in electrodes	BBB	Brain endothelial	+	Astroglia, muscle	[21]
+	+	+	+	–	–	BBB	hBMVEC cell line	+	hAST glia cell line	[51]
–	+	+	+	EVOM2 volt-ohm meter	Au/Ag/AgCl film	BBB	bEnd.3 cell line	–	Glia or glioma cell line	[16,19,52]
+	+	+	–	EVOM volt-ohm meter	Transparent Au film	Gut	Caco-2 cell line	+	–	Present model
+	+	+	–			Lung	A-549 cell line	+	–	
+	+	+	+			BBB	hCMEC/D3 cell line	+	–	
+	+	+	+			BBB	Brain endothelial	–	Pericyte, glial cell	

Abbreviations: ND, no data.

and under fluid flow. Integrated, complex microfluidic devices with co-culture systems were already described for gut [32] and lung [47] barrier models imitating micromovements, but no BBB model was established in an integrated chip with all the functions we described in the present manuscript.

4. Conclusion and perspectives

The aim of the study was to develop a general-purpose device that can be used to investigate multiple types of biological barriers as mono-, double- or triple cultures monitoring the electric conductivity and molecular permeability of the (co-)cultured cells under no flow or low flow conditions, at the same time allowing microscopic visualization of the whole membrane surface. The miniaturized chip was successfully used to model three different biological barriers with four types of cell cultures. Human intestinal epithelial, lung alveolar epithelial and brain endothelial cells grew all well in the new microdevice, and showed cell morphology and barrier functions similar to cultures on inserts. A similar co-culture of epithelial and endothelial cells may represent an anatomically more realistic model of the intestinal epithelium in the device and a novel approach to study oral absorption of drugs. The biochip was also suitable for modeling the BBB: formation of barriers was observed for both the brain endothelial cell line and the co-culture model. The triple primary co-culture blood–brain barrier model was established on a lab-on-a-chip device and investigated under fluid flow for the first time. The barrier-inducing effect of flow could be observed for the brain endothelial cell line, and further modification of the chip will permit the study of different flow and shear stress conditions. The device is expected to be a versatile tool for further examination of biological barriers, among them endothelial barrier functions under flow conditions.

Conflict of interest

There is a pending patent application on this topic. Authors declare that in connection to the present work there is no other potential conflict of interest.

Acknowledgements

This work was supported by the following grants: OTKA K-101821, OTKA NN-102624 and TÁMOP-4.2.2.A-11/1/KONV-2012–0047. Fruzsina Walter received a fellowship for young researchers from the Hungarian Academy of Sciences. Hereby we acknowledge the help of Alexandra Bocsik and Dr. Lóránd Kiss for providing cell culture insert permeability and resistance data.

Appendix A. Supplementary data

Supplementary data associated with this article can be found, in the online version, at http://dx.doi.org/10.1016/j.snb.2015.07.110

References

[1] M.A. Deli, Potential use of tight junction modulators to reversibly open membraneous barriers and improve drug delivery, Biochim. Biophys. Acta 1788 (2009) 892–910.
[2] M.A. Deli, C.S. Ábrahám, Y. Kataoka, M. Niwa, Permeability studies on in vitro blood–brain barrier models: physiology, pathology, and pharmacology, Cell. Mol. Neurobiol. 25 (2005) 59–127.
[3] E. Hellinger, S. Veszelka, A.E. Tóth, F.R. Walter, Á. Kittel, M.L. Bakk, K. Tihanyi, V. Háda, S. Nakagawa, T.D. Duy, M. Niwa, M.A. Deli, M. Vastag, Comparison of brain capillary endothelial cell-based and epithelial (MDCK-MDR1, Caco-2, and VB-Caco-2) cell-based surrogate blood–brain barrier penetration models, Eur. J. Pharm. Biopharm. 82 (2012) 340–351.
[4] Q. Ramadan, H. Jafarpoorchekab, C. Huang, P. Silacci, S. Carrara, G. Koklü, J. Ghaye, J.J. Ramsden, C. Ruffert, G. Vergeres, M.A.M. Gijs, NutriChip: nutrition analysis meets microfluidics, Lab Chip 13 (2013) 196–203.
[5] L. Kiss, F.R. Walter, A. Bocsik, S. Veszelka, B. Ózsvári, L.G. Puskás, P. Szabó-Révész, M.A. Deli, Kinetic analysis of the toxicity of pharmaceutical excipients Cremophor EL and RH40 on endothelial and epithelial cells, J. Pharm. Sci. 102 (2013) 1173–1181.
[6] L. Kiss, É. Hellinger, A.M. Pilbat, Á. Kittel, Z. Török, A. Füredi, G. Szakács, S. Veszelka, P. Sipos, B. Ózsvári, L.G. Puskás, M. Vastag, P. Szabó-Révész, M.A. Deli, Sucrose esters increase drug penetration, but do not inhibit P-glycoprotein in Caco-2 intestinal epithelial cells, J. Pharm. Sci. 103 (2014) 3107–3119.
[7] S. Bakand, C. Winder, C. Khalil, A. Hayes, An experimental in vitro model for dynamic direct exposure of human cells to airbone contaminants, Toxicol. Lett. 165 (2006) 1–10.
[8] L. Wang, R. Taneja, W. Wang, L.J. Yao, R.A. Veldhuizen, S.E. Gill, D. Fortin, R. Inculet, R. Malthaner, S. Mehta, Human alveolar epithelial cells attenuate pulmonary microvascular endothelial permeability under septic conditions, PLoS ONE 8 (2013) e55311.
[9] B.B. Weksler, E.A. Subileau, N. Perrière, P. Charneau, K. Holloway, M. Leveque, H. Tricoire-Leignel, A. Nicotra, S. Bourdoulous, P. Turowski, D.K. Male, F. Roux, J. Greenwood, I.A. Romero, P.O. Couraud, Blood–brain barrier-specific properties of a human adult brain endothelial cell line, FASEB J. 19 (2005) 1872–1874.
[10] B. Weksler, I.A. Romero, P.O. Couraud, The hCMEC/D3 cell line as a model of the human blood brain barrier, Fluids Barriers CNS 10 (2013) 16.
[11] A.E. Tóth, F.R. Walter, A. Bocsik, P. Sántha, S. Veszelka, L. Nagy, L.G. Puskás, P.O. Couraud, F. Takata, S. Dohgu, Y. Kataoka, M.A. Deli, Edaravone protects against methylglyoxal-induced barrier damage in human brain endothelial cells, PLoS ONE 9 (2014) e100152.
[12] M.A. Deli, Drug transport and the blood–brain barrier, in: K. Tihanyi, M. Vastag (Eds.), Solubility, Delivery and ADME Problems of Drugs and Drug-Candidates, Bentham Science Ltd., Washington, 2011, pp. 144–165.
[13] A.E. Tóth, S. Veszelka, S. Nakagawa, M. Niwa, M.A. Deli, Patented in vitro blood–brain barrier models in CNS drug discovery, Recent Pat. CNS Drug Discov. 6 (2011) 107–118.
[14] S. Nakagawa, M.A. Deli, S. Nakao, M. Honda, K. Hayashi, R. Nakaoke, Y. Kataoka, M. Niwa, Pericytes from brain microvessels strengthen the barrier integrity in primary cultures of rat brain endothelial cells, Cell. Mol. Neurobiol. 27 (2007) 687–694.
[15] S. Nakagawa, M.A. Deli, H. Kawaguchi, T. Shimizudani, T. Shimono, Á. Kittel, K. Tanaka, M. Niwa, A new blood–brain barrier model using primary rat brain endothelial cells, pericytes and astrocytes, Neurochem. Int. 54 (2009) 253–263.
[16] R. Booth, H. Kim, Characterization of a microfluidic in vitro model of the blood–brain barrier (μBBB), Lab Chip 12 (2012) 1784–1792.
[17] B. Prabhakarpandian, M.C. Shen, J.B. Nichols, I.R. Mills, M. Sidoryk-Wegrzynowicz, M. Aschner, K. Pant, SyM-BBB: a microfluidic Blood Brain Barrier model, Lab Chip 13 (2013) 1093–1101.
[18] W. Neuhaus, R. Lauer, S. Oelzant, U.P. Fringeli, G.F. Ecker, C.R. Noe, A novel flow based hollow-fiber blood–brain barrier in vitro model with immortalized cell line PBMEC/C1-2, J. Biotechnol. 125 (2006) 127–141.
[19] R. Booth, S. Noh, H. Kim, A multiple-channel, multiple-assay platform for characterization of full-range shear stress effects on vascular endothelial cells, Lab Chip 14 (2014) 1880–1890.
[20] S.K. Mahto, V. Charwat, P. Ertl, B. Rothen-Rutishauser, S.W. Rhee, J. Sznitman, Microfluidic platforms for advanced risk assessments of nanomaterials, Nanotoxicology 9 (2015) 381–395.
[21] L. Cucullo, M. Hossain, W. Tierney, D. Janigro, A new dynamic in vitro modular capillaries-venules modular system: cerebrovascular physiology in a box, BMC Neurosci. 14 (2013) 18.
[22] E. Hellinger, M.L. Bakk, P. Pócza, K. Tihanyi, M. Vastag, Drug penetration model of vinblastine-treated Caco-2 cultures, Eur. J. Pharm. Sci. 41 (2010) 96–106.
[23] S. Veszelka, M. Pásztói, A.E. Farkas, I. Krizbai, T.K. Ngo, M. Niwa, C.S. Ábrahám, M.A. Deli, Pentosan polysulfate protects brain endothelial cells against bacterial lipopolysaccharide-induced damages, Neurochem. Int. 50 (2007) 219–228.
[24] S. Veszelka, A.E. Tóth, F.R. Walter, Z. Datki, E. Mózes, L. Fülöp, Z. Bozsó, É. Hellinger, M. Vastag, B. Orsolits, Z. Környei, B. Penke, M.A. Deli, Docosahexaenoic acid reduces amyloid-β induced toxicity in cells of the neurovascular unit, J. Alzheimers Dis. 36 (2013) 487–501.
[25] P. Hülper, S. Veszelka, F.R. Walter, H. Wolburg, P. Fallier-Becker, J. Piontek, I.E. Blasig, M. Lakomek, W. Kugler, M.A. Deli, Acute effects of short-chain alkylglycerols on blood–brain barrier properties of cultured brain endothelial cells, Br. J. Pharmacol. 169 (2013) 1561–1573.
[26] S. Liebner, M. Corada, T. Bangsow, J. Babbage, A. Taddei, C.J. Czupalla, M. Reis, A. Felici, H. Wolburg, M. Fruttiger, M.M. Taketo, H. von Melchner, K.H. Plate, H. Gerhardt, E. Dejana, Wnt/beta-catenin signaling controls development of the blood–brain barrier, J. Cell Biol. 183 (2008) 409–417.
[27] S.H. Ramirez, S. Fan, M. Zhang, A. Papugani, N. Reichenbach, H. Dykstra, A.J. Mercer, R.F. Tuma, Y. Persidsky, Inhibition of glycogen synthase kinase 3β (GSK3β) decreases inflammatory responses in brain endothelial cells, Am. J. Pathol. 176 (2010) 881–892.
[28] N. Perrière, P. Demeuse, E. Garcia, A. Regina, M. Debray, J.P. Andreux, P. Couvreur, J.M. Scherrmann, J. Temsamani, P.O. Couraud, M.A. Deli, F. Roux, Puromycin-based purification of rat brain capillary endothelial cell cultures. Effect on the expression of blood–brain barrier-specific properties, J. Neurochem. 93 (2005) 279–289.

[29] E.A. Jähne, D.E. Eigenmann, M. Culot, R. Cecchelli, F.R. Walter, M.A. Deli, R. Tremmel, G. Fricker, M. Smiesko, M. Hamburger, M. Oufir, Development and validation of a LC–MS/MS method for assessment of an anti-inflammatory indolinone derivative by in vitro blood–brain barrier models, J. Pharm. Biomed. Anal. 98 (2014) 235–246.
[30] Y. Imura, Y. Asano, K. Sato, E. Yoshimura, A microfluidic system to evaluate intestinal absorption, Anal. Sci. 25 (2009) 1403–1407.
[31] L.M. Griep, F. Wolbers, B. de Wagenaar, P.M. ter Braak, B.B. Weksler, I.A. Romero, P.O. Couraud, I. Vermes, A.D. van der Meer, A. van den Berg, BBB on chip: microfluidic platform to mechanically and biomechanically modulate blood–brain barrier function, Biomed. Microdevices 15 (2013) 145–150.
[32] H.J. Kim, D. Huh, G. Hamilton, D.E. Ingber, Human gut-on-a-chip inhabited by microbial flora that experiences intestinal peristalsis-like motions and flow, Lab Chip 12 (2012) 2164–2165.
[33] D.D. Nalayanda, C. Puleo, W.B. Fulton, L.M. Sharpe, T.H. Wang, F. Abdullah, An open-access microfluidic model for lung-specific functional studies at an air–liquid interface, Biomed. Microdevices 11 (2009) 1081–1089.
[34] S.H. Kim, S.M. Hwang, J.M. Lee, J.H. Kang, I.Y. Chung, B.G. Chung, Epithelial-to-mesenchymal transition of human lung alveolar epithelial cells in a microfluidic gradient device, Electrophoresis 34 (2013) 441–447.
[35] K.L. Sellgren, E.J. Butala, B.P. Gilmour, S.H. Randell, S. Grego, A biomimetic multicellular model of the airways using primary human cells, Lab Chip 14 (2014) 3349–3358.
[36] A.K. Achyuta, A.J. Conway, R.B. Crouse, E.C. Bannister, R.N. Lee, C.P. Katnik, A.A. Behensky, J. Cuevas, S.S. Sundaram, A modular approach to create neurovascular unit-on-a-chip, Lab Chip 13 (2013) 542–553.
[37] O.F. Khan, M.V. Sefton, Endothelial cell behaviour within a microfluidic mimic of the flow channels of a modular tissue engineered construct, Biomed. Microdevices 13 (2011) 69–87.
[38] L.T. Chau, B.E. Rolfe, J.J. Cooper-White, A microdevice for the creation of patent, three-dimensional endothelial cell-based microcirculatory networks, Biomicrofluidics 5 (2011) 34115–3411514.
[39] S. Kim, H. Lee, M. Chung, N.L. Jeon, A label-free DC impedance-based microcytometer for circulating rare cancer cell counting, Lab Chip 13 (2013) 1489–1500.
[40] C. Fede, I. Fortunati, L. Petrelli, D. Guidolin, R. De Caro, C. Ferrante, G. Albertin, An easy-to-handle microfluidic device suitable for immunohistochemical procedures in mammalian cells under flow conditions, Eur. J. Histochem. 58 (2014) 2360.
[41] L. Cucullo, P.O. Couraud, B. Weksler, I.A. Romero, M. Hossain, E. Rapp, D. Janigro, Immortalized human brain endothelial cells and flow-based vascular modeling: a marriage of convenience for rational neurovascular studies, J. Cereb. Blood Flow Metab. 28 (2008) 312–328.
[42] S. Veszelka, A. Kittel, M.A. Deli, Tools of modelling blood–brain barrier penetrability, in: K. Tihanyi, M. Vastag (Eds.), Solubility, Delivery and ADME Problems of Drugs and Drug-Candidates, Bentham Science Ltd., Washington, 2011, pp. 166–188.
[43] H.H. Sigurdsson, J. Kirch, C.M. Lehr, Mucus as a barrier to lipophilic drugs, Int. J. Pharm. 453 (2013) 56–64.
[44] J. Pusch, M. Votteler, S. Göhler, J. Engl, M. Hampel, H. Walles, K. Schenke-Layland, The physiological performance of a three-dimensional model that mimics the microenvironment of the small intestine, Biomaterials 32 (2011) 7469–7478.
[45] F. Hervé, N. Ghinea, J.M. Scherrmann, CNS delivery via adsorptive transcytosis, AAPS J. 10 (2008) 455–472.
[46] C. Greß, M. Jeziorski, M. Saumer, K.H. Schäfer, Simulation of in-vivo-equivalent epithelial barriers using a micro fluidic device, Biomed. Microdevices 16 (2014) 191–198.
[47] D. Huh, B.D. Matthews, A. Mammoto, M. Montoya-Zavala, H.Y. Hsin, D.E. Ingber, A mechanosensitive transcriptional mechanism that controls angiogenesis, Science 328 (2010) 1662–1668.
[48] L. Bol, J.C. Galas, H. Hillaireau, I. Le Potier, V. Nicolas, A.M. Haghiri-Gosnet, E. Fattal, M. Taverna, A microdevice for parallelized pulmonary permeability studies, Biomed. Microdevices 16 (2014) 277–285.
[49] S.K. Mahto, J. Tenenbaum-Katan, A. Greenblum, B. Rothen-Rutishauser, J. Sznitman, Microfluidic shear stress-regulated surfactant secretion in alveolar epithelial type II cells in vitro, Am. J. Physiol. Lung Cell Mol. Physiol. 306 (2014) L672–L683.
[50] V. Siddharthan, Y.V. Kim, S. Liu, K.S. Kim, Human astrocytes/astrocyte-conditioned medium and shear stress enhance the barrier properties of human brain microvascular endothelial cells, Brain Res. 1147 (2007) 39–50.
[51] Y. Takeshita, B. Obermeier, A. Cotleur, Y. Sano, T. Kanda, R.M. Ransohoff, An in vitro blood–brain barrier model combining shear stress and endothelial cell/astrocyte co-culture, J. Neurosci. Methods 232 (2014) 165–172.
[52] R. Booth, H. Kim, Permeability analysis of neuroactive drugs through a dynamic microfluidic in vitro blood–brain barrier model, Ann. Biomed. Eng. 42 (2014) 2379–2391.

Biographies

Fruzsina R. Walter obtained her MSc in biology at the University of Szeged, Hungary in 2010. She conducts her PhD studies (delivery of drugs to the central nervous system by opening the blood brain barrier) at the Biological Research Centre, Szeged, Hungary. She is currently a junior research associate in the Institute of Biophysics of the Centre. Her present works include the development and study of novel culture models of the blood–brain and other barriers using microfluidic devices. She received several prizes and recognitions for her achievements as a research student.

Sándor Valkai is a staff scientist of the Institute of Biophysics, Biological Research Center of the Hungarian Academy of Sciences. He received his MS diploma in physics in 1995 at József Attila University Szeged, Hungary. He got a PhD degree at the Veszprém University, Veszprém, Hungary in 1999. He was a post doc at Bar-Ilan University, Ramat Gan, Israel between 1999 and 2001. From 2002, he deals with integrated optics and nanotechnology in BRC, Szeged. He is co-author of several scientific papers and patents.

András Kincses is a PhD student of the University of Szeged, Hungary, working in the Institute of Biophysics, Biological Research Centre, under the supervision of A.D. His research interest is connected mainly with elaborating alternative electrophysiological techniques for measurement of electric signals associated to cell physiological processes. As a visiting student, he has been invited to the Max Planck Institute of Biophysics, Frankfurt am Main, Germany, and to the Technical University of Denmark, Copenhagen. He is the first author or co-author of several scientific publications.

András Petneházi and **Tamás Czeller** have prepared their BSc theses in the Institute of Biophysics, BRC, concerning the biological application of various lab-on-a-chip devices. The diploma works were carried out under the supervision of M.D. and A.D., in the framework of the undergraduate degree program "Molecular Bionics" of the University of Szeged.

Szilvia Veszelka is a postdoctoral research associate at the Biological Research Centre, Szeged, Hungary. She received both her MSc in 2003 and PhD degree in 2007 at the University of Szeged, Hungary. After obtaining her PhD thesis (protection against blood–brain barrier damages in pathological conditions) she started a new project on drug targeting to brain by different nanoparticles decorated with ligands of solute carriers or transporters. She was awarded two research grants for young investigators from Gedeon Richter Plc., Hungary. Her present studies are funded by a postdoctoral research grant from the Hungarian Scientific Research Fund.

Pál Ormos is the director general of the Biological Research Center of the Hungarian Academy of Sciences. He has MSc (1975) and PhD (1982) in physics from Jozsef Attila University Szeged. He is an ordinary member of the Hungarian Academy of Sciences (1994). P. Ormos is honorary president of the Hungarian Biophysical Society. Between 2002 and 2005 he served as vice president of IUPAP (International Union of Pure and Applied Physics). P. Ormos's research is focused on single particle observation, optical micromanipulation and nanobiotechnology. He is author or co-author of *ca.* 100 publications and there are over 4000 citations to them. He is an elected Fellow of the American Physical Society.

Mária A. Deli is a group leader and scientific advisor at the Biological Research Centre, Szeged, Hungary, a Center of Excellence of the European Union. She graduated as an MD and received a PhD degree from the University of Szeged. Her main research interests include culture models of biological barriers, blood–brain barrier protection in pathologies like Alzheimer's disease and diabetes, drug targeting to brain by different strategies, blood–brain barrier models for central nervous system drug testing. She has published 81 PubMed indexed research articles including 9 reviews, and 12 book chapters (independent citations over 2400, Hirsch index: 31). Present research team includes 3 postdoctoral researchers, 3 PhD students and 8 undergraduate students.

András Dér is a group leader and scientific advisor of the Institute of Biophysics, Biological Research Center of the Hungarian Academy of Sciences, Szeged, Hungary. He received an MS diploma in physics in 1980 at József Attila University Szeged, Hungary, a CSc (PhD) and a DSC degree from the Hungarian Academy of Sciences in 1988 and 1999, respectively. He has been the co-president of the Biophysics Committee of the Hung. Acad. Sci., and the vice president of the Hungarian Biophysical Society. His major research area is protein dynamics and bioelectronics. Together with his colleagues, he is named as inventor on several granted and pending patents about the photonic application of biomaterials.

II.

Kincses A, Santa-Maria AR, Walter FR, Dér L, Horányi N, Lipka DV, Valkai S, Deli MA, Dér A. A chip device to determine surface charge properties of confluent cell monolayers by measuring streaming potential. Lab. Chip. 2020;20(20):3792-3805. IF: 6.774

Lab on a Chip

PAPER

Cite this: *Lab Chip*, 2020, **20**, 3792

A chip device to determine surface charge properties of confluent cell monolayers by measuring streaming potential†

András Kincses,[ab] Ana R. Santa-Maria, [ac] Fruzsina R. Walter, [ad] László Dér,[a] Nóra Horányi,[a] Dóra V. Lipka,[a] Sándor Valkai, [a] Mária A. Deli *[a] and András Dér *[a]

Received 29th May 2020,
Accepted 4th September 2020

DOI: 10.1039/d0lc00558d

rsc.li/loc

Cell surface charge is an important element of the function of biological barriers, but no chip device has been described to measure cell surface charge properties of confluent barrier cell monolayers. The aim of this study was the design and fabrication of a dynamic lab-on-a-chip (LOC) device which is suitable to monitor transcellular electrical resistance, as well as streaming potential parallel to the surface of cell layers. We successfully measured the streaming potential of a biological barrier culture model with the help of our previously published versatile lab-on-a-chip device equipped with two Ag/AgCl electrodes. The inclusion of these "zeta electrodes", a voltage preamplifier and an oscilloscope in our set-up made it possible to successfully record signals describing the surface charge properties of brain endothelial cell monolayers, used as a barrier model in our experiments. Data obtained on the new chip device were verified by comparing streaming potential results measured in the LOC device and zeta potential results by the commonly used laser-Doppler velocimetry (LDv) method and model simulations. Changes in the negative surface charge of the barrier model by treatments with neuraminidase enzyme modifying the cell membrane glycocalyx or lidocaine altering the lipid membrane charge could be measured by both the upgraded LOC device and LDv. The new chip device can help to gain meaningful new information on how surface charge is linked to barrier function in both physiological and pathological conditions.

Introduction

The physical and physico-chemical parameters of mammalian cells and their outer membrane are important to determine their integrity and function. In general, plasma membranes possess an overall negative charge which is derived from sulfate and sialic acid residues of the cell surface glycocalyx and negative lipid headgroups phosphatidylserine and phosphatidylinositol of the lipid bilayer.[1,2] Basic biological processes regulated by membrane charge include binding and sorting of charged proteins[1] and processes like immune homeostasis and cancer cell attachment, migration and metastasis formation.[3]

Biological barriers are layers of tightly attached epithelial or endothelial cells specialized for the protection of the organism from the environment and special organs within the body.[4] The negative surface charge of the cell layers is an important element of the defense system of barriers. The role of the negatively charged glycocalyx of the vascular endothelial barrier for example is well known in the protection of the cardiovascular system which can be damaged in diseases like atherosclerosis, ischemia due to blood vessel occlusion, diabetes, nephropathy, inflammation and sepsis.[5,6] The glycocalyx of biological barriers is also important in microbiological infections: the neuraminidase enzyme of different bacteria and viruses contribute to their virulence: for example, the neuraminidase of influenza viruses, causing pandemics, facilitates virus release by cleaving sialic acid residues.[7]

An important inner biological barrier, the blood–brain barrier (BBB), is a complex interface separating the central nervous system and the blood circulation. Cerebral endothelial cells lining the blood vessels in the brain have very specific properties within the vascular system.[8] Brain capillary endothelial cells have an inherent role in forming the gatekeeping functions of the BBB, which consist of interendothelial tight junctions, low amount of intracellular vesicles, specialized and polarized influx and efflux transport systems.[9,10] The overall negative surface charge of endothelial

[a] *Institute of Biophysics, Biological Research Centre, Szeged, Hungary. E-mail: deli.maria@brc.hu, der.andras@brc.hu*
[b] *Doctoral School of Multidisciplinary Medical Sciences, University of Szeged, Hungary*
[c] *Doctoral School of Biology, University of Szeged, Hungary*
[d] *Department of Cell Biology and Molecular Medicine, University of Szeged, Hungary*

† Electronic supplementary information (ESI) available. See DOI: 10.1039/d0lc00558d

cells of brain microvessels is higher than that of other vascular endothelial cells measured by laser-Doppler velocimetry (LDv).[2] On one hand, this negative charge of cerebral endothelial cells correlated with their higher phosphatidylserine and phosphatidylinositol content in the plasma membrane.[2] On the other hand, the glycocalyx of cerebral endothelial cells is denser and covers larger areas of the microvessel lumen, than in the heart or lung.[11] In addition, after vascular injury induced by lipopolysaccharide, the endothelial glycocalyx coverage decreased in the brain but almost completely disappeared in the peripheral organs heart and lung, indicating that the brain specific ultrastructure of the glycocalyx is an important element of the defense system of the BBB.[11] This surface glycocalyx on brain endothelial cells is built from a mesh of glycolipids, sialo-glycoconjugates and heparan sulfate proteoglycans.[12,13] The negative surface charge at the BBB is not only providing an extra barrier function for the brain endothelial layer, but is also important in the regulation of the passage of charged molecules including drugs, delivery vectors and nanoparticles[12,14–17] across the monolayer.

Therefore, a quantitative description of the surface electric properties of cell layers forming biological barriers is essential for the broader understanding of their function in physiological processes and diseases. A well-measurable physical quantity to characterize the charge density of surfaces in contact with fluids is the so-called zeta potential.[18] Counter-ions of the liquid solution are distributed close to the charged surface of the particle, where, subject to Coulomb force and Brownian motion, form a diffuse, electric double layer. Part of the ions inside the double layer is occluded in an adsorbed layer of water molecules (the "shear layer"), which, under flow conditions, does not move with the stream. The surface potential, therefore, cannot be measured directly, only the potential difference between the surface of the shear layer and the bulk of the liquid solution, which is called zeta potential. The most widely used method to measure zeta potential of suspended particles in a solvent (colloid particles or cells in an aqueous electrolyte) is LDv, which is able to detect the electrophoretic mobility of the microscopic particles with high precision,[19] from which the zeta potential can be calculated. The group of Castanho measured the zeta potential of different mammalian cells in single cell suspension by the LDv method and revealed that brain endothelial cells have more negative zeta potential than other types of cells or endothelial cells from other vascular bed.[2] Using this technique, we have directly measured zeta potential changes in brain endothelial cells treated with lidocaine, a cationic lipophilic drug molecule and discovered that lidocaine can alter of the passage of positively charged molecules across a BBB culture model indicating possible drug interactions due to charge at the level of BBB.[17]

While the surface charge of individual cells can be determined by LDv, for the *in situ* measurement of zeta potential of biological barrier layers forming large surfaces, this method cannot be applied. Nevertheless, in the vicinity of macroscopic surfaces (*e.g.*, when fluids are moving due to pressure difference through a channel of charged walls), a special electrokinetic technique, the streaming potential measurement can be used, instead, to determine the zeta potential at the channel wall.[20,21] Streaming potential refers to the transient potential difference developing under fluid flow conditions inside the channel along the flow direction, due to the migration of mobile counter-ions from the vicinity of the charged surface of the channel. Streaming potential, measured *via* a pair of electrodes, is considered to be proportional to the zeta potential of the surface, under laminar flow conditions.[20]

Experiments to measure streaming potential in animals or in *ex vivo* tissues have been made since the late 60's (Table 1). Streaming potentials due to the bloodstream in rabbit aorta and vena cava were measured by microelectrodes inserted into the vessels (measurement direction parallel to the vessel surface), and the endothelial surface lining these large vessels were highly negatively charged at physiological pH.[22] In addition to these studies, parts of the gastrointestinal tract, namely the small intestine,[23] and the buccal mucosa[24] were also investigated by streaming potential measurements. In the latter case, however, the fluid flow was typically directed across the epithelial barrier layers (measurement direction perpendicular to the surface). Although, these pioneering papers have given important insight into the major role of surface charge of biological barriers in basic physiological mechanisms, with the increasing use of cell cultures in biomedical research new methods and devices are needed.

In vitro culture models of biological barriers are widely used tools for basic and applied research.[25,26] In the past 10 years besides static models cultured on inserts[26,27] dynamic lab-on-a-chip (LOC)/organ-on-chip (OC) devices were developed to study cell–cell interactions, molecular pathways, pathological conditions and drug delivery in biological barriers.[28–31] These models incorporate the use of fluid flow enabling the investigation of physiological-like functions such as receptor and mechanosensor expression, transport mechanisms, pathologies and drug delivery.[32–40] LOC/OC devices became important tools since they provide controlled conditions for cellular signaling and external stimulus and are able to track the development and changes in the barrier function. Specific advantages of these biochips are the possibility to monitor barrier integrity in real time, constant fluid flow to mimic blood flow and shear stress, and the opportunity of switching medium composition for treatments with the help of valves and pumps. System-integrated electrodes can be readily accommodated to LOC devices to measure the impedance spectrum[41] or the trans-endothelial/epithelial electrical resistance (TEER),[37,42] to characterize the integrity of barrier-forming cellular monolayers. An alternative method to monitor cell layer integrity by high-throughput optical screening is the use of a microplate-compatible resonant waveguide grating imager.[43,44] Cells in LOC/OC devices, similarly to cells cultured on inserts, can also be monitored with phase

Table 1 Studies measuring streaming potential on tissues and cells

Method to measure surface charge/zeta potential				Tissue/cell			
Streaming potential/ measurement direction	Chip device	Verification by LDv	Built in TEER electrodes	Tissue/cell type	Human	Biological barrier	Ref.
Yes/parallel	No	No	No	Aorta and vena cava	No	Yes	22
Yes/perpendicular	No	No	No	Small intestine	No	Yes	23
Yes/perpendicular	No	No	No	Buccal mucosa	No	Yes	24
No (electro-osmosis)/parallel	No	No	No	BGM (kidney)	No	Yes	45
				Hep-2 (laryngeal carcinoma)	Yes	No	
				RPMI-1846 (melanoma)	No	No	
Yes/parallel	No	No	No	3T12 (fibroblast)	No	No	46
Yes/perpendicular	No	Yes	No	HEK293 (kidney epithelial)	Yes	Yes	47, 48
				EA926 (endothelial)	Yes	Weak	
				Caco-2	Yes	Yes	
Yes/parallel	Yes	Yes	Yes	hCMEC/D3 cell line	Yes	Yes	Present model

contrast microscopy, while good quality immunostaining and pharmacologically relevant permeability assays are extra features in two-compartment models.[31,37]

Despite the recent boom in LOC devices, no biochip to determine the surface charge of intact cell layers forming biological barriers has been published, yet. Table 1 summarizes the studies in which the measurement of streaming potential of biological cell surfaces, including culture models, was investigated.

In Table 1 we refer to four studies performed on cultured cells in which cell surface charge properties were determined.[45–48] One of them used electroosmosis,[45] three of them streaming potential,[46–48] but none of them were using an LOC device. Other differences, as compared to the present study, include the use of non-barrier forming cells[46] and measurement of streaming potential across the cell layer (measurement direction perpendicular to the surface).[47,48]

Hence, our aim was to develop a new LOC device to directly assess the surface charge of barrier cell monolayers by applying a fluid flow parallel to the barrier surface. To achieve this goal, we added Ag/AgCl electrodes for the detection of streaming potential under microfluidic flow conditions to our previously published LOC device,[37] allowing measurement of streaming potential on a culture model of a biological barrier. With this setup, we characterized the zeta potential of a simple ionic model membrane, Nafion, and of human brain endothelial cell (BEC) monolayers as a simplified model of the BBB. LDv data and model simulations were compared to the streaming potential results and show that the zeta potential of the cell surface is proportional to the peak value of the streaming potential detected by our LOC validating measurements with the new device.

Materials & methods

LOC and electrode fabrication process

The device was formed by top and bottom channels, separated by a porous polyester (PET) membrane with 0.45 μm pore size, 2×10^6 cm^{-2} pore density and 23 μm thickness (It4ip, Belgium) (Fig. 1A). The geometry of the channels enabled the measurement of trans-endothelial electric resistance (TEER) and performance of permeability assays (Fig. 1B).[37] The channels were fabricated from poly(dimethylsiloxane) (PDMS, Sylgard 184, Dow Corning GmbH, Germany) by injection molding. The length, width and height of the top and bottom channels were 36 mm × 2 mm × 1 mm and 57 mm × 2 mm × 2 mm, respectively. The initiator and base polymer were mixed in 1 : 10 ratio, and subsequently degassed by vacuum. The mixture was injected in brass molds that were the negatives of the channels. The PDMS was cured on 80 °C for 15 min to reach a rigid structure. To bind the channels to each other, the surfaces of the PDMS channels were treated with oxygen plasma. The vacuum chamber of the plasma cleaner (PDC-002, Harrick Plasma, USA) was evacuated to 200 mtorr then a steady 400 mtorr pressure was set by oxygen stream. When the 400 mtorr oxygen pressure became stable, radio frequency (RF) excitation was used for oxygen plasma treatment for 45 seconds. Thus, the PDMS channels became adhesive and could be assembled with the porous membrane between.

For the top and bottom side of the LOC device, plastic microscope slides (polystyrene, Ted Pella USA) were used. The top slide and the flat part of the male Luer lock (Rotilabo, Carl Roth, Germany) inlets/outlets were drilled with a diameter of 2 mm using a commercial drilling machine (Fig. 1A). The inlets were glued on the top slide using a photoresin (Norland Optical Adhesive 81, Norland Products, USA). The bottom side of the Luer locks were painted with the photoresin then placed above the holes on the top slide. After 30 seconds of exposure with a UV lamp (Newport New Illumination System, Newport Corp, USA), the resin reached the required structural rigidity. The gold electrodes for TEER measurement were formed on plastic microscope slides using sputter-coating (K975X, Emitec, France). The thickness of the gold layer was 25 nm, providing low enough resistance (*ca.* 10 Ohms), and approximately 70% transmission in the visible spectrum, to allow TEER measurements and simultaneous microscopic observation.[37] Therefore, the cell growth could be monitored with a phase

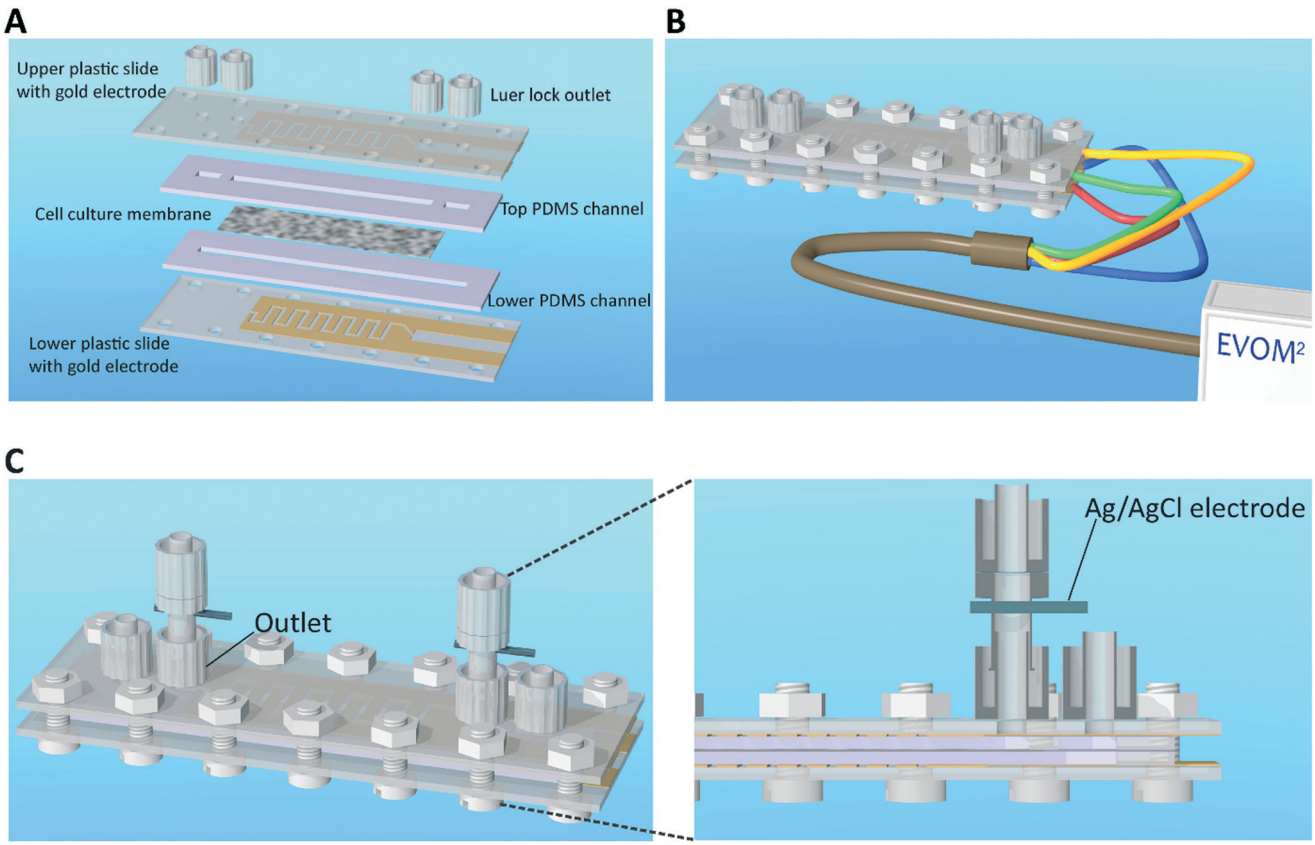

Fig. 1 The structure of the biochip. (A) The two PDMS channels are separated by a porous PET culture membrane. The top and bottom plastic slides coated with the gold electrodes are closing down the two channels. The PDMS and the plastic slides are assembled with plastic screws to avoid shortcut between the electrodes. Luer-lock inlets/outlets on the top slide provide easy access to the channels. The culture medium is circulated in the top channels, while the bottom channel is closed down using male Luer cups (not shown). (B) Copper wires are glued to gold electrodes using conductive epoxy, so the instrument (EVOM^2) to measure transendothelial electric resistance can be connected easily. (C) The biochip and the zeta electrodes. The PDMS channels and the plastic slides containing the electrodes for transendothelial electric resistance measurement were joined together with screws. The female Luer inlets were located on the top and provided easy access for both top and bottom channels. The Ag/AgCl electrodes were fit in a drilled channel of male–female Luer lock caps and fixed using Norland Optical Adhesive, thus the electrodes were easy to mount to the biochip for the experiments.

contrast microscope throughout the whole length of the channel. Conductive epoxy glue (CW2400, Chemtronics) was applied in order to link copper wires to the electrodes, and a 4-channel voltohmmeter (EVOM,^{2} World Precision Instruments, USA) could be connected to the LOC device. The top and bottom slides and the PDMS channels were screwed together with plastic screws to avoid shortcut of the TEER electrodes (Fig. 1B, ESI† Video V1). The ready-to-use device was sterilized with oxygen plasma for 5 min and 70% ethanol for 30 min before cells were seeded to the system.

For the detection of streaming potentials Ag/AgCl electrodes were prepared and placed in Luer lock connectors (Fig. 1C), so they could be easily connected to the inlet and outlet side of the biochip. The silver wires (10 mm long, 0.5 mm width) were polished with sandpaper and washed with ethanol, then were soldered to copper wires. The connectors were drilled at their diameter, and the silver wires were fitted in. Small drops of the Norland photoresin were applied at openings between the connector and the silver cord to fix them, and were exposed to UV light using a mercury arc lamp for 30 seconds. The end of the copper wire connecting the silver was sealed with silicon glue to avoid shortcut during the subsequent electrolytic chloridisation. For this, the wires were immersed in 3 M KCl solution, one at the time, and a 3 mA DC current was applied for 1 minute. The ready Ag/AgCl electrodes were rinsed with distilled water and dried under N2.

Cell culture

To model the BBB, the hCMEC/D3 human brain endothelial cell line was used (Merck, Germany).[49] Cell cultures (≤passage 35) were kept in MCDB 131 medium (Pan Biotech) supplemented with 5% fetal bovine serum (FBS, Sigma), Glutamax (100×, Life Technologies, USA), lipid mixture (100×, Life Technologies, USA), 10 μg ml^{-1} ascorbic acid, 550 nM hydrocortisone, 100 μg ml^{-1} heparin, 1 ng ml^{-1} human basic fibroblast growth factor (bFGF, Roche, USA), insulin (2.5 μg ml^{-1}), transferrin (2.5 μg ml^{-1}), sodium selenite (2.5 ng ml^{-1}) provided as a mix (ITS, Life Technologies, USA), and 50 μg

ml^{-1} gentamicin. Membranes in the LOC device were coated with 0.5% gelatin from porcine skin (Sigma) and incubated at 37 °C for 20 min. hCMEC/D3 cells were seeded at a number of 1×10^5 into the device. On day 4 cells received LiCl (10 mM) to elevate barrier tightness.[27] As described in our previous work, cell cultures were kept for 3 days under static conditions in the device.[37] A syringe (20 ml plastic disposable syringe with Luer cone, Braun) containing the culture medium was placed in a syringe pump (Legato 110, KDS products, USA) and connected to the device. The tubes (1 mm inner, 3 mm outer diameter, Carl Roth, Germany) were connected to the inlets/outlets *via* female Luer-locks (Rotilabo, Carl Roth, Germany) to allow feeding during cell growth and constant medium-supply. During the cell growth phase, the syringe pump was programed to change the medium above the cell monolayer (static condition) with 500 μl min^{-1} flow rate every 8 hours. The transparency of the gold electrodes lets us monitor the growth of the cell monolayer by phase contrast microscopy on the entire surface, and TEER was measured every day. If the cell layer was not continuous as reflected in low TEER values and visually detected holes, the device was excluded from the experiments. Before the cell layer reached full confluence, a constant stream of culture medium was introduced by a peristaltic pump (Masterflex, Cole-Parmer, USA) for 24 hours (1 ml min^{-1}, flow condition) before zeta measurement and permeability studies.

Cell culture treatments

Lidocaine (Sigma L7757) was dissolved in water at 30 °C to prepare a 20 mM stock solution. Working solutions of 1 mM concentration were prepared freshly before each experiment in culture medium and added to the cells.[17] Neuraminidase from *Clostridium perfringens* (Sigma N2876) was dissolved in Dulbecco's modified Eagle's medium (DMEM) and aliquots of a 10 U ml^{-1} stock were stored at −20 °C. A new neuraminidase stock vial was thawed before each experiment. For the treatment neuraminidase was applied at 0.1, 0.3 and 1 U ml^{-1} concentrations to the cells based on a preliminary study and literature data.[50]

Zeta potential measurements: detection of streaming potential

Development of streaming potential is a well-known electrokinetic phenomenon occurring in microfluidic channels.[51,52] If the inner surface of the channel is covered with charges (intrinsic or adsorbed), it attracts counterions from the solution, and keeps them near the surface. Due to a balance of Coulomb attraction and Brownian motion, a diffuse double layer is formed by the mobile ions and the fixed surface charges, the Gouy–Chapman layer (GCL). As a consequence, an electric potential gradient develops perpendicular to the membrane plane, screening the surface potential of the membrane across the GCL. If fluid flow is applied in the channel, a major part of the counterion cloud of GCL, divided by a "slipping plane" to a moving part and a layer sticking the channel wall, will be grabbed by the solution under Poiseuille flow. The resulting flow of net charge along the channel represents an electric current called streaming current, and the accompanying streaming potential can be detected by an electrode pair separated alongside the channel. The streaming potential under stationary conditions is proportional to the surface potential of the shear plane called zeta potential, according to the Helmholtz–Smoluchowski equation.[18] Since the zeta potential can be relatively easily measured by electrokinetic methods, this is the very quantity that is used to characterize surface charge densities of artificial membranes or colloid particles. In this work, we measure a nonstationary (transient) streaming potential, in order to maximize the signal amplitude by applying high inlet flow rates. We provide both theoretical and experimental evidence that the amplitude of the transient signal is proportional to the zeta-potential at the surface, in this case, too (for more details, see below, and under the Simulation section).

The transient signal was gained and filtered with a low-noise voltage pre-amplifier (SR560, Stanford Research Systems, USA) (Fig. 2A), recorded by a digital oscilloscope (Wave Ace, Teledyne LeCroy, USA), and further analyzed *via* the Wavestudio software (Teledyne LeCroy, USA). The amplitude of the transient streaming potential signals was calculated with Matlab (MathWorks, USA). The difference between the baseline and the maximum of the curve defined the amplitude. The noise of the signals was eliminated with the function estimation of smoothing splines (Fig. 3A).

Experimental validation of the system was performed by using a Nafion membrane (Ion Power, USA) inserted between the two PDMS channels. For the measurements performed on the confluent monolayer of hCMEC/D3 after 24 h flow, first, the background streaming potential was registered under a 1 ml min^{-1} flow rate, then cells were treated with 1 mM lidocaine for 30 min at 37 °C or with 1 U ml^{-1} neuraminidase in a serum-free medium for 1 h at 37 °C. After treatments, streaming potential was measured again with the same electrodes and under the same conditions, and changes were calculated. In case of cell monolayers in the control group, instead of any treatment, the medium was changed and incubated for 30 min or 1 h at 37 °C, before the streaming potential was measured.

Zeta potential measurements: laser-Doppler velocimetry

LDv measures the electrophoretic mobility of charged particles with two collimated, monochromatic, and coherent laser light beams, forming a set of straight fringes by interference.[19] The moving particles go through the fringes and reflect light to a photodetector. The frequency of the reflected light's intensity fluctuation is proportional to the Doppler shift between the scattered and incident light, and the velocity of the particles is proportional to the Doppler shift. Using the Smoluchowski equation the zeta potential ζ can be calculated as follows:

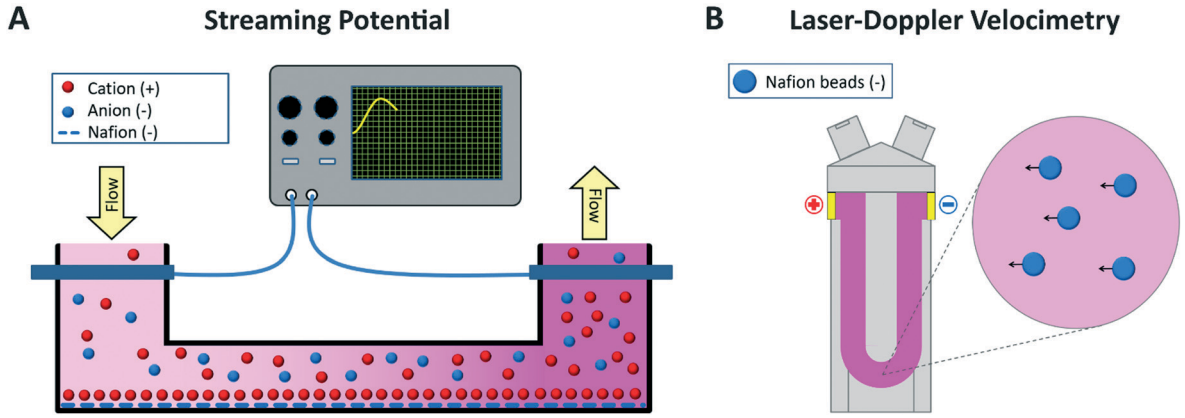

Fig. 2 Methods of zeta potential measurement. (A) Streaming potential. The counterions of the solution has a higher local concentration close to the negatively charged surface due to the electric double layer. The ion concentration of the diffuse layer was constant (fix cations close to the surface) while the cations of the slipping plane move towards the outlet under flow conditions and temporarily accumulate in the larger vicinity of the electrode resulting in a potential difference compared to the reference (inlet) electrode. (B) Laser-Doppler velocimetry. Electric field was applied on a suspension of charged particles (*e.g.* the Nafion beads) in the capillary channel and the beads moved toward the direction of the field. The electrophoretic mobility is measured with the intensity shift between two collimated, monochromatic, and coherent laser beams, thus the zeta potential of the particles can be calculated.

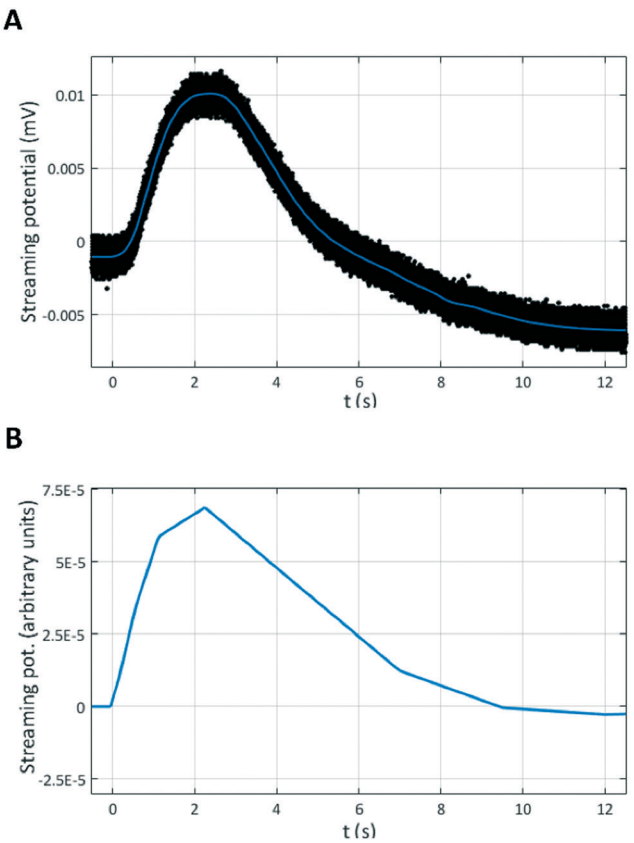

Fig. 3 Comparison of the registered streaming potential and the model simulations. In both cases the reference was on the low-pressure end so the positive potential difference corresponds to negative zeta potential since it measured the concentration of the counterions. (A) The registered signal on Nafion membrane measured in the biochip. (B) The result of the simulation. The streaming potential is shown in arbitrary units because the geometry of the model was proportionally decreased as compared to the chip device. The dynamics of the transient streaming potential signal is identical.

$$\xi = \frac{4\pi\mu\eta}{\varepsilon}$$

where μ is the electrophoretic mobility, η is the viscosity of the solvent and ε is the dielectric constant.

In the experiments a Zetasizer Nano ZS instrument (Malvern, UK) was used. First, LDv was performed using Nafion beads (Ion Power, USA) as a simple model for ionic surface changes. Nafion belongs to a class of polymers with ionic properties, which unique characteristic results from the incorporation of perfluorovinyl ether groups terminated with sulfonate groups onto a tetrafluoroethylene strength.[53] To alter the negative surface charge of the Nafion particles cationic polyethylenimine (PEI) polymer with good attachment properties was used. Nafion beads were stored in a mixture of water and ethanol. To measure the LDv of the Nafion beads they were transferred into the same ionic solution used for measuring the surface charge of endothelial cells. First, 2 × 1 ml Nafion stock solution was spun down with ultracentrifugation (T-1270 fixed angle titanium rotor, Sorvall WX+100 ultracentrifuge, ThermoFisher Scientific, USA) at 45000 rpm for 30 min on 4 °C. The pellet in one of the vials was resuspended in 2 ml phosphate-buffered saline (PBS) solution containing Ca^{2+} and Mg^{2+}, while the other vial was resuspended in 3 ml PEI. Both samples were sonicated for 60 min. The PEI-treated sample was ultracentrifuged once more with the same settings and was resuspended in 2 ml of PBS containing Ca^{2+} and Mg^{2+} and sonicated for 1 hour. This step was repeated once more to remove any PEI which was not attached to the Nafion beads. Samples were measured by Zetasizer Nano ZS using a disposable zeta potential cuvette with gold plated beryllium/copper electrodes (DST1070, Malvern, UK). Before measurements cuvettes were rinsed with 100% ethanol for activation and washed twice with

distilled water. Then zeta cuvettes were calibrated with zeta standard solution (Malvern, UK) as described by the manufacturer's protocol. Samples were measured at 25 °C, with a minimum of 6 rounds (12 runs each), with an applied 40 V voltage (Fig. 2B).

Zeta potential of hCMEC/D3 brain endothelial cells was measured similarly.[17] Before the cells in Petri dishes reached full confluence were trypsinized and 10^5 cells were re-suspended for treatment in the appropriate buffer. As described in our previous work, 1 mM lidocaine was added to the cell suspension and incubated at 37 °C for 30 min.[17] For neuraminidase treatment, cells in suspension were incubated with 1 U ml^{-1} of neuraminidase in a serum-free medium for 1 h at 37 °C before measurement. The Zetasizer software v.7.12. calculated the zeta potential using the Smoluchowski equation.

Evaluation of barrier integrity

hCMEC/D3 cultured in the LOC device received fresh medium every 8 hours automatically, and TEER measurement was performed each day to follow barrier formation. After the 48 h flow in the device treatments followed by permeability measurements were done to determine the integrity of the cell layers. Permeability for fluorescein isothiocyanate-labeled 10 kDa dextran (FD10, Sigma) was done as described previously.[37] In the lower compartment the cell culture medium was changed to Ringer-Hepes buffer (118 mM NaCl, 4.8 mM KCl, 2.5 mM $CaCl_2$, 1.2 mM $MgSO_4$, 5.5 mM D-glucose, 10 mM Hepes, at pH 7.4) supplemented with 1% FBS and 1% ITS. In the upper compartment of the device the culture medium was changed for Ringer-Hepes containing 10 μg ml^{-1} FD10 for control biochips, and Ringer-Hepes containing 10 μg ml^{-1} FD10 and 1 mM lidocaine in the lidocaine treatment group. For the neuraminidase treatment cell culture medium was replaced for serum-free medium containing 1 U ml^{-1} of neuraminidase and incubated for 1 h at 37 °C. After streaming potential was measured, permeability measurement was done replacing the cell culture medium as described above. The devices were kept in a CO_2 incubator, on a horizontal shaker (150 rpm), for 30 min during permeability measurements, then samples were collected from both compartments of the device and concentrations of the molecular marker were measured by fluorescent spectrophotometry (Fluostar Optima, BMG Labtechnologies, Germany) with 485 nm excitation and 520 nm emission wavelengths. Apparent permeability coefficient (P_{app}) was calculated as described previously.[54]

Fluorescent immunostaining

Permeability measurements were followed by immunohistochemical stainings for morphological characterization.[17] Brain endothelial cells were fixed with cold acetone–methanol solution (1 : 1) for 2 min, washed with PBS and stained for junctional associated protein β-catenin. To block the non-specific binding sites cells were incubated with 3% bovine serum albumin (BSA) in PBS for 1 h at room temperature. Incubation with the primary antibody polyclonal rabbit anti-β-catenin (Sigma, C2206; 1 : 200) lasted overnight at 4 °C. The next day cell culture membranes were incubated with secondary antibody anti-rabbit labeled with Cy3 (Sigma C2306; 1 : 400) and bis-benzimide H33342 (Merck, Germany) for nucleus staining, for 1 h at room temperature. Between incubations membranes with cells were washed three times with PBS. Pictures for the junctional staining were visualized by a Leica TGS SP5 confocal laser scanning microscope (Leica Microsystems, Germany).

Surface glycocalyx staining

Endothelial cells were cultured on rat tail collagen coated glass cover slips. After reaching confluence cells were treated either with culture medium (control group) or with neuraminidase as described in the Cell culture treatment section. After treatment cells were fixed with 1% paraformaldehyde in PBS for 15 min at room temperature. To visualize the surface glycocalyx fixed but unpermeabilized cells were incubated with wheat germ agglutinin (WGA) lectin conjugated with Alexa Fluor 488 (Invitrogen, W11261). WGA is specific for sialic acid and *N*-acetyl-D-glucosamine residues within the glycocalyx. The final concentration of WGA was 5 μg ml^{-1} in PBS and the incubation lasted for 10 min at room temperature.[55] After thorough washing steps preparations were mounted and pictures were taken with an Olympus FV1000 confocal microscope at different random positions. Minimum of 5 pictures was taken from each group at each experiment. The images were analyzed for staining intensity using the FIJI (ImageJ) software.

Simulations

Model calculations were carried out on a flow channel by the COMSOL Multiphysics work package (Comsol Inc., USA) run on a personal computer, to describe time- and zeta potential dependence of the transient streaming potential signal. To optimize simulation time and disencumber processor capacity, a rectangular channel of proportionally reduced size and simplified geometry was used in the simulations. The average flow velocity at the inlet (3.8×10^{-4} m s^{-1}) was adjusted to the reduced size in order to be able to mimic the time course of the measured transient electric signal. The dimensions of the channel were 100 μm × 200 μm × 1200 μm. In the middle of this channel a 200 μm by 300 μm inner wall segment, representing the slipping plane, was carrying a surface charge density of 0.172 C m^{-2}. The electrolyte comprised of a NaCl–water solution of 137 mM concentration, with ambient pressure and temperature values, to mimic typical measuring conditions. For details of the simulation see ESI† Fig. S1. The simulations were carried out by solving coupled differential equations of the electrostatics, transport of diluted species and creeping flow work packages (ESI† Fig. S1), using the Poisson approximation (1)–(3) and the Nernst–Planck (4), and Navier–

Stokes equations for the creeping flow of an incompressible fluid (5)–(6), respectively:

$$\nabla\cdot\boldsymbol{D} = \rho_{\mathrm{V}} \tag{1}$$

$$-\boldsymbol{n}\cdot\boldsymbol{D} = \sigma_{\mathrm{S}} \tag{2}$$

$$\boldsymbol{E} = -\nabla V \tag{3}$$

$$\frac{\partial c_j}{\partial t} + \nabla\cdot\left(-D_j\nabla c_j - z_j u_{\mathrm{m},j} F c_j \nabla V\right) + \boldsymbol{u}\cdot\nabla c_j = 0 \tag{4}$$

$$0 = \nabla\cdot[-p\boldsymbol{I} + \mu(\nabla\boldsymbol{u} + (\nabla\boldsymbol{u})^T)] + \boldsymbol{F} \tag{5}$$

$$\rho\nabla\cdot(\boldsymbol{u}) = 0 \tag{6}$$

Here $\boldsymbol{D}$ and $\boldsymbol{E}$ are the electric displacement and field strength, respectively, ρ_{V} and σ_{S} are volume and surface charge densities, $\boldsymbol{n}$ is the normal vector of the surface, V is the electric potential, c_j is the concentration of the jth ion of z_j valency and $u_{\mathrm{m},j}$ mobility, F is the Faraday constant, $\boldsymbol{u}$ is the flow velocity, p is the pressure, $\boldsymbol{I}$ is the volumetric current flux, μ is the dynamic viscosity, $\boldsymbol{F}$ is the volumetric force, and $(\nabla\boldsymbol{u})^T$ is the shear stress term. The simulations were carried out in two steps: first, under no-flow conditions a stationary state was developed, while in the second step, a creeping flow was also introduced. The coupled differential equations were solved by the implicit method of backward differentiation formula (BDF).

Statistics

Data are presented as means ± SD. Statistical significance between groups was determined by one-way ANOVA with Bonferroni multiple comparison tests, by unpaired *t*-test or by paired *t*-test (GraphPad Prism 5.0, GraphPad software, USA). The number of parallel samples were minimum 3, and significance was considered at $p < 0.05$. Experiments were repeated at least two times with multiple parallels.

Results and discussion

Design and operation of the device

The basic structure of the barrier device mimics that of the culture inserts: top and bottom channels separated by a porous PET membrane (Fig. 1A). The two parallel channels were made of PDMS. The geometry of the top and bottom channels are 36 mm × 2 mm × 1 mm and 42 mm × 2 mm × 2 mm, respectively, which 90% overlap providing higher sensitivity for *in vitro* permeability assays. It should be noted that the height of the top channels was reduced to half as compared to the device in our previous publication.[37] Plastic slides with transparent gold TEER electrodes cover the two channels (Fig. 1A). The 25 nm thick gold electrodes were formed with a masking technique using sputter-coated gold deposition.[37] A four-point probe configuration was designed for the precise impedance measurement, which electrically covered and enabled monitoring of the whole surface of the PET culture membrane (36 mm × 2 mm). Copper wires were bound to the transparent gold electrodes using conductive epoxy, thus the EVOM voltohmmeter could be connected to the device (Fig. 1B).

The plastic tubes and the zeta electrodes were connected to the device *via* Luer lock inlets. The Ag/AgCl zeta electrodes were inserted in Luer connectors, so they could be mounted easily (Fig. 1C). A programmable syringe pump fed the cells during the growth period (3 days) every 8 hours, while the TEER values were recorded and the monolayer was monitored with a phase contrast microscope, each day. Automatic feeding decreased the chances of contamination, too. The devices were connected in line (3 to 6 at one experiment), thus the flow rate and shear stress (0.4 dyn) were the exact same in all cultures. Before the cell monolayers reached full confluence, a peristaltic pump was introduced for constant flow, to mimic the shear stress of the bloodstream in veins for 1 day. The flow rate was 500 μl min^{-1} during feeding, 1 ml min^{-1} during the constant flow.

The streaming potential was measured with the Ag/AgCl electrodes (Fig. 1C) between the inlet and outlet sides of the top channel (Fig. 2). For the recording, the flow was periodically stopped and restarted after equilibration of the ions close to the surface of the cell monolayer. Please note that contrary to the usual streaming potential measurements working with moderate flow rates, we do not operate our device under stationary conditions where the forward streaming current and the backward conductive current keep an equilibrium, but rather measure transient signals (Fig. 3A) by applying a strong input flow, in order to increase the signal-to-noise ratio. Although, this case is beyond the scope of the Helmholtz–Smoluchowski equation establishing a linear relationship between the zeta and steady-state streaming potentials, here we present experimental and theoretical evidence for the proportionality of the zeta potential and the amplitude of the transient streaming potential in our approach, as well.

The streaming potential feature: experimental validation of the method

In this work, the streaming potential was measured either on a test membrane or on cell monolayers, in the form of a transient potential difference evolving between the inlet and outlet electrodes, due to migration of ions from the vicinity of the negatively charged surface of the channel under flow conditions (Fig. 2A). The negative charge derives from the overwhelming anionic groups on the surface of the confluent cell monolayer due to the lipid headgroups[2] and the surface glycocalyx in the BBB experiments,[15] or from the sulfate groups of the Nafion membrane in the control measurements. The electric double layer close to a charged surface has a different ion concentration compared to the solution. If flow is applied to the system, the mobile part of the GCL containing an excess number of positive counterions

move towards the outlet electrode, and temporarily increase the positive charge density in the larger volume of the socket of the electrode, giving rise to an increase in electric potential, as compared to the reference electrode (Fig. 3A). As we show by both model calculations (Fig. 3B) and control experiments using the LDv method, the amplitude of this transient streaming potential signal is proportional to the zeta potential of the membrane surface.

A highly negatively charged Teflon derivative, the sulfonated tetrafluoroethylene-based fluoropolymer-copolymer called Nafion was selected to perform the proof-of-concept experiments by the streaming potential electrodes incorporated in the chip. Since Nafion is available both in 183 μm thick membrane sheets and in liquid suspension, it is suitable for both the transient streaming potential measurements and for LDv (Fig. 4A and B), where the latter can serve as a control for calibration.

For the streaming potential study, the PET membrane of the chip was replaced by a Nafion membrane, and the adjacent microfluidic channels were filled up by PBS, in order to mimic the ionic conditions of the incubating solution of endothelial cells, most frequently used in our earlier BBB chip experiments.[37] Following the application of an inflow on the upper microfluidic channel of the device (Fig. 2A), a well-measurable transient electric potential change could be recorded under 1 ml min^{-1} flow rate, using a voltage preamplifier and an oscilloscope (Fig. 3A). The sign of the transient signal corresponded to a displacement of positive charges in the direction of the flow, indicating an overall negative zeta potential of the surface of the channel. After a 1 minute post-measurement incubation time without flow, the signal could be quantitatively reproduced. As a single-parameter descriptor of the transient signal, we chose its amplitude for comparison with the results of subsequent measurements. Note that here the convention of the sign was the opposite compared to the traditional streaming potential measurements,[56] as the reference electrode was on the low-pressure end of the channel. Hence, the sign of the measured signal was the opposite of that of the zeta potential since the amplitude was proportional to the concentration of the counterions. According to the convention, the amplitude of the streaming potential of the untreated Nafion membrane was found to be −1.06 ± 0.0625 mV (Fig. 4A).

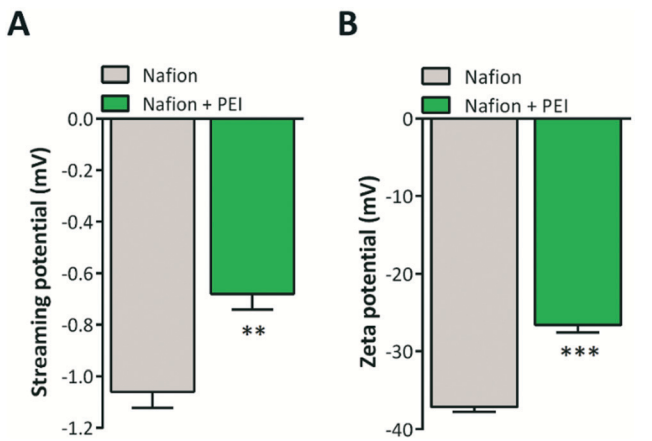

Fig. 4 Measurement of the surface charge of Nafion by streaming potential and by laser-Doppler velocimetry (LDv) methods. (A) Nafion film replaced the culture membrane in the biochip. It was treated with polyethylenimine and the streaming potential was measured before and after the treatment. Values are presented as means ± SD, $n = 4$. Data was analysed by unpaired t-test. **, $p < 0.01$, compared to control. (B) Nafion beads were treated with PEI and the samples were measured with LDv before and after the treatment. Values are presented as means ± SD, $n = 5$. Data was analysed by unpaired t-test. ***, $p < 0.001$, compared to control groups.

To change the surface charge density, the Nafion membrane, was treated for 30 min with PEI, known to be able to attach *via* highly positively charged ethyleneimine residues to the surface. Its access quantity was subsequently washed away with PBS, and the streaming potential was measured again. The result showed a pronounced decrease of the absolute value of the amplitude to −0.68 ± 0.061 mV (Fig. 4A). Control measurements without Nafion membrane showed negligible streaming potential signal, indicating that the zeta potential of the PDMS channel walls was insignificant, as compared to the highly negatively charged Nafion membranes.[57]

In order to calibrate the results gained by the transient streaming potential method with well-established techniques, LDv was applied to measure the zeta potential of Nafion beads prepared of identical material characteristics to those of the membrane. The Nafion stock solution (pH = 1.5) had a −76.2 ± 2.08 mV zeta potential measured with Malvern Zetasizer Nano ZS. Then the stock was centrifuged and resuspended in PBS (pH = 7.2), therefore the Nafion beads had the same ionic conditions as in the streaming potential experiments, and had a zeta potential of −37.13 ± 0.63 mV. Another batch of beads was then treated with PEI, and subsequently re-centrifuged and resuspended in PBS. The PEI-treated beads showed a similar ratio of increase in zeta potential up to −26.58 ± 0.94 mV (Fig. 4B), as it was observed for the streaming potentials of analogously treated Nafion membranes (Fig. 4A).

Based on the fact that the ratios of the zeta and streaming potentials of the native and PEI-treated Nafion surfaces were the same within the experimental error, a proportionality between the data measured by the two different methods were suggested. Below, we present both theoretical and further experimental evidence supporting this finding.

The streaming potential feature: simulations

In order to give a theoretical background for the measured transient streaming potential signals, we carried out model calculations on a flow channel by the COMSOL Multiphysics work package. The dynamics of the system was modelled in two steps: 1) to establish stationary conditions without flow, first the system was let to equilibrate according to the Poisson–Boltzmann–Nernst–Planck approximation, assuming

electro-neutrality of the channel-fluid system; 2) in the second step, a creeping flow with an average velocity of 3.8×10^{-4} m s^{-1} was applied (ESI† Fig. S2)to the inlet of the channel, and the electric potential was measured on two probe planes placed in front of and behind the charged surface, along the long axis of the channel. A typical voltage signal received by subtracting the two potentials is shown in Fig. 3B, faithfully reflecting the time-evolution of the measured signal (Fig. 3A). In order to establish the connection between the simulated signal amplitudes and the zeta potential, the latter was swept two orders of magnitude, and the simulated time-evolution of the streaming potential functions was recorded (ESI† Fig. S3, Video V2). Fig. 5B shows the dependence of the amplitudes of these curves as a function of the zeta potential, showing a clear linear relationship, in full concert with the experiments (see the previous section, and Fig. 5A).

The above experimental and model calculation results proved that the concept of upgrading our chip device by a streaming potential unit, to detect the zeta potential of the membrane insert and monitor its changes, is feasible. Nevertheless, it remained an important question whether the method is appropriate (*i.e.* sensitive enough) to characterize changes in the surface charge properties of cellular monolayers, such as those in biological barriers. In the forthcoming sections, we address this problem *via* the experimental investigation of an *in vitro* BBB model system.

Effects of surface charge modifications and measurement of streaming potential on a cell culture model of the BBB

There is an increasing number of direct and indirect evidence that simple physical parameters such as surface charge density or the related zeta potential might control physiological functions of barrier properties.[2,17] The main sources of the, usually negative, surface charge densities of cells are the lipid head groups of the plasma membrane, and the so-called glycocalyx, composed of highly negatively charged polysaccharide chains at the surface of the cells (Fig. 6A). Glycocalyx forms a continuous coat on the luminal surface and plays important roles as both a mechanosensor[55] and as a physical barrier for nanoparticle permeability.[16] The negative surface charge derived from the lipid head groups of the BBB regulates both drug delivery to the brain[14] and drug interaction at the level of brain endothelial cells.[17] Therefore, the surface charge density of brain endothelial cells can be modified by both enzymatic digestions of the glycocalyx or cationic lipophilic molecules that are inserted into the plasma membrane (Fig. 6A). To determine changes in the surface charge of individual cells LDv measurements are used.[2,17]

In our study, we measured the streaming potential on confluent monolayers of barrier cells cultured in a LOC device for the first time. We used two clinically relevant surface charge modulators (Fig. 6A). The antiarrhythmic intravenous drug, lidocaine incorporates into the plasma membrane of vascular endothelial cells and as we demonstrated in a recent study it changes the zeta potential of brain endothelial cells.[17] Neuraminidase, a glycoside-hydrolase enzyme, cleaves sialic acids and reduces the amount of negative charge on the glycocalyx, thus mimics glycocalyx shedding observed in sepsis.[6] Cleavage of glycocalyx elements turns cellular surface charge more positive, although this change has not been measured directly on brain endothelial cells yet. The efficiency of cleavage of sialic acid residues from the glycocalyx by neuraminidase was determined by the sialic acid-specific lectin WGA-Alexa 488 staining, followed by confocal microscopy and image analysis for staining intensity (Fig. 6B and C). A concentration-dependent effect of the

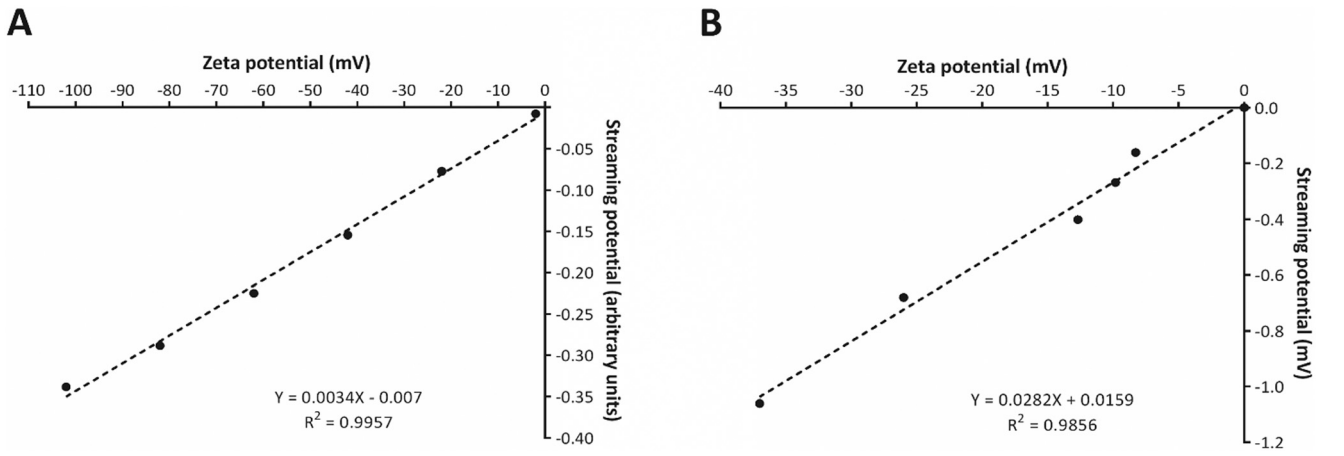

Fig. 5 Correlation between streaming potential and laser-Doppler velocimetry. (A) Correlation of the simulation. The zeta potential was set in the channel as a charged section of the wall and the corresponding streaming potential was calculated by the simulation. (B) The streaming potential and laser-Doppler velocimetry data measured on Nafion or the confluent brain endothelial cell layers were plotted and fitted with linear regression. The two goodness-of-fits are R^2 = 0.996 and R^2 = 0.986 respectively, which shows a clear linear relationship between the zeta and streaming potential.

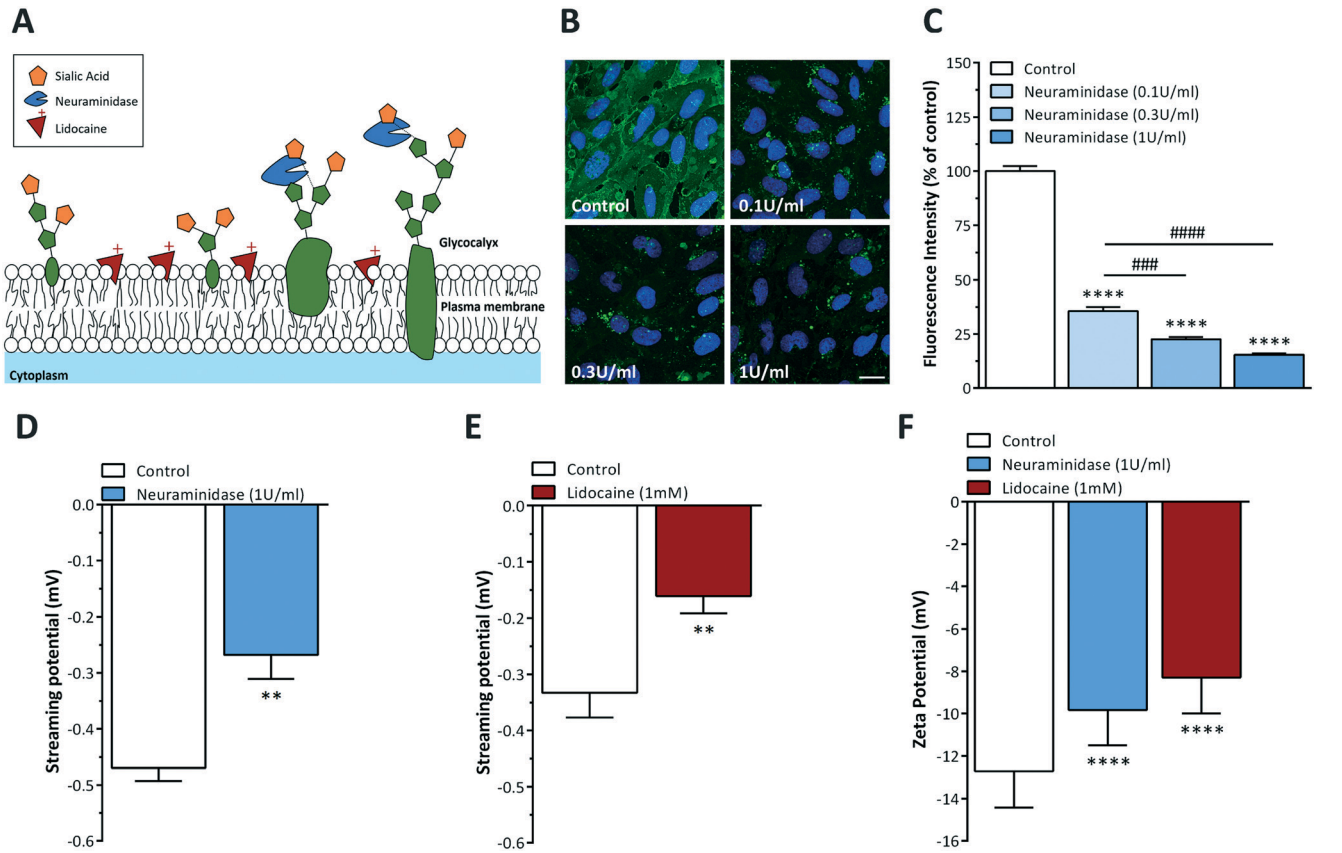

Fig. 6 Measurement of surface charge and its modification on brain endothelial cells by streaming potential in the chip device and by laser-Doppler velocimetry (LDv). (A) The two strategies to modify the zeta potential were the cleavage of the glycocalyx or the insertion of positively charged molecules in the membrane. Neuraminidase enzyme cleaves the sialic acids of the polysaccharide sidechains, thus decreases the amount of negative charges on the cell surface. Lidocaine incorporates into the cell membrane and makes it more positive. (B) Representative pictures of the staining with wheat germ agglutinin (WGA) lectin labeled with Alexa 488 with or without treatments with different concentrations of neuraminidase, bar: 20 μm. (C) Image analysis of the fluorescent intensity of the lectin labeling on pictures taken by confocal microscopy. Values are presented as means ± SD, n = 30–66. Data was analysed by one-way ANOVA with Bonferroni post-test. ****, #### $p < 0.0001$, ### $p < 0.001$. (D and E) Streaming potential values measured in the chip device. Values are presented as means ± SD, n = 4. Data was analysed by unpaired t-test. **, $p < 0.01$, compared to control. (F) Zeta potential results obtained with LDv method. Values are presented as means ± SD, n = 12–60. Data was analysed by one-way ANOVA with Bonferroni post-test. ****, $p < 0.0001$, compared to control.

enzyme on lectin staining was obtained: neuraminidase treatment at 1 U ml^{-1} concentration reduced the labeling by 80% on the surface of BEC after 1 h treatment, while lower concentrations were less effective (Fig. 6B and C).

The effects of the two different treatments were tested by measuring transient streaming potential signals on the chip (Fig. 6D and E). To this end, a fluid flow of 1 ml min^{-1} was applied on the upper channel of the device, containing the brain endothelial cell monolayer and the flow of charges was registered. As shown in Fig. 6D and E, both treatments increased the streaming potential of the cell monolayers. Neuraminidase treatment was performed at a concentration of 1 U ml^{-1}, since it was the most effective concentration in reducing sialic acids from the glycocalyx (Fig. 6B and C). Addition of neuraminidase increased the streaming potential of cell layers to −0.268 ± 0.086 mV from −0.470 ± 0.047 mV (Fig. 6D). Lidocaine, the other surface charge modulator in our experiments, is widely used as an anaesthetic or antiarrhythmic drug. We demonstrated in our previous study by LDv that it modifies the zeta potential of BEC.[17] Since we found no toxic effect of lidocaine at 1 mM concentration,[17] this concentration was used on the BEC monolayers cultured in the LOC device. In Fig. 6E, the streaming potential is shown to increase from −0.333 ± 0.089 mV to −0.161 ± 0.061 mV upon lidocaine treatment. For comparison with the results obtained by the streaming potential measurements, single-cell experiments were performed using the same treatments but the LDv method. As shown in Fig. 6F, neuraminidase treatment significantly increased the surface charge of BEC to −9.83 ± 1.67 mV, while lidocaine elevated it to −8.29 ± 1.71 mV from the −12.7 ± 1.71 mV measured in basal conditions when no treatment was applied. The lower, 0.1 U ml^{-1} and 0.3 U ml^{-1} concentrations of neuraminidase resulted in smaller changes in the zeta potential of BEC (ESI† Fig. S4), in accordance with the glycocalyx staining results (Fig. 6B and C).

After completing the experiments on both Nafion and cells, the streaming potential amplitudes recorded on the

LOC device and the zeta potential values measured by the LDv technique were compared to seek possible correlation. Fig. 5B shows the streaming potential results plotted as a function of zeta potential, including the Nafion results. The graph was fitted with linear regression, and the result showed a clear linear relationship between the data gathered by the two methods, with a goodness-of-fit of $R^2 = 0.988$.

The results clearly prove the feasibility of the new "zeta-feature" of the device, at the same time provide a calibration factor for the determination of the zeta potential of the cell layer. It was also shown that the sensitivity of the technique is sufficient to measure changes in the surface charge properties of the BBB layer that was demonstrated to be linked to altered penetration of charged molecules and nanoparticles.[2,16,17] The question arises, however, whether the changes in surface charge measured by streaming or zeta potential were accompanied by alterations in barrier parameters, such as permeability for ions (TEER) or neutral hydrophilic molecules.

Barrier integrity of cell monolayers in the LOC device

To investigate if zeta potential changes are linked to changes in passive paracellular permeability or are independent indicators of function further experiments were performed. The tightness of the paracellular pathway, restricted by tight intercellular junctions, can be tested with hydrophilic molecules.[9,25,58,59] Electrical impedance measurement at low frequency (called as TEER) is the most sensitive method to characterize the paracellular barrier integrity for ions.[25,60] The TEER (measured at 12.5 Hz) of the BBB model was determined both in the device (Fig. 7) and in culture inserts (ESI† Fig. S5). The resistance of the BEC cultures in the LOC device did not change after treatments (Fig. 7A) and the same result was shown on culture inserts for neuraminidase (ESI† Fig. S5A). Since the paracellular permeability for both ions and neutral hydrophilic molecules is regulated by the tight intercellular junctions, changes in the cell surface zeta potential are not expected to affect this pathway. The removal of the sialic acid residues from the glycocalyx or the insertion of a positively charged molecule in the plasma membrane of the cells did not result in any statistical difference in the paracellular permeability for dextran as compared to the control group, as it was expected for a neutral large tracer molecule. The same was observed on culture inserts as shown in ESI† Fig. S5B. These data are in agreement with our previous results describing that treatment of BBB culture models with lidocaine did not change the permeability of neutral hydrophilic markers such as dextran.[17] In concordance with TEER and permeability data the cell morphology of BEC was unchanged as the same immunostaining pattern was observed for the junctional linker protein β-catenin after treatments as compared to the control cells (Fig. 7C). Similar BEC morphology was also observed after neuraminidase treatment by phase contrast microscopy (ESI† Fig. S5C). These control experiments prove that modulation of endothelial cellular surface charge with neuraminidase or lidocaine did not affect barrier integrity of the cell layers and that both TEER and zeta potential, two independent essential parameters can be measured with the device.

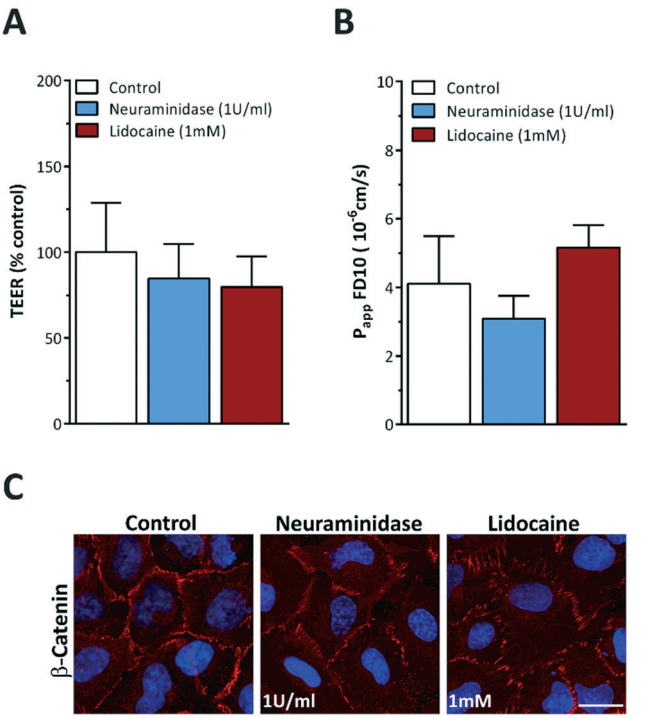

Fig. 7 The effects of the treatments modifying the surface charge of confluent brain endothelial cells on the paracellular barrier properties measured in the chip device. (A) Transendothelial electric resistance (TEER) results were normalized to the values of the control group which received culture medium instead of treatments for the same period. (B) Apparent permeability coefficient (P_{app}) of the brain endothelial monolayers for the neutrally charged fluorescently labeled 10 kDa dextran (FD10), a marker of paracellular permeability. (C) Cell morphology was characterized by immunostaining for β-catenin, a linker protein of adherens junctions, and visualised by confocal microscopy. Bar: 20 μm.

Conclusions and outlook

We successfully measured the streaming potential of a biological barrier culture model with the help of our versatile lab-on-a-chip device upgraded with two Ag/AgCl electrodes. The inclusion of the "zeta electrodes", a voltage preamplifier and an oscilloscope in our set-up made it possible to successfully record signals describing the surface charge properties of brain endothelial cell monolayers, used as a barrier model in our experiments. The new technique was verified by comparing streaming potential data obtained in the LOC device and zeta potential results by the commonly used LDv method. Changes in the negative surface charge of the barrier model by treatments with neuraminidase enzyme modifying the plasma membrane glycocalyx or lidocaine altering the lipid membrane charge could be measured by both the novel LOC device and LDv. The device as we proved earlier can be used for different types of biological barriers,

such as respiratory and intestinal epithelial cell cultures and co-culture models of the BBB.[37] Potential application of the new LOC zeta device can be two-fold. Surface charge and its changes can be measured by registering the streaming potential on other epithelial and endothelial barrier systems including lung, intestine, kidney and cornea. On the other hand, changes in either the glycocalyx of the vascular or other barriers caused by pathologies such as diabetes, sepsis, hypertension or virus infection or changes in the plasma membrane caused by charged molecules or drugs can be modeled and directly measured on intact cell layers. Our technique is, in principle, compatible with further miniaturization of the channel to adapt the system for screening purposes. The new device can help to gain meaningful novel information on how surface charge is linked to barrier function in both physiological and pathological conditions.

Author contribution

Conceptualization, A. K., A. R. S. M., M. A. D., A. D.; methodology, A. K., A. R. S. M., S. V., M. A .D. and A. D.; formal analysis, A. K., A. R. S. M., F. R. W., S. V., L. D., A. D.; investigation, A. K., A. R. S. M., F. R. W., N. H., D. V. L., A. D..; resources, A. K., A. R. S. M., L. D., S. V., A. D., data curation, A. K., A. R. S. M., F. R. W., S. V., L. D., A. D.; writing – original draft preparation, A. K., A. R. S. M., F. R. W., M. A. D., A. D.; writing – review and editing, A. K., A. R. S. M., F. R. W., L. D., S. V., M. A. D., A. D.; visualization, A. K., A. R. S. M., S. V., L. D.; project administration, F. R. W., M. A. D. and A. D.; supervision, M. A. D. and A. D., funding acquisition, M. A. D. and A.D.

Conflicts of interest

There is no conflict of interest to declare.

Acknowledgements

This work was supported by National Research, Development and Innovation Office, Hungary [grant numbers GINOP-2.3.2-15-2016-00001, GINOP-2.3.2-15-2016-00037, OTKA K-108697, NNE 129617 as part of the M-Era.NET2 nanoPD project]. A. R. S.-M. was supported by the European Training Network H2020-MSCA-ITN-2015 [grant number 675619]. FRW is currently supported by the National Research, Development and Innovation Office, Hungary [grant number OTKA PD-128480], by the János Bolyai Research Fellowship of the Hungarian Academy of Sciences, and by the New National Excellence Program Bolyai+ fellowship (UNKP-19-4-SZTE-42) of the Ministry for Innovation and Technology, Hungary.

References

1 T. Yeung, G. E. Gilbert, J. Shi, J. Silvius, A. Kapus and S. Grinstein, *Science*, 2008, **319**, 210–213.
2 M. M. Ribeiro, M. M. Domingues, J. M. Freire, N. C. Santos and M. A. Castanho, *Front. Cell. Neurosci.*, 2012, **6**, 44.
3 L. Möckl, *Front. Cell Dev. Biol.*, 2020, **8**, 253.
4 M. A. Deli, *Biochim. Biophys. Acta*, 2009, **1788**, 892–910.
5 B. M. van den Berg, M. Nieuwdorp, E. S. Stroes and H. Vink, *Pharmacol. Rep.*, 2006, **58**, 75–80.
6 S. Dogné and B. Flamion, *Am. J. Pathol.*, 2020, **190**, 768–780.
7 F. Krammer, G. J. D. Smith, R. A. M. Fouchier, M. Peiris, K. Kedzierska, P. C. Doherty, P. Palese, M. L. Shaw, J. Treanor, R. G. Webster and A. García-Sastre, *Nat. Rev. Dis. Primers*, 2018, **4**, 3.
8 N. J. Abbott, A. A. Patabendige, D. E. Dolman, S. R. Yusof and D. J. Begley, *Neurobiol. Dis.*, 2010, **37**, 13–25.
9 M. A. Deli, *Solubility, Delivery and ADME Problems of Drugs and Drug-Candidates*, ed. K. Tihanyi and M. Vastag, Bentham Science Ltd., Wasington DC, 2011, vol. 8, pp. 145–165.
10 P. Campos-Bedolla, F. R. Walter, S. Veszelka and M. A. Deli, *Arch. Med. Res.*, 2014, **45**, 610–638.
11 Y. Ando, H. Okada, G. Takemura, K. Suzuki, C. Takada, H. Tomita, R. Zaikokuji, Y. Hotta, N. Miyazaki, H. Yano, I. Muraki, A. Kuroda, H. Fukuda, Y. Kawasaki, H. Okamoto, T. Kawaguchi, T. Watanabe, T. Doi, T. Yoshida, H. Ushikoshi, S. Yoshida and S. Ogura, *Sci. Rep.*, 2018, **8**, 17523.
12 F. Hervé, N. Ghinea and J. M. Scherrmann, *AAPS J.*, 2008, **10**, 455–472.
13 B. M. Fu and J. M. Tarbell, *Wiley Interdiscip. Rev.: Syst. Biol. Med.*, 2013, **5**, 381–390.
14 M. M. Ribeiro, A. R. Pinto, M. M. Domingues, I. Serrano, M. Heras, E. R. Bardaji, I. Tavares and M. A. Castanho, *Mol. Pharmaceutics*, 2011, **8**, 1929–1940.
15 G. Li and B. M. Fu, *J. Biomech. Eng.*, 2011, **133**, 021002-1-12.
16 M. Mészáros, G. Porkoláb, L. Kiss, A. M. Pilbat, Z. Kóta, Z. Kupihár, A. Kéri, G. Galbács, L. Siklós, A. Tóth, L. Fülöp, M. Csete, Á. Sipos, P. Hülper, P. Sipos, T. Páli, G. Rákhely, P. Szabó-Révész, M. A. Deli and S. Veszelka, *Eur. J. Pharm. Sci.*, 2018, **123**, 228–240.
17 A. R. Santa-Maria, F. R. Walter, S. Valkai, A. R. Brás, M. Mészáros, A. Kincses, A. Klepe, D. Gaspar, M. A. Castanho, L. Zimányi, A. Dér and M. A. Deli, *Biochim. Biophys. Acta, Biomembr.*, 2019, **1861**, 1579–1591.
18 R. J. Hunter, *Zeta Potential in Colloid Science*, Academic Press, San Diego, 1981.
19 E. Malher, D. Martin, C. Duvivier, B. Volochine and J. F. Stoltz, *Biorheology*, 1982, **19**, 647–654.
20 I. B. Oldham, F. J. Young and J. F. Osterle, *J. Colloid Sci.*, 1963, **18**, 328–336.
21 R. A. Van Wagenen and J. D. Andrade, *J. Colloid Interface Sci.*, 1980, **76**, 305–314.
22 P. N. Sawyer, E. Himmelfarb, I. Lustrin and H. Ziskind, *Biophys. J.*, 1966, **6**, 641–651.
23 D. H. Smyth and E. M. Wright, *J. Physiol.*, 1966, **182**, 591–602.
24 R. B. Gandhi and J. R. Robinson, *Pharm. Res.*, 1991, **8**, 1199–1202.
25 M. A. Deli, C. S. Ábrahám, Y. Kataoka and M. Niwa, *Cell. Mol. Neurobiol.*, 2005, **25**, 59–127.

26 H. C. Helms, N. J. Abbott, M. Burek, R. Cecchelli, P. O. Couraud, M. A. Deli, C. Förster, H. J. Galla, I. A. Romero, E. V. Shusta, M. J. Stebbins, E. Vandenhaute, B. Weksler and B. Brodin, *J. Cereb. Blood Flow Metab.*, 2016, **36**, 862–890.

27 S. Veszelka, A. Tóth, F. R. Walter, A. E. Tóth, I. Gróf, M. Mészáros, A. Bocsik, É. Hellinger, M. Vastag, G. Rákhely and M. A. Deli, *Front. Mol. Neurosci.*, 2018, **11**, 166.

28 C. M. Sakolish, M. B. Esch, J. J. Hickman, M. L. Shuler and G. J. Mahler, *EBioMedicine*, 2016, **5**, 30–39.

29 M. W. van der Helm, A. D. van der Meer, J. C. T. Eijkel, A. van den Berg and L. I. Segerink, *Tissue Barriers*, 2016, **4**, e1142493.

30 S. R. A. Kratz, G. Höll, P. Schuller, P. Ertl and M. Rothbauer, *Biosensors*, 2019, **9**, 110.

31 I. Raimondi, L. Izzo, M. Tunesi, M. Comar, D. Albani and C. Giordano, *Front. Bioeng. Biotechnol.*, 2020, **7**, 435.

32 W. Neuhaus, R. Lauer, S. Oelzant, U. P. Fringeli, G. F. Ecker and C. R. Noe, *J. Biotechnol.*, 2006, **125**, 127–141.

33 R. Booth and H. Kim, *Lab Chip*, 2012, **12**, 1784–1792.

34 B. Prabhakarpandian, M. C. Shen, J. B. Nichols, I. R. Mills, M. Sidoryk-Wegrzynowicz, M. Aschner and K. Pant, *Lab Chip*, 2013, **13**, 1093–1101.

35 L. Cucullo, M. Hossain, W. Tierney and D. Janigro, *BMC Neurosci.*, 2013, **14**, 18.

36 Q. Ramadan, H. Jafarpoorchekab, C. Huang, P. Silacci, S. Carrara, G. Koklü, J. Ghaye, J. Ramsden, C. Ruffert, G. Vergeres and M. A. M. Gijs, *Lab Chip*, 2013, **13**, 196–203.

37 F. R. Walter, S. Valkai, A. Kincses, A. Petneházi, T. Czeller, S. Veszelka, P. Ormos, M. A. Deli and A. Dér, *Sens. Actuators, B*, 2016, **222**, 1209–1219.

38 Y. I. Wang, C. Carmona, J. J. Hickman and M. L. Shuler, *Adv. Healthcare Mater.*, 2018, **7**, 1–29.

39 B. M. Maoz, A. Herland, E. A. FitzGerald, T. Grevesse, C. Vidoudez, A. R. Pacheco, S. P. Sheehy, T. E. Park, S. Dauth, R. Mannix, N. Budnik, K. Shores, A. Cho, J. C. Nawroth, D. Segrè, B. Budnik, D. E. Ingber and K. K. Parker, *Nat. Biotechnol.*, 2018, **36**, 865–874.

40 T. E. Park, N. Mustafaoglu, A. Herland, R. Hasselkus, R. Mannix, E. A. FitzGerald, R. Prantil-Baun, A. Watters, O. Henry, M. Benz, H. Sanchez, H. J. McCrea, L. C. Goumnerova, H. W. Song, S. P. Palecek, E. Shusta and D. E. Ingber, *Nat. Commun.*, 2019, **10**, 2621.

41 C. M. Lo, C. R. Keese and I. Giaever, *Exp. Cell Res.*, 1993, **204**, 102–109.

42 B. Srinivasan, A. R. Kolli, M. B. Esch, H. E. Abaci, M. L. Shuler and J. J. Hickman, *J. Lab. Autom.*, 2015, **20**, 107–126.

43 N. Orgovan, B. Kovacs, E. Farkas, B. Szabó, N. Zaytseva, Y. Fang and R. Horvath, *Appl. Phys. Lett.*, 2014, **104**, 083506.

44 E. Farkas, A. Szekacs, B. Kovacs, M. Olah, R. Horvath and I. Szekacs, *J. Hazard. Mater.*, 2018, **351**, 80–89.

45 R. M. Fike and C. J. van Oss, *In Vitro*, 1976, **12**, 428–436.

46 R. A. Van Wagenen, J. D. Andrade and J. B. Hibbs Jr, *J. Electrochem. Soc.*, 1976, **123**, 1438–1444.

47 P. Vandrangi, P. Jreij, T. E. Rajapaksa, N. Bansal, D. D. Lo and V. G. J. Rodgers, *Rev. Sci. Instrum.*, 2012, **83**, 074302.

48 P. Vandrangi, D. D. Lo, R. Kozaka, N. Ozaki, N. Carvajal and V. G. J. Rodgers, *Biotechnol. Bioeng.*, 2013, **110**, 2742–2748.

49 B. B. Weksler, E. A. Subileau, N. Perrière, P. Charneau, K. Holloway, M. Leveque, H. Tricoire-Leignel, A. Nicotra, S. Bourdoulous, P. Turowski, D. K. Male, F. Roux, J. Greenwood, I. A. Romero and P. O. Couraud, *FASEB J.*, 2005, **19**, 1872–1874.

50 A. Singh, S. C. Satchell, C. R. Neal, E. A. McKenzie, J. E. Tooke and P. W. Mathieson, *J. Am. Soc. Nephrol.*, 2007, **18**, 2885–2893.

51 D. Gross and W. S. Williams, *J. Biomech.*, 1982, **15**, 277–295.

52 Z. A. Kostiuchenko, J. Z. Cui and S. G. Lemay, *J. Phys. Chem. C Nanomater Interfaces*, 2020, **124**, 2656–2663.

53 K. A. Mauritz and R. B. Moore, *Chem. Rev.*, 2004, **104**, 4535–4585.

54 E. Hellinger, S. Veszelka, A. E. Tóth, F. R. Walter, A. Kittel, M. L. Bakk, K. Tihanyi, V. Háda, S. Nakagawa, T. D. Duy, M. Niwa, M. A. Deli and M. Vastag, *Eur. J. Pharm. Biopharm.*, 2012, **82**, 340–351.

55 K. B. Betteridge, K. P. Arkill, C. R. Neal, S. J. Harper, R. R. Foster, S. C. Satchell, D. O. Bates and A. H. J. Salmon, *J. Physiol.*, 2017, **595**, 5015–5035.

56 F. D. Morgan, E. R. Williams and T. R. Madden, *J. Geophys. Res., [Solid Earth Planets]*, 1989, **94**, 12449–12461.

57 R. Peng and D. Li, *Nanoscale*, 2016, **8**, 12237–12246.

58 N. J. Abbott, L. Rönnbäck and E. Hansson, *Nat. Rev. Neurosci.*, 2006, **7**, 41–53.

59 M. Cereijido, R. G. Contreras, L. Shoshani, D. Flores-Benitez and I. Larre, *Biochim. Biophys. Acta*, 2008, **1778**, 770–793.

60 K. Benson, S. Cramer and H. J. Galla, *Fluids Barriers CNS*, 2013, **10**, 5.